Potential-Dependent Adsorption Behavior of Fluorescent Species at Liquid|Liquid Interfaces Studied by Polarization-Modulation Total Internal Reflection Fluorescence Spectroscopy

Doctoral Dissertation

Potential-Dependent Adsorption Behavior of Fluorescent Species at Liquid|Liquid Interfaces Studied by Polarization-Modulation Total Internal Reflection Fluorescence Spectroscopy

Division of Material Chemistry, Graduate School of Natural Science and Technology, Kanazawa University

Student ID: 1524022006

Name: Sho Yamamoto

Chief Advisor: Hirohisa Nagatani

January 5, 2018

Abstract

Polarization-modulation total internal reflection fluorescence (PM-TIRF) spectroscopy was developed to study the adsorption behavior of fluorescent species at liquid|liquid interfaces. In the PM-TIRF experiments, the fluorescence signal from the interfacial region is analyzed as a function of the periodic modulation of linear-polarizations (p and s) of the incident excitation beam, which enables us to measure interfacial species *in situ* without controversial contribution of bulk species. The potential dependences of molecular orientation and adsorption state of fluorescent species at the water|1,2-dichloroethane (DCE) interface were analyzed by PM-TIRF spectroscopy.

Water-soluble *meso*-substituted porphyrins, 5,10,15,20-tetrakis(*N*-methylpyridyl)porphyrin (H_2TMPyP^{4+}) and 5,10,15,20-tetrakis(4-sulfonatophenyl)porphyrin (H_2TPPS^{4-}), indicated that the free base forms were adsorbed with relatively lying orientations at the polarized water|DCE interface. Their solvation states at the interface were significantly modified from those in the bulk solution. The diprotonated species, H_4TPPS^{2-}, formed J-aggregates at the interface, where the aggregation was controlled reversibly as a function of the externally applied potential. In the case of protoporphyrin IX (H_2PP^{2-}), the monomers were adsorbed with relatively standing orientation and the long axis of the J-aggregates was nearly in plane of the interface. The monomer and its aggregates at the interface were characterized separately by using appropriate excitation wavelengths.

PM-TIRF spectroscopy was also applied to elucidate the interfacial mechanism of water-soluble 8-quinolinol complexes at the water|DCE interface. In the case of a bidentate ligand, 8-quinolinol-5-sulfonate (HQS^-), the stoichiometry of the metal complex formation in the aqueous solution varies from 1:1 to 1:3 as a function of pH. PM-TIRF analysis revealed that the hydration states of 1:2 Al(III) and Zn(II) complexes ($Al(QS)_2^-$ and $Zn(QS)_2^{2-}$) were analogous to those in the aqueous solution. On the other hand, in the case of a tridentate 8-quinolinol-2-carboxylate (HQC^-), the solvation state of the 1:2 complex ($Zn(QC)_2^{2-}$) was dependent on the potential,

indicating that the axial coordination of water molecules to metal center plays important roles in the interfacial mechanism. These results demonstrated the potential ability of PM-TIRF spectroscopy for direct characterization of the species oriented at liquid|liquid interfaces.

Contents

1. Introduction

1-1. Liquid|Liquid Interfaces

A liquid|liquid interface is a boundary between two immiscible solutions with a thickness of ~1 nm,[1, 2] where several elementary steps take place, such as transfer and adsorption of species, heterogeneous reaction, electron transfer etc. The liquid|liquid interface is used for the study of mass transport reaction in vivo and solvent extraction, where transfer and adsorption processes of reactants play important roles in the reaction mechanism.[3, 4] Some specific features of interfacial species have been reported in terms of molecular assembly and solvation by means of surface-sensitive spectroscopy.[5-7] The self-assembly process is often involved with the molecular orientation of the species adsorbed at the interface. The adsorbed species with a specific orientation tend to form their self-aggregates easily at the liquid|liquid interface in comparison with homogeneous solution systems.[5-7]

A liquid|liquid interface is regarded as a model of biomembrane because the charge transfer processes are closely associated with biological systems. The interfacial mechanism has been evaluated at an interface between two immiscible electrolyte solutions (ITIES) by various electrochemical approaches to understand mass-transfer mechanism and distribution equilibrium in separation sciences, nanomaterial formation, pharmacokinetic applications etc.[8, 9] At ITIES, the charge transfer processes can be controlled as a function of the Galvani potential difference between two liquid phases ($\Delta_o^w\phi$) (**Figure 1-1**).[8, 9] ITIES consisting of water and an organic

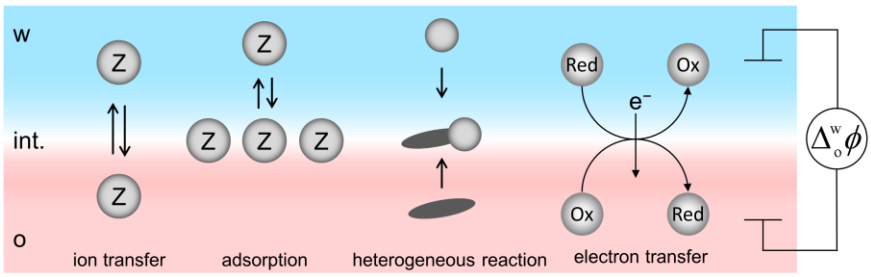

Figure 1-1. Schematic representation elementary steps at ITIES.

solvent with high dielectric constant, such as 1,2-dichloroethane (DCE) and nitrobenzene, is often used in electrochemistry. When an ion (x^{z+}) is initially present in the aqueous phase, x^{z+} can be partitioned between the aqueous (w) and organic (o) phases.

$$x_w^{z+} \rightleftharpoons x_o^{z+} \tag{1-1}$$

The ion transfer reactions at ITIES is controlled by $\Delta_o^w\phi$ and then the distribution of x^{z+} across the interface is given by the Nernst equation:[8, 9]

$$\Delta_o^w\phi = \Delta_o^w\phi^\circ + \frac{RT}{zF}\ln\frac{a_x^o}{a_x^w} \tag{1-2}$$

where $\Delta_o^w\phi^\circ$, z, F, R, T, a_x^w and a_x^o are the standard ion transfer potential and charge number of x^{z+}, Faraday constant, gas constant, temperature, the activities of x^{z+} in the aqueous and organic phases, respectively. $\Delta_o^w\phi$ is represented as the difference of the inner potentials of each phase.

$$\Delta_o^w\phi = \phi^w - \phi^o \tag{1-3}$$

$\Delta_o^w\phi^\circ$ relates to the standard Gibbs free energy of ion transfer ($\Delta G_t^{\circ,w\to o}$) from the aqueous to organic phases.

$$\Delta G_t^{\circ,w\to o} = zF\Delta_o^w\phi^\circ \tag{1-4}$$

In the adsorption process of ionic species at ITIES, two adsorption planes, i.e., aqueous and organic sides, are considered in a simplified phenomenological model (**Figure 1-2**).[10, 11] Assuming that the interaction between the adsorbed species is negligible, the adsorption processes at both aqueous and organic sides of the interface are described by the Langmuir-type adsorption isotherm. In the case of the adsorption of ionic species in the aqueous phase, the surface coverage (θ) is given by the following equation.[11]

$$\frac{d\theta}{dt} = k_a^w c^w(1-\theta) - k_d^w\theta \tag{1-5}$$

where k_a^w and k_d^w are the rate constants for the adsorption and desorption at the aqueous plane. c^w is the bulk aqueous concentration. Assuming that k_a^w and k_d^w are potential dependent in the

Butler–Volmer formalism, the potential dependent surface coverage at the aqueous side of the interface can be given by[11]

$$k_{\mathrm{a}}^{\mathrm{w}} = k_{\mathrm{a}}^{\mathrm{w}\circ} \exp\left(\frac{\alpha z F}{RT} \Delta_{\mathrm{aw}}^{\mathrm{w}} \phi \right) \tag{1-6}$$

$$k_{\mathrm{d}}^{\mathrm{w}} = k_{\mathrm{d}}^{\mathrm{w}\circ} \exp\left(\frac{(\alpha - 1) z F}{RT} \Delta_{\mathrm{aw}}^{\mathrm{w}} \phi \right) \tag{1-7}$$

$k_{\mathrm{a}}^{\mathrm{w}\circ}$ and $k_{\mathrm{d}}^{\mathrm{w}\circ}$ are rate constants for the adsorption and desorption at the potential of zero charge, respectively. α is overall transfer coefficient for the adsorption process. $\Delta_{\mathrm{aw}}^{\mathrm{w}} \phi$ corresponds to the potential difference between the bulk aqueous phase and interface, which is interpreted as a part of Galvani potential difference between two phases (**Figure 1-2**). $\Delta_{\mathrm{aw}}^{\mathrm{w}} \phi$ is represented as

$$\Delta_{\mathrm{aw}}^{\mathrm{w}} \phi = b^{\mathrm{w}} \Delta_{\mathrm{o}}^{\mathrm{w}} \phi \tag{1-8}$$

b^{w} is determined by the potential distribution across the interface. Considering that the potential difference between two adsorption planes ($\Delta_{\mathrm{aw}}^{\mathrm{ao}} \phi$) is negligible, that is $b^{\mathrm{w}} + b^{\mathrm{org}} = 1$, the potential difference at the organic phase ($\Delta_{\mathrm{o}}^{\mathrm{ao}} \phi$) is expressed as $\Delta_{\mathrm{o}}^{\mathrm{ao}} \phi = b^{\mathrm{org}} \Delta_{\mathrm{o}}^{\mathrm{w}} \phi = (1 - b^{\mathrm{w}}) \Delta_{\mathrm{o}}^{\mathrm{w}} \phi$. From eqs. (1-5)–(1-8), the potential dependent surface coverage (θ^{w}) at the aqueous side of the interface can be given by[11]

$$\theta^{\mathrm{w}} = \frac{c^{\mathrm{w}} \exp[(b^{\mathrm{w}} z F \Delta_{\mathrm{o}}^{\mathrm{w}} \phi - \Delta G_{\mathrm{a}}^{\circ}) / RT]}{1 + c^{\mathrm{w}} \exp[(b^{\mathrm{w}} z F \Delta_{\mathrm{o}}^{\mathrm{w}} \phi - \Delta G_{\mathrm{a}}^{\circ}) / RT]} \tag{1-9}$$

where

$$\Delta G_{\mathrm{a}}^{\circ} = -RT \ln\left(\frac{k_{\mathrm{a}}^{\circ} c^{\circ}}{k_{\mathrm{d}}^{\circ}} \right) \tag{1-10}$$

$\Delta G_{\mathrm{a}}^{\circ}$ is the Gibbs free energy of adsorption. When the concentration c^{w} is also described by the Nernst equation (eq. 1-2), the surface coverage of the adsorbed species should be maximized at its ion transfer potential (**Figure 1-3**).

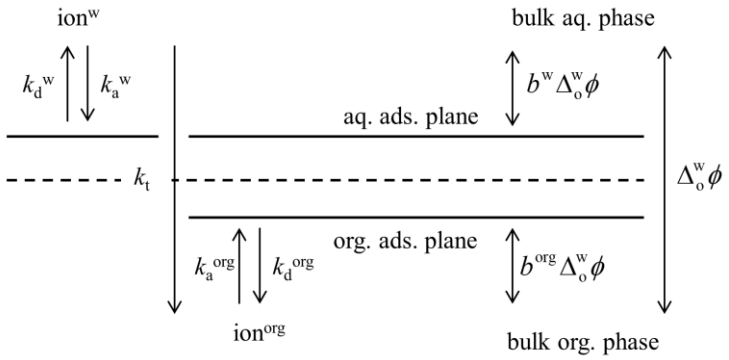

Figure 1-2. Schematic representation of the interfacial structure and adsorption processes.[13]

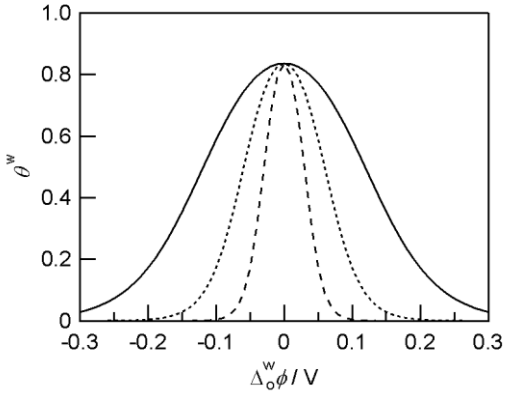

Figure 1-3. Potential dependent surface coverage calculated from eqs. (1-2) and (1-9). The charge number z, was taken as +1 (solid line), +2 (dotted line) and +4 (dashed line). The values for c^w, b^w, $\Delta_o^w\phi^\circ$ and ΔG_a° were taken as 1.0×10^{-3} mol dm^{-3}, 0.5, 0 V and –40 kJ mol^{-1}, respectively.

1-2. Spectroscopic Characterization of Species at Liquid|Liquid Interfaces

The heterogeneous reaction at liquid|liquid interfaces often involves the interfacial adsorption process of reactants. The interfacial mechanism and kinetics are then significantly affected by the adsorption state of the reactants. Therefore, characterizations of interfacial species at molecular level such as solvation structure, molecular orientation and intermolecular interaction are important to elucidate the heterogeneous reaction mechanism.[12, 13] A number of spectroscopic techniques have been developed to characterize interfacial species at liquid|liquid interfaces. The reactivity and characterization of interfacial species are generally evaluated by either electrochemical techniques or spectroscopies.[12-14] However, it is extremely difficult to characterize the interfacial species *in situ* by using conventional spectroscopies since ion transfer reactions (or ion partitioning) could take place simultaneously with their adsorption processes at liquid|liquid interfaces. In such cases, weak signals of the interfacial species cannot readily be differentiated from bulk solution species.

Total internal reflection (TIR) spectroscopy is one of the most powerful techniques to investigate the reaction mechanism at a liquid|liquid interface.[7, 14] In TIR mode, a laser beam is introduced from a medium 1 with higher refractive index (n_1) to a medium 2 with lower index (n_2) (**Figure. 1-4**). When the angle of the incident (ψ_i) is larger than the critical angle (ψ_c), the

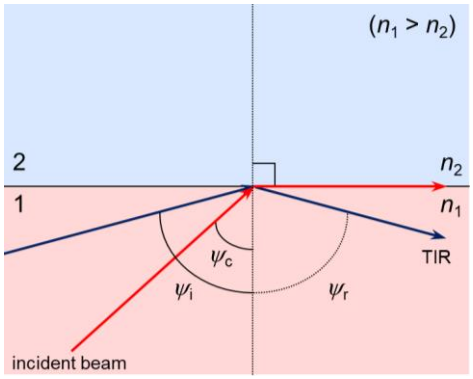

Figure 1-4. Schematic representation of reflection of the incident beam at an interface between two liquid media. ψ_i and ψ_r are the angles of incidence and reflectance, respectively. ψ_c is the critical angle.

beam is totally reflected at the interface, which is given by the Snell's law:

$$\psi_c = \sin^{-1}(n_2 / n_1) \qquad (1\text{-}11)$$

Under a TIR condition, the beam can penetrate into the medium 2, which is called evanescent wave. The penetration depth (d_p) relates to the wavelength (λ_L) of the incident beam.[15]

$$d_p = \frac{\lambda_L}{4\pi\sqrt{n_1^2 \sin^2 \psi_i - n_2^2}} \qquad (1\text{-}12)$$

The evanescent wave can penetrate ~100 nm at the water|DCE interface in the UV-visible region (e.g. $d_p \approx 80$ nm with $\lambda_L = 404$ nm, $\psi_i = 75°$, $n_{water} = 1.33$. $n_{DCE} = 1.44$). TIR spectroscopy enable us to excite species selectively in the evanescent region. In particular, total internal reflection fluorescence (TIRF) spectroscopy has provided various insights of interfacial species with its high sensitivity.[16-18] When dye species are dissolved in the incident medium, however, the optical signals from the interfacial region are weak and buried in strong signals from the bulk solution species.

Surface second harmonic generation (SSHG) spectroscopy is extremely sensitive to molecules adsorbed at the interface between two centrosymmetric phases such as liquid surfaces, solid|liquid and liquid|liquid interfaces.[5, 19-23] SHG is one of the non-linear optical phenomena, where the two photons with frequency ω_f are converted to one photon with frequency ω_{SH} ($\omega_{SH} = 2\omega_f$). In the electric dipole approximation, the second harmonic (SH) signal is only generated from oriented molecules adsorbed at the interface. Although SSHG spectroscopy is a quite useful technique to characterize interfacial species with high selectivity, the self-absorption of SH signals by bulk species at resonant wavelengths through the optical path is still a serious problem. The requirements of a high-power laser system and a strict optical setup may also reduce general versatility of this technique.

At polarized liquid|liquid interfaces, the transfer and adsorption processes of ionic species are controlled as a function of $\Delta_o^w\phi$ and thus an ac potential-modulation applied to the interface induces a perturbation of spectroelectrochemical signal arising from the interfacial region.

Potential-modulated fluorescence (PMF) spectroscopy has been employed to analyze the charge transfer reaction at liquid|liquid interfaces.[24-29] In PMF measurements, the ion transfer and adsorption processes are distinguishable through the complex analysis of PMF signals within the framework of simple phenomenological models at a polarized liquid|liquid interface.[11] The direct characterization of interfacial species was also achieved under limited conditions. The sensitivity and selectivity for the adsorbed species are still insufficient in the case that the transfer and adsorption processes takes place in the same potential region.

Polarization modulation infrared reflection absorption spectroscopy (PM-IRRAS) has been used to determine the molecular orientation and the conformation of layered materials formed at solid and liquid surfaces.[30-34] In PM-IRRAS, the linear polarizations of the incident light are periodically modulated and the selectivity for oriented species is drastically improved by analyzing corresponding ac optical signals. A similar approach has also been applied to total reflection X-ray absorption fine structure (TR-XAFS) at liquid surfaces and liquid|liquid interfaces.[35-37] Polarized TR-XAFS measurements, where the linear polarization of incident X-rays is controlled by a diamond retarder crystal, allowed us to estimate the solvation structure of metalloporphyrins at interfaces *in situ*.[38-40] However, the application of PM-IRRAS and polarized TR-XAFS to liquid|liquid systems is rigidly limited by strong attenuation or scattering of incident beam and optical signal by solvent molecules in infrared and X-ray regions.

1-3. Objective of This Study

The direct characterization of interfacial species is a challenging task by means of conventional technique because of the contribution of bulk species. In this dissertation, a novel spectroscopic technique, polarization-modulation total internal reflection fluorescence (PM-TIRF) spectroscopy is introduced. In PM-TIRF technique, TIRF spectroscopy is combined with polarization modulation of an excitation beam to remove unfavorable contribution from the bulk species, which allows us to characterize the species oriented at a liquid|liquid interface with high sensitivity and selectivity. PM-TIRF spectroscopy was applied to investigate the potential-dependent adsorption behavior of fluorescent species at the water|1,2-dichloroethane (DCE) interface.

This dissertation consists of three parts in **Results and Discussion** (Chapter 4). Section 4-1 introduces PM-TIRF analysis based on the molecular orientation of interfacial species, and the potential dependent adsorption behavior of *meso*-substituted water-soluble porphyrins are discussed. In addition, the solvation state of the interfacial species is characterized by PM-TIRF spectroscopy. In Section 4-2, the aggregation of anionic water-soluble porphyrins is analyzed as a function of the applied potential. Furthermore, the adsorption behavior of H_2PP^{2-} at the phospholipid-adsorbed water|DCE interface is investigated in order to evaluate its binding characteristics on cell membrane. Chapter 4-3 relates the effect of metal ions and pH conditions on the adsorption states of water-soluble 8-quinolinol complexes in detail.

2. Principle of Polarization-Modulation Total Internal Reflection Fluorescence (PM-TIRF) Spectroscopy

A novel *in situ* spectroscopic method, polarization-modulation total internal reflection fluorescence (PM-TIRF) spectroscopy, has been developed to measure fluorescent species adsorbed with a certain orientation at a liquid|liquid interface. In PM-TIRF experiments, the fluorescence signal from the interfacial region is analyzed as a function of periodic modulation of linear-polarizations (p and s polarizations) of an excitation beam. PM-TIRF spectroscopy can effectively extract the fluorescence signals of interfacially oriented species from the signals arising throughout the optical path in the incident medium because no PM-TIRF signal arises from bulk species. Here, the principle of PM-TIRF technique is described in detail.

The fluorescence intensity emitted form a molecule adsorbed at an interface is determined by the molecular orientation and polarizations of the excitation beam. Assuming that a transition dipole moment is in a molecular axis (**Figure 2-1**, light blue arrow), the fluorescence intensity

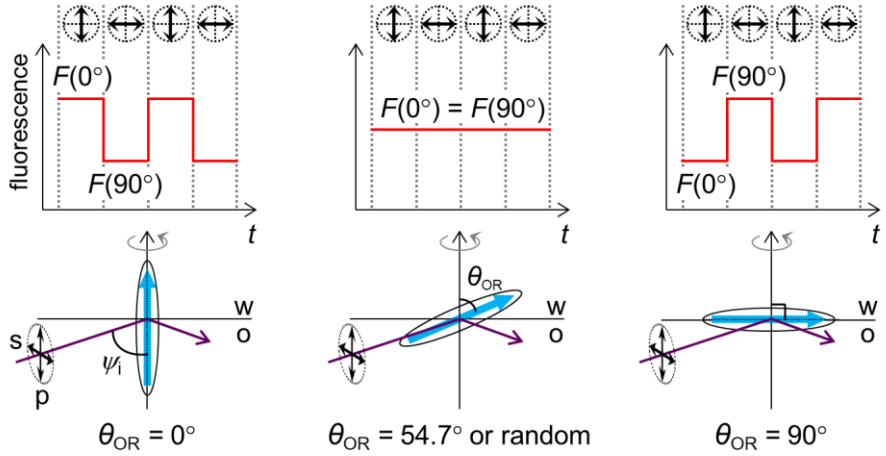

Figure 2-1. Schematic representation of the fluorescence signal from molecules oriented at θ_{OR}. The polarization angle (Ψ) of incident excitation beam is periodically modulated between 0° (p) and 90° (s). The blue arrows depict the transition dipole moment.

from a molecule oriented at an angle (θ_{OR}) with respect to the interface normal can be given by[24, 41, 42]

$$F(\Psi) = C[\sin^2\theta_{OR}\cos^2(90°-\Psi) + (\cos^2\psi_i \sin^2\theta_{OR} + 2\sin^2\psi_i \cos^2\theta_{OR})\sin^2(90°-\Psi)] \quad (2\text{-}1)$$

where ψ_i is the angle of the incident beam, Ψ is the angle of polarization of excitation beam with respect to the normal to the interface and C is a proportional factor. The Ψ values for the p- and s-polarized excitation beams are 0° and 90°, respectively. **Figure 2-1** schematically illustrates the polarization angle dependence of the fluorescence intensity $F(\Psi)$ under TIR conditions. The intensity of $F(0°)$ under the p-polarized excitation beam for molecules oriented at $0° \le \theta_{OR} < 54.7°$ is larger than $F(90°)$ under the s-polarized excitation, while an opposite relationship is obtained in the case of $54.7° < \theta_{OR} \le 90°$. At $\theta_{OR} = 54.7°$ or random orientation, the fluorescence intensity is constant irrespective of Ψ, i.e. $F(0°) = F(90°)$ (**Figure 2-2**).

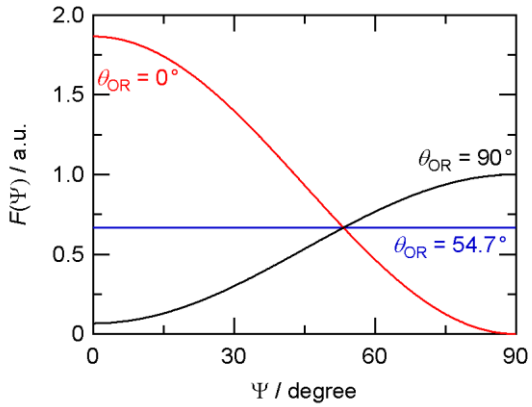

Figure 2-2. Polarization angle dependence of the fluorescence intensity ($F(\Psi)$) calculated from eq. 2-1. The Ψ was defined as the angle with respect to the interface normal, where 0° and 90° relate to the p- and s-polarization, respectively. The orientation angle (θ_{OR}) was taken as 0°, 54.7° and 90°. The values of other parameters were taken as $C = 1$, $\psi_i = 75°$, and θ_{OR} = 0°, 54.7°, 90°, respectively.

In the present work, the PM-TIRF signal ($\Delta F^{p\text{-}s}$) is defined as

$$\Delta F^{p\text{-}s} = F(0°) - F(90°) \qquad (2\text{-}2)$$

The signs of $\Delta F^{p\text{-}s}$ can be diagnostic criteria for the relative orientation of interfacial molecule, in which positive and negative values indicate relatively standing and lying molecular orientations with respect to interface (**Figure 2-3**). When a molecule is oriented at $\theta_{OR} = 54.7^{\circ}$ or random orientation, $\Delta F^{p\text{-}s}$ is zero. In PM-TIRF spectroscopy, the fluorescence signal arising from bulk solution species with random orientation is effectively cancelled out by periodic polarization modulation.

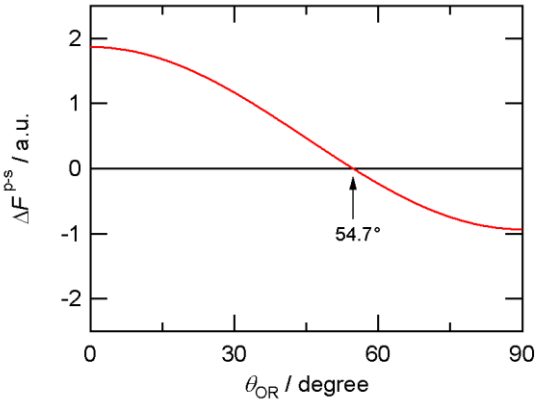

Figure 2-3. Orientation angle dependence of PM-TIRF signal ($\Delta F^{p\text{-}s}$) calculated from eqs. 2-1 and 2-2. The orientation angle (θ_{OR}) of an adsorbed molecule was varied between 0° and 90°. The values of other parameters were taken as $C = 1$, $\psi_i = 75^{\circ}$, respectively.

3. EXPERIMENTAL SECTION

3-1. Reagents.

5,10,15,20-tetrakis(*N*-methylpyridyl)porphyrin (H_2TMPyP^{4+}) tetratosylate salt (Dojindo Laboratories), 5,10,15,20-tetrakis(4-sulfonatophenyl)porphyrin (H_2TPPS^{4-}) disulfuric acid tetrahydrate (Dojindo Laboratories) and protoporphyrin IX (H_2PP^{2-}) disodium salt (TCI) were used as received. Tris(2,2′-bipyridine)ruthenium(II) ($Ru(bpy)_3^{2+}$) chloride (>98%) was purchased from Aldrich. The composition of the electrochemical cell is represented in **Figure 3-1**. The porphyrin derivatives and $Ru(bpy)_3^{2+}$ were dissolved in the aqueous phase. A nonionic surfactant, sorbitan monolaurate (Span 20) was purchased from TCI and dissolved in DCE phase (**Cell II**). A neutral glycerophospholipid, 1,2-dimyristoyl-*sn*-glycero-3-phosphocholine (DMPC) (TCI, ≥ 97%) was initially dissolved in chloroform at 1.0×10^{-3} mol dm^{-3} and then added to the DCE phase (**Cell IV**). Aluminum chloride (Aldrich, >98%) and zinc chloride (Nacalai Tesque, >98%) were used without further purification. 8-quinolinol-5-sulfonate (HQS^-, TCI, >98%) and 8-quinolinol-2-carboxylate (HQC^-, Aldrich, >98%) were used as ligands. The quinolinol complexes were formed in the aqueous solution (**Cell V**). The molecular structures of fluorescent dyes, surfactans, and quinolinol derivatives are shown in **Figure 3.2**. The supporting electrolytes were 1.0×10^{-2} mol dm^{-3} LiCl (**Cell I**, **II**, and **IV**) or Li_2SO_4 (**Cell III and V**) for the aqueous phase and 5.0×10^{-3} mol dm^{-3} bis(triphenylphosphoranylidene)ammonium tetrakis(pentafluorophenyl)borate (BTPPATPFB) for the organic phase, respectively. BTPPATPFB was prepared by metathesis of bis(triphenylphosphoranylidene)ammonium chloride (BTPPACl) (Aldrich, >97%) and lithium tetrakis(pentafluorophenyl)borate ethyl ether complex (TCI, ≥70%).[43] The aqueous solutions were prepared with purified water by a Milli-Q system (Millipore, Direct-Q3UV). 1,2-dichloroethane (DCE) (Nacalai Tesque, HPLC grade, >99.7%) was used as an organic solvent. DCE and water were saturated with each other. All other reagents used were of analytical grade or higher. The pH of the aqueous phase was

adjusted by (1.0–3.0) × 10^{-3} mol dm^{-3} LiH_2PO_4/LiOH buffer and 5.0 × 10^{-3} mol dm^{-3} H_2SO_4 for pH 6.1−7.5 and pH 1.3−2.3 conditions, respectively.

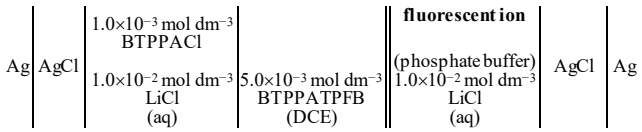

(Cell I)

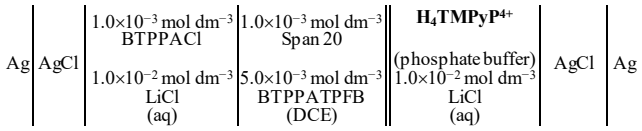

(Cell II)

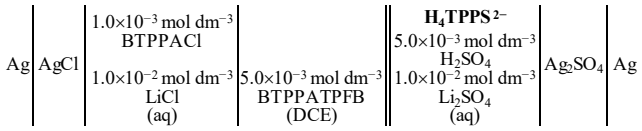

(Cell III)

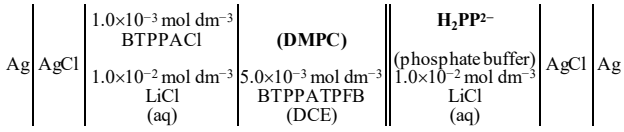

(Cell IV)

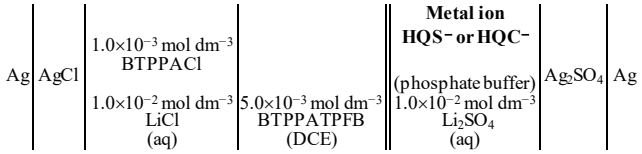

(Cell V)

Figure 3-1. Schematic representation of the electrochemical cells.

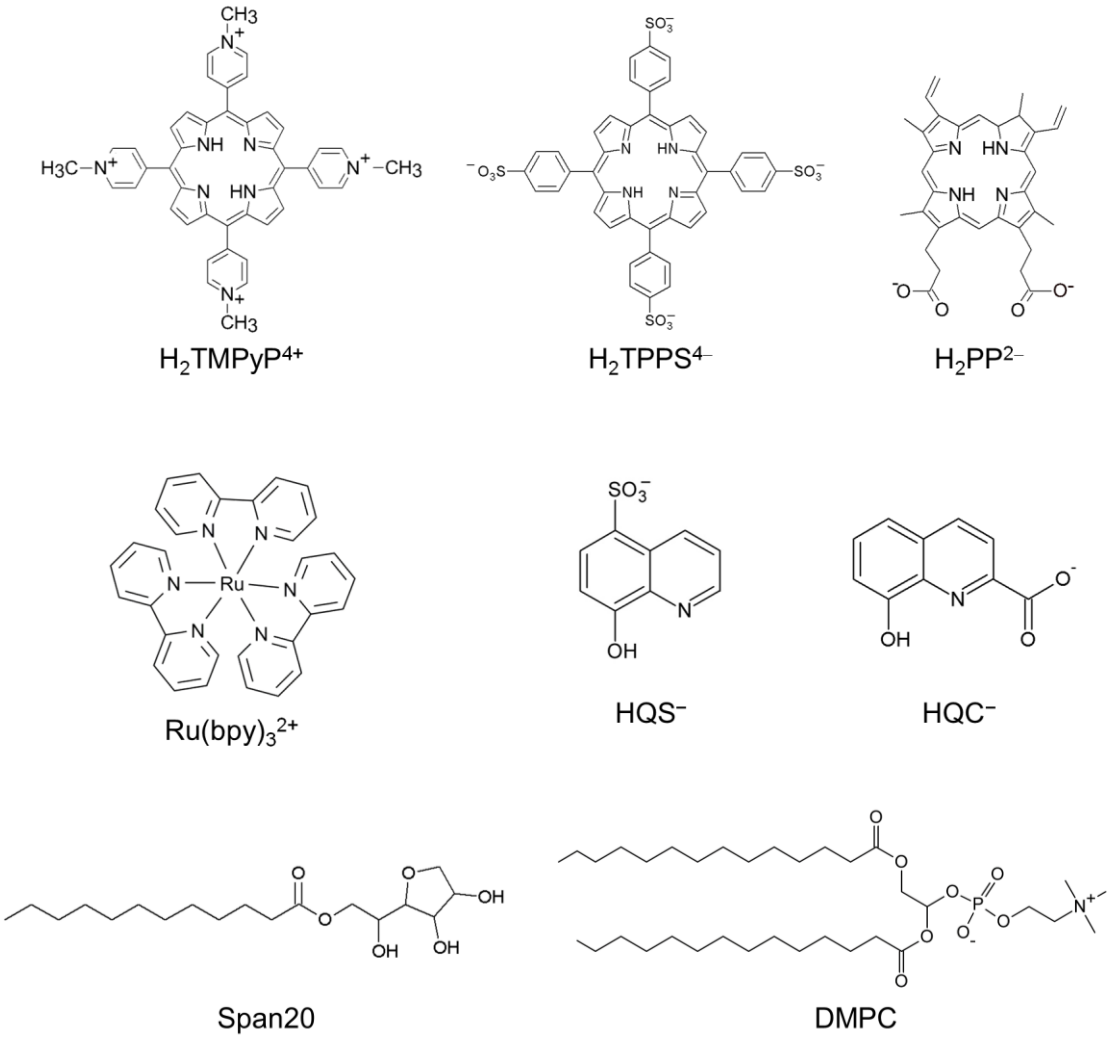

Figure 3-2. Molecular Structures.

3-2. Electrochemical Setup

The electrochemical cell used in all measurements is shown in **Figure 3-3**. The water|DCE interface with a geometrical area of 0.50 cm^2 was polarized by a four-electrode potentiostat (Hokuto Denko, HA-1010mM1A). The platinum counter (CE) and reference electrodes (RE: Ag/AgCl or Ag/Ag_2SO_4 with Luggin capillary) were used in both phases. The Galvani potential difference ($\Delta_o^w\phi \equiv \phi^w - \phi^o$) was estimated by taking the formal transfer potential ($\Delta_o^w\phi^{o\prime}$) of tetramethylammonium ions as −0.160 V.

In ac voltammetry, the applied potential is modulated with a fixed frequency. The ac current ($\tilde{I} = I_{re} + jI_{im}$) was analyzed by a digital lock-in amplifier (NF LI5640), which is converted to admittance ($Y = Y_{re} + jY_{im}$). In the absence of charge transfer across the interface, the admittance can be represented as a linear combination of the solution resistance (R_s) and capacitance (C_{dl}) (eq. 3-1).[44, 45]

$$Y = \frac{\tilde{I}}{\tilde{E}} = \frac{1}{R_s} + j\omega C_{dl} \qquad (3\text{-}1)$$

where $\tilde{I}$ and $\tilde{E}$ are the ac current and ac potential, respectively. j is the imaginary number and ω is the angular frequency ($\omega = 2\pi f_{ac}$, f_{ac}: the potential modulation frequency), respectively. R_s and C_{dl} is calculated from the equation (3-2) and (3-3).

$$R_s = \frac{Y_{re}}{Y_{re}^2 + Y_{im}^2} \qquad (3\text{-}2)$$

$$\frac{1}{\omega C_{dl}} = \frac{Y_{im}}{Y_{re}^2 + Y_{im}^2} \qquad (3\text{-}3)$$

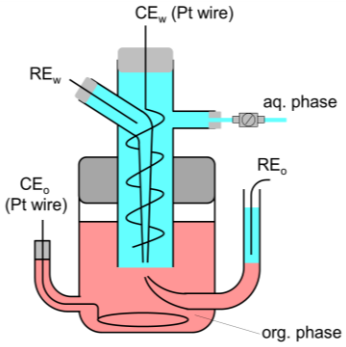

Figure 3-3. Schematic drawing of the electrochemical setup.

3-3. PM-TIRF Spectroscopy

The spectroelectrochemical cell used in all measurements was analogous to one reported previously (**Figure 3-4**).[46] The water|DCE interface was illuminated under the total internal reflection (TIR) condition from organic phase by a cw laser diode at 376 nm (Coherent, OBIS 375LX-50), 404 nm (Coherent, CUBE 405-50C) or 488 nm (Coherent, OBIS 488LS-60). The critical angle for the water|DCE interface is 67.6° and the angle of incidence to the interface (ψ_i) was ca. 75°. The laser radiation was attenuated to 25 mW to avoid the photobleaching of fluorescent species. The fluorescence emitted from the interfacial region was collected perpendicularly to the interface by an optical fiber fitted to a photomultiplier tube (PMT) through

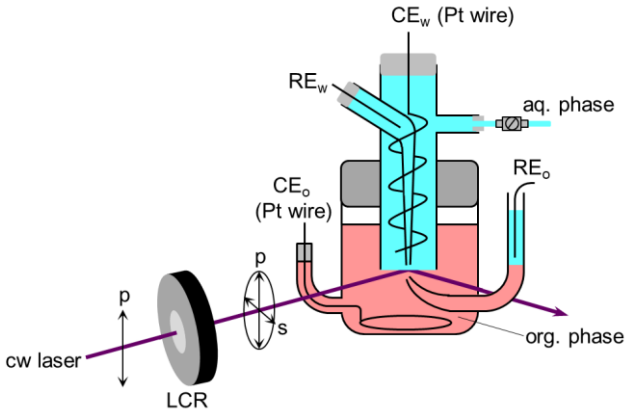

Figure 3-4. Schematic drawing of the spectroelectrochemical setup for PM-TIRF measurement.

a monochromator (Shimadzu, SPG-120S). The linear polarization of an incident excitation beam was periodically modulated from p- (parallel to the plane of incidence) to s-polarization (perpendicular to the plane of incidence) at 13 Hz by a liquid crystal retarder (LCR) thermostated at 323 K (Thorlabs, LCC1111T-A, LCC25/TC200). The polarization-modulated fluorescence signal was analyzed by a digital lock-in amplifier (NF, LI5640) as a function of periodic modulation of linear polarizations. All experiments were carried out in a thermostated room at 298 ± 2 K.

The polarization modulation efficiency (P_m, $0 < P_m \leq 1$) of a liquid crystal retarder (LCR) in the present experimental setup was defined as the fraction of the p- or s-polarized components in the excitation beam through LCR. The P_m values in the p- and s-polarized modes, P_m^p and P_m^s, are expressed by eqs. 3-4 and 3-5 under respective polarization modes, respectively.

$$P_m^p = \frac{I^p}{I^p + I^s} \tag{3-4}$$

$$P_m^s = \frac{I^s}{I^p + I^s} \tag{3-5}$$

The intensities of p- and s-polarized incident beams, I^p and I^s, were measured by a Glan-Thompson prism (Sigma Koki, GTPC-10-33SN) and a Si photodiode (Hamamatsu Photonics, S1133-01) placed after LCR. The P_m value will be unity for perfect conversion between p- and s-polarization. As shown in **Figure 3-5**, the maximum I^p and I^s were observed under respective polarization conditions of LCR. In the present study, the $P_m (= P_m^p = P_m^s)$ values were obtained as 0.85 at 376 nm, 0.95 at 404 nm and 0.97 at 488 nm, respectively, indicating that 15, 5, and 3% of the s-polarized component remain in the p-polarized mode of LCR or *vice versa* (**Figure 3-5**).

When P_m is not equal to 1, the excitation beam consists of both the p- and s-polarized components under polarization modulation. The total intensities of the modulated fluorescence in the p- and s-polarization modes, F_m^p and F_m^s, can be represented by

$$F_m^p = P_m F(0°) + (1 - P_m) F(90°) \tag{3-6}$$

$$F_{\mathrm{m}}^{\mathrm{s}} = P_{\mathrm{m}}F(90°) + (1 - P_{\mathrm{m}})F(0°) \qquad (3\text{-}7)$$

From eqs. 3-6 and 3-7, $\Delta F^{\mathrm{p\text{-}s}}$ with $P_{\mathrm{m}} < 1$ is rewritten as

$$\Delta F^{\mathrm{p\text{-}s}} = F_{\mathrm{m}}^{\mathrm{p}} - F_{\mathrm{m}}^{\mathrm{s}} = (2P_{\mathrm{m}} - 1)(F(0°) - F(90°)) \qquad (3\text{-}8)$$

P_{m} value depends on the liquid crystal retarder (LCR) used and excitation wavelength.

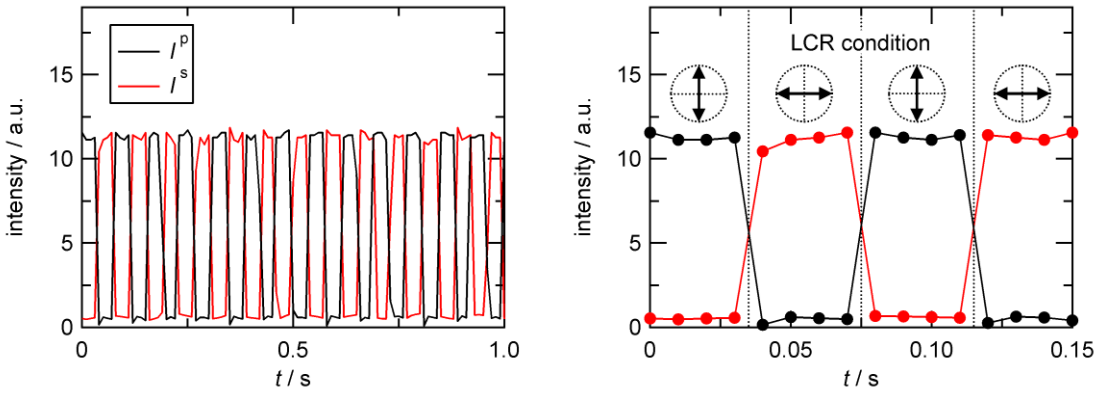

Figure 3-5. Typical time dependences of polarization-modulated light intensity through LCR at 13 Hz. The black and red lines refer to the intensities of the p- and s-polarized components of the excitation beam. The wavelength of the excitation beam was 404 nm.

3-4. Potential Modulated Fluorescence (PMF) Spectroscopy

The spectroelectrochemical cell used is analogous to the electrochemical cell as shown in **Figure 3-3**. PMF measurements were performed in the same manner as described elsewhere.[11, 24, 46] The water|DCE interface was illuminated under TIR condition from organic phase by a cw laser diode at 404 nm (Coherent, CUBE 405-50C). The critical angle for the water|DCE interface is 67.6° and the angle of incidence to the interface (ψ_i) was ca. 75°. Instead of LCR, Fresnel rhomb waveplate (Sigma koki) was placed in front of the cell. The polarization angle of the excitation beam was selected by using Fresnel rhomb half-waveplate. The laser radiation was attenuated to 25 mW to avoid the photobleaching of fluorescent species. The fluorescence emitted from the interfacial region was collected perpendicularly to the interface by an optical fiber fitted to a photomultiplier tube (PMT) through a monochromator (Shimadzu, SPG-120S). The real (ΔF_{re}) and imaginary (ΔF_{im}) components of ac modulated fluorescence, PMF signal, were analyzed by a digital lock-in amplifier (NF LI5640). ΔF_{re} and ΔF_{im} relate to the interfacial mechanism as detailed below.

In PMF measurement, $\Delta_o^w\phi$ is modulated as described by the following equation.[11, 24, 46]

$$\Delta_o^w\phi = \Delta_o^w\phi_{dc} + \Delta_o^w\phi_{ac}\exp(j\omega t) \qquad (3\text{-}9)$$

where $\Delta_o^w\phi_{dc}$ is dc potential applied at the interface, $\Delta_o^w\phi_{ac}$ is the amplitude of the ac potential modulation, j is imaginary number and ω is the angular frequency. When the interfacial processes of fluorescent ions are potential dependent, the fluorescence intensity from the interfacial region is also modulated at the frequency of the potential modulation. The ac modulated fluorescence, PMF signal, associates with two interfacial processes: quasi-reversible ion transfer process and adsorption at the interface. The PMF response associated with the quasi-reversible ion transfer (ΔF_t) in a TIR mode is proportional to ac faradic current ($i_{f,ac}$) given by following equation.

$$\Delta F_t = \frac{4.606\varepsilon\Phi_f I_0}{j\omega zFS\cos\psi_i} i_{f,ac} \qquad (3\text{-}10)$$

where ε, Φ_f and I_0 are the molar absorption coefficient, the fluorescence quantum yield and the excitation photon flux, respectively. S is the illuminated interfacial area. Equation (3-10) can be separated to the real ($\Delta F_{t,\,re}$) and imaginary ($\Delta F_{t,\,im}$) part.[5] In the case of cationic species, the frequency dependence of $\Delta F_{t,\,re}$ and $\Delta F_{t,\,im}$ for the ion transfer process appears in fourth quadrant in complex plane, where $\Delta F_{t,\,re}$ and $\Delta F_{t,\,im}$ are almost same value with each other although it depends on the kinetics of the ion transfer process.

Assuming that the interactions between species adsorbed at the interface are negligible, the adsorption process is described by the Langmuir-type adsorption isotherm (cf. Section 1-1). Then, PMF response for the adsorption of fluorescent ion from the aqueous phase is given by following equation as a function of the ac modulated surface coverage (θ_{ac}).

$$\Delta F_a = 2.303\varepsilon\Phi_f I_0 \Gamma_s S\theta_{ac} \tag{3-11}$$

where

$$\theta_{ac} = \frac{bzF\Delta_o^w\phi_{ac}}{RT}\left[\frac{k_{a,dc}\alpha c_0(1-\theta_{dc}) - k_{d,dc}(\alpha-1)\theta_{dc}}{k_{a,dc}c_{dc} + k_{d,dc} + j\omega}\right] \tag{3-12}$$

And Γ_s is the saturated interfacial concentration. α is overall transfer coefficient for adsorption process. c_0 is the bulk concentration, θ_{dc} is the dc surface coverage, and $k_{a,dc}$ and $k_{d,dc}$ are the dc components of the adsorption and desorption rate constants at given potentials, respectively. Equation (3-11) can also be separated to the real and imaginary components.[5] The magnitude and ratio of the real and imaginary components of PMF response for the adsorption process depend on the frequency of potential modulation. The complex plane plot of PMF response for adsorption process shows semicircle in fourth quadrant ($\Delta F_{re} > 0$ and $\Delta F_{im} < 0$). The frequency analysis of PMF provides us kinetic parameters for interfacial processes such as rate constants for adsorption and ion transfer of the ionic species. In the case of adsorption process from the organic phase, the PMF signal should show the reversed sign because the dependence of the surface coverage on the potential is opposite to the case of the adsorption process from the aqueous phase.

3-5. Quasi Elastic Laser Scattering (QELS) Technique

QELS technique has been employed to measure the interfacial tension at liquid|liquid interfaces.[47-52] The thermal fluctuation (capillary wave) is spontaneously generated at a liquid|liquid interface. When the laser beam passes through a diffraction grating and the interface perpendicularly, the incident beam is diffracted on the grating and scattered by the capillary waves (**Figure 3-6**).[47-52] Assuming that the scattered angle (θ_{scat}) is sufficiently small, the θ_{scat} is given by the following equation.[51, 52]

$$K = k \sin \theta_{scat} \qquad (3\text{-}13)$$

K and k are the wavenumbers of the incident beam and the capillary wave, respectively. The θ_{scat} is also associated with the order of the diffraction spot (n).

$$n\lambda = d \sin \theta_{scat}, \qquad (3\text{-}14)$$

where λ_L is the wavelength of the incident beam. From the eqs. (3-13) and (3-14), the k value is obtained as

$$k = \frac{2\pi n}{d} \qquad (3\text{-}15)$$

The frequency of the incident beam is shifted as $f_L \pm f_0$, where f_0 is the frequency of capillary wave. The interfacial tension (γ_i) can be calculated from the frequency of maximum intensity associated with the mean frequency of the capillary waves, which is given by Lamb's equation.[47-50]

$$f_0 = \frac{1}{2\pi} \sqrt{\frac{\gamma_i k^3}{\rho^w + \rho^{org}}} \qquad (3\text{-}16)$$

where ρ^w and ρ^{DCE} are the density of water (0.9970 g cm^{-3}) and DCE (1.246 g cm^{-3}), respectively. The k value can be selected by choosing the diffraction spot.

The electrocapillary curves at 298 ± 2 K were measured at the polarized water|DCE interface by QELS. A cylindrical glass cell with a geometrical interfacial area of 15.9 cm^2 was used in the interfacial tension measurements with the same cell composition displayed in **Figure 3-2 (Cell**

III and **IV)**. A cw laser at 660 nm (Coherent, CUBE 660-60C) passed through the interface perpendicularly from the bottom of a cylindrical glass cell. The diffraction grating with a line spacing of 0.320 mm was placed after the water|DCE interface. The optical beat of third-order diffraction spot was detected by a Si photodiode (Hamamatsu Photonics, S1133-01) with a wide bandwidth amplifier (Melles Griot, 13AMP005). The power spectra of the diffraction spot were obtained by using a fast-Fourier transform analyzer (Stanford Research Systems, SR770). The effective value of k was estimated as 552.4 cm^{-1} by taking the value of the interfacial tension of the neat water|DCE interface as 28.5 m N m^{-1}.[48, 49]

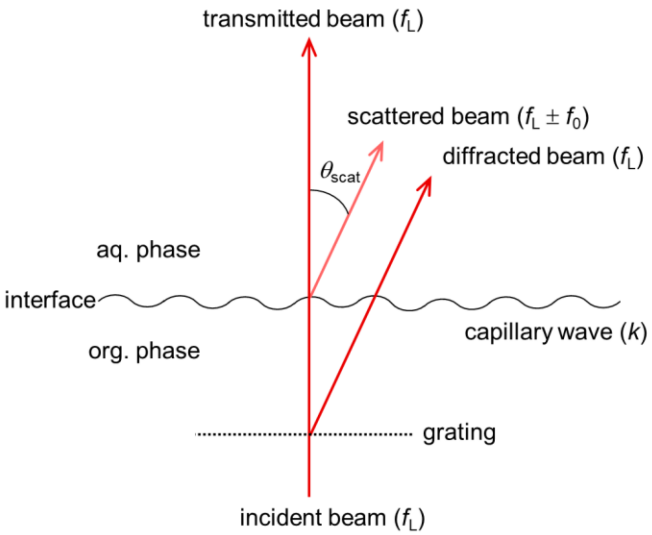

Figure 3-6. Schematic drawing of QELS.

3-6. Absorption and Fluorescence Measurements

The UV-Vis absorption spectra of fluorescent species in the aqueous solution were measured by UV-Vis spectrophotometer (JASCO, V-630). The optical path was 1.0 mm. The fluorescence spectra were measured as the similar manner in PM-TIRF measurements. Simply, the sample in the cuvette with the optical path of 1.0 cm was irradiated with a cw laser diode at 376 nm (Coherent, OBIS 375LS-50), 404 nm (Coherent, CUBE 405-50C) or 488 nm (Coherent, OBIS 488LS-60). The laser radiation was attenuated to 25 mW to avoid the photobleaching of fluorescent species. The fluorescence was corrected from the bottom of the cuvette by an optical fiber fitted to a photomultiplier tube (PMT) through a monochromator (Shimadzu, SPG-120S). The fluorescence spectra in the organic solution were measured for the species partitioned into the DCE solution after the electrochemical measurements.

4. RESULTS AND DISCUSSION

4-1 Potential-Dependent Adsorption and Orientation of *Meso*-Substituted Porphyrins at the Water|1,2-Dichloroethane Interface

4-1-1. Introduction

The interfacial processes of several porphyrin derivatives have been investigated by PMF spectroscopy.[11, 25, 27, 53, 54] For instance, the characterization of the interfacial species has been achieved for *meso*-tetrakis(*N*-methylpyridyl)porphyrin (H_2TMPyP^{4+}) and *meso*-tetrakis(4-sulfonatophenyl)porphyrin (H_2TPPS^{4-}) systems,[25] where PMF technique demonstrated the specific solvation structure of interfacial species modified from both aqueous and organic bulk species. Although the detailed PMF analysis elucidated the dynamic behavior of monomeric ions such as ion transfer and adsorption processes, the characterization of interfacial species was available within limited experimental conditions since a large change in molecular emission property caused by molecular aggregation and ion-association complicate the signal analysis.

PM-TIRF spectroscopy was applied to *meso*-substituted water-soluble porphyrins, 5,10,15,20-tetrakis(*N*-methylpyridyl)porphyrin (H_2TMPyP^{4+}) and 5,10,15,20-tetrakis(4-sulfonatophenyl)porphyrin (H_2TPPS^{4-}). In Section 4-1, the potential-dependent adsorption and orientation behavior of H_2TMPyP^{4+} and H_2TPPS^{4-} at the water|DCE interface are discussed in detail. Potential dependence of the molecular orientation of the interfacial species are estimated from PM-TIRF analysis. In addition, the wavelength dependence of PM-TIRF signal, "PM-TIRF spectrum", indicates specific solvation and adsorption states of the porphyrins at the water|DCE interface.

4-1-2. Ion Transfer of Porphyrins across the Water|DCE Interface.

Figure 4-1-1 shows cyclic voltammograms (CVs) measured in the presence of 2.0×10^{-5} mol dm^{-3} H_2TMPyP^{4+} and H_2TPPS^{4-} under neutral conditions (**Cell I**, **Figure 3-1**), where both porphyrins exist as the free base form in the aqueous solution. The well-defined voltammetric responses were observed in each system. In **Figure 4-1-1a**, the positive and negative current peaks obtained for H_2TMPyP^{4+} correspond to the diffusion controlled ion transfer of tetracationic species from water to DCE and that of the reverse process across the interface, respectively, since the peak currents exhibited a linear relationship with square root of potential sweep rate. The formal ion transfer potential of H_2TMPyP^{4+} was determined as $\Delta_o^w\phi^{o'}_{H^2TMPyP^{4+}} = 0.07$ V. The current increases at the negative edge of potential window is attributed to the ion transfer of tosylate anions ($\Delta_o^w\phi^{o'}_{tosylate} = -0.28$ V) as a counter ion of H_2TMPyP^{4+}.[55] The ion transfer responses of H_2TPPS^{4-} were obtained at $\Delta_o^w\phi^{o'}_{H_2TPPS^{4-}} = -0.20$ V (**Figure 4-1-1b**). In addition, the broad positive current responses at $0.20\,\text{V} < \Delta_o^w\phi < 0.30\,\text{V}$ and the gradual increase of currents

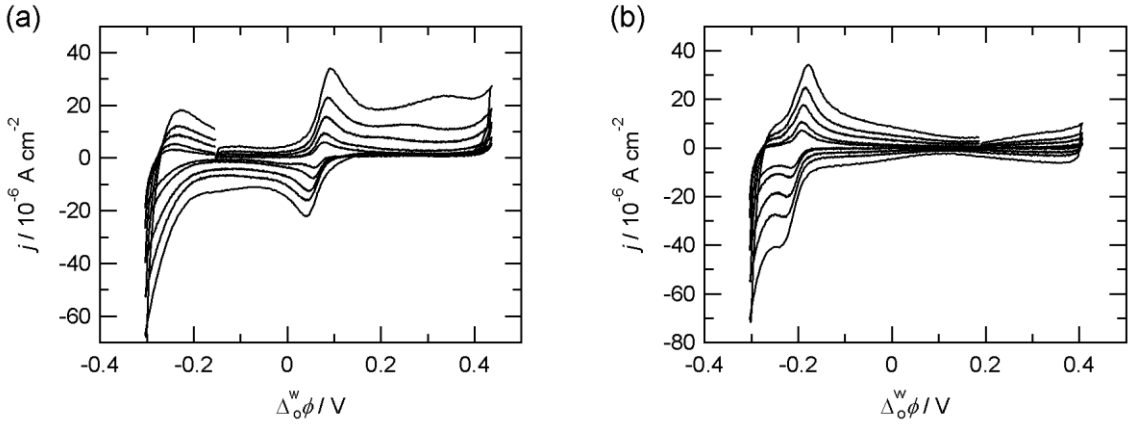

Figure 4-1-1. Typical cyclic voltammograms measured for (a) H_2TMPyP^{4+} and (b) H_2TPPS^{4-} at the water|DCE interface. The potential sweep rates were 10, 20, 50, 100 and 200 mV s^{-1}. The concentration of porphyrin derivatives in the aqueous phase was 2.0×10^{-5} mol dm^{-3}. The pH values of the aqueous phase were (a) pH 7.1 and (b) pH 6.9, respectively.

prior to the ion transfer ($\Delta_o^w\phi < 0.10$ V) were observed for H_2TMPyP^{4+} and H_2TPPS^{4-}, respectively. These increases is associated with the adsorption of the porphyrins at the water|DCE interface.[25] In ac voltammetry, the well-defined ion transfer responses of H_2TMPyP^{4+} and H_2TPPS^{4-} were obtained around at 0.07 V and –0.20 V, respectively (**Figure 4-1-2**). In **Figure 4-1-2a**, the increase in the real (Y_{re}) and imaginary (Y_{im}) components of the admittance was also observed at $\Delta_o^w\phi < -0.20$ V due to the ion transfer of tosylate anion. In the H_2TPPS^{4-} system, Y_{re} and Y_{im} were considerably increased particularly at $\Delta_o^w\phi^{o'}_{H_2TPPS^{4-}} (= -0.20\ \text{V}) < \Delta_o^w\phi$ (**Figure 4-1-2b**). These results indicate that H_2TPPS^{4-} is preferably adsorbed at the interface in comparison with H_2TMPyP^{4+}.

The PMF responses of H_2TMPyP^{4+} and H_2TPPS^{4-} were in good agreement with the previous report (**Figure 4-1-3**).[25] PMF signals were measured by p- and s-polarized beams. The magnitude of PMF signal for adsorption process is affected by the molecular orientation of fluorescent ions.[24] In H_2TMPyP^{4+} system (**Figure 4-1-3a**), the PMF response with negative ΔF_{re} and positive ΔF_{im} was observed around at 0.07 V, which is associated with ion transfer process

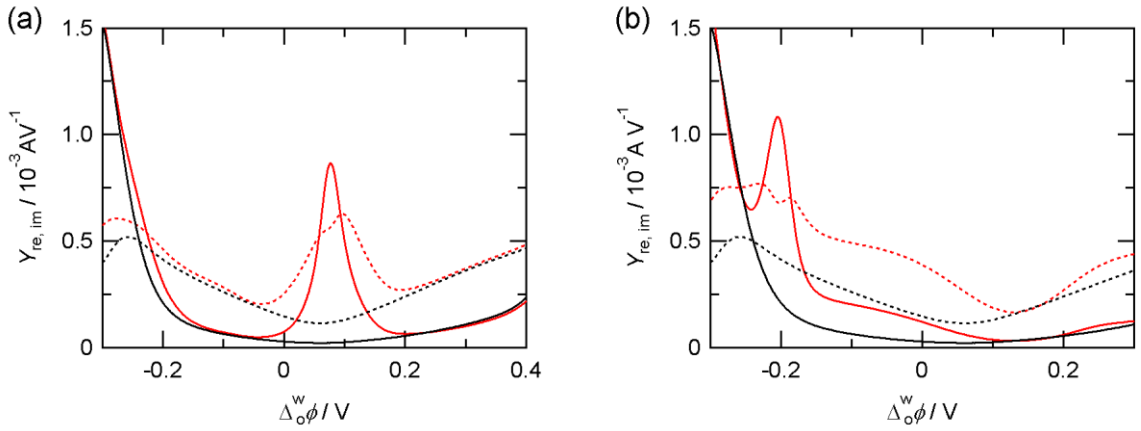

Figure 4-1-2. Real (solid line) and imaginary (dashed line) components of the admittance measured for (a) H_2TMPyP^{4+} and (b) H_2TPPS^{4-} at the water|DCE interface. The black lines depict the admittances in the absence of the porphyrin. The potential modulation was 10 mV at 7 Hz. The pH values of the aqueous phase were (a) pH 7.1 and (b) pH 6.9, respectively.

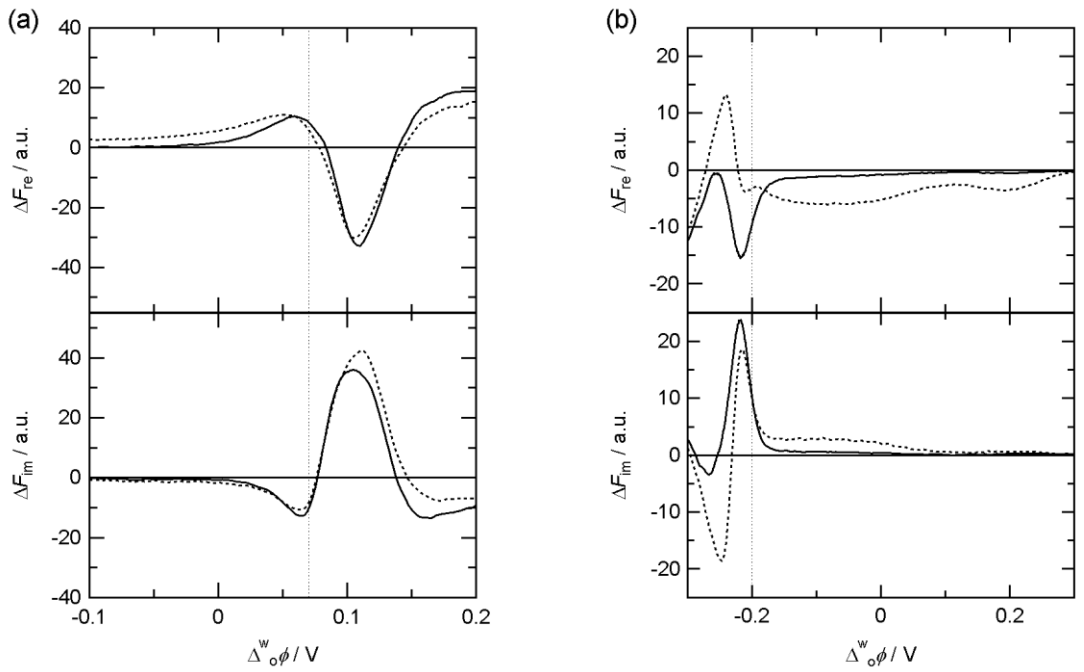

Figure 4-1-3. Potential dependence of PMF responses measured for (a) H_2TMPyP^{4+} and (b) H_2TPPS^{4-} at the water|DCE interface. The solid and dotted lines show the PMF responses measured by p- and s-polarized light, respectively. The potential sweep rate was 5 mV s^{-1}. The potential modulation was 10 mV at 3 Hz. The fluorescence intensity was detected at (a) 660 and (b) 649 nm. The vertical dotted lines depict (a) $\Delta^{w}_{o}\phi^{o'}_{H_2TMPyP^{4+}} = 0.07$ V and (b) $\Delta^{w}_{o}\phi^{o'}_{H_2TPPS^{4-}} = -0.20$ V.

of H_2TMPyP^{4+}. In addition, the phase shift in ΔF_{re} and ΔF_{im} was observed around at $0.10\,\mathrm{V} < \Delta^{w}_{o}\phi < 0.15\,\mathrm{V}$. This phase shift is associated with the adsorption process of H_2TMPyP^{4+} from the organic side of the interface. In the case of anionic species, PMF signal should be expressed as $\Delta F_{re} < 0$ and $\Delta F_{im} > 0$ for ion transfer or adsorption processes from the aqueous phase, while PMF response with the reversed sign, $\Delta F_{re} > 0$ and $\Delta F_{im} < 0$, should be interpreted as the adsorption from the organic phase (cf. **section 3-4**). As shown in **Figure 4-1-3b**, the PMF response of H_2TPPS^{4-} was significantly affected by the polarization of the incident beam. The PMF responses with $\Delta F_{re} > 0$ and $\Delta F_{im} < 0$ were observed at $-0.20\,\mathrm{V} < \Delta^{w}_{o}\phi < 0.10\,\mathrm{V}$, which is

associated with the adsorption of H_2TPPS^{4-} at the aqueous side of the interface. These PMF responses were enhanced under the s-polarized excitation. The polarization dependence of the PMF response for adsorption process suggests that H_2TPPS^{4-} is lying at the interface (cf. Chapter 2). In addition, a sharp PMF response with $\Delta F_{re} < 0$ and $\Delta F_{im} > 0$ was observed at –0.22 V by using p-polarized beam. This PMF response is attributed to the ion transfer of H_2TPPS^{4-}.[25] However, the PMF response for the ion transfer process of H_2TPPS^{4-} was overlapped with that for adsorption process at the organic side of the interface at $-0.30\,\mathrm{V} < \Delta_o^w\phi < -0.20\,\mathrm{V}$. Thus, the sharp PMF response for the adsorption with large $\Delta F_{re} > 0$ and $\Delta F_{im} < 0$ was observed by s-polarized beam, indicating H_2TPPS^{4-} adsorbed with lying orientation.

4-1-3. Potential Dependence of Molecular Orientation of Porphyrins at the Water|DCE Interface

The PM-TIRF spectroscopy was employed to study the potential dependent adsorption behavior of the porphyrins in detail. **Figures 4-1-4a** shows the potential dependences of PM-TIRF signal ($\Delta F^{p\text{-}s}$) measured in the H_2TMPyP^{4+} system. The PM-TIRF response was recorded at 660 nm for H_2TMPyP^{4+}, where these porphyrins emit relatively strong fluorescence in both aqueous and organic solutions under present excitation conditions. In principle, the PM-TIRF signal is observed only from the species adsorbed at the interface with a certain orientation. (cf. PM-TIRF signal measured for tris(2,2′-bipyridine)ruthenium(II) ($Ru(bpy)_3^{2+}$) in **Appendix**) The nonzero $\Delta F^{p\text{-}s}$ values are, therefore, indicative of a selective detection of the species oriented at the interface. The potential dependence of $\Delta F^{p\text{-}s}$ is useful in evaluating the molecular orientation of the interfacial species as a function of $\Delta_o^w\phi$. As shown in **Figure 4-1-4a**, the negative PM-TIRF signals, $\Delta F^{p\text{-}s} < 0$, were observed over the potential window, suggesting that H_2TMPyP^{4+} were adsorbed with relatively lying orientations at the polarized water|DCE interface. For the π–π^* transition in porphyrin systems, the two absorption and respective emission transition

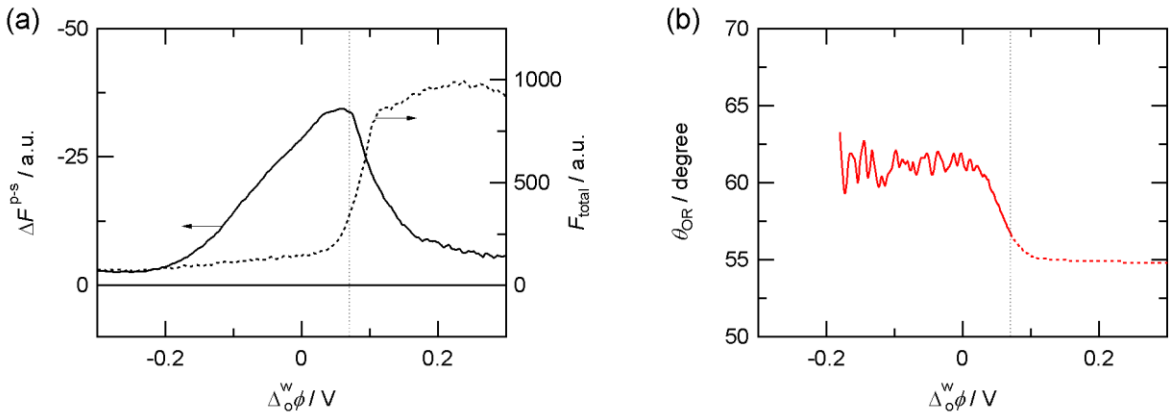

Figure 4-1-4. The potential dependence of (a) PM-TIRF responses (ΔF^{p-s}) (solid) and F_{total} (dashed) and (b) the orientation angles (θ_{OR}) estimated from eqs. 4-1, 4-3 and 4-4 for H_2TMPyP^{4+} system. The potential sweep rate was 5 mV s^{-1}. The fluorescence intensity was detected at 660 nm. The vertical dotted lines depict $\Delta_o^w\phi^{\circ'}_{H_2TMPyP^{4+}} = 0.07$ V .

dipole moments are perpendicular to each other and parallel to the porphyrin ring (in plane).[56, 57] Hence, the orientation of a molecule is considered as equal to that of a porphyrin ring. The average orientation angle (θ_{OR}) of interfacial species can be expressed by eq. 2-1 with a monodispersed distribution of θ_{OR}. To cancel the proportional factor C in eq. 2-1, the θ_{OR} value is determined by the ratio of $F(90°)$ to $F(0°)$

$$\frac{F(90^\circ)}{F(0^\circ)} = \frac{\sin^2\theta_{OR}}{\cos^2\psi_i \sin^2\theta_{OR} + 2\sin^2\psi_i \cos^2\theta_{OR}} \qquad (4\text{-}1)$$

The individual magnitudes of $F(90°)$ and $F(0°)$ were estimated from eq. 3-8 and total fluorescence intensity (F_{total}). F_{total} includes the fluorescence emitted from all species existing in the interfacial region and bulk solutions.

$$F_{total} = \frac{1}{2}\left(F_m^p + F_m^s\right) + F_{bulk} = \frac{P_m}{2}\left(F(0^\circ) + F(90^\circ)\right) + F_{bulk} \qquad (4\text{-}2)$$

where the F_{bulk} term arises from only the randomly oriented bulk solution species in the evanescent wave region at the aqueous side of the interface and on the optical path of the

excitation beam in the organic phase. The F_{total} value was measured as the mean value of fluorescence intensities obtained by p- and s-polarized excitation beams at a given potential (**Figure 4-1-4a**, dashed line). Then, $F(0°)$ and $F(90°)$ for the molecules adsorbed at the interface are expressed by the following equations derived from eqs. 3-8 and 4-2.

$$F(0°) = \frac{1}{P_{\mathrm{m}}}(F_{\mathrm{total}} - F_{\mathrm{bulk}}) + \frac{1}{4P_{\mathrm{m}} - 2}\Delta F^{\mathrm{p\text{-}s}} \tag{4-3}$$

$$F(90°) = \frac{1}{P_{\mathrm{m}}}(F_{\mathrm{total}} - F_{\mathrm{bulk}}) - \frac{1}{4P_{\mathrm{m}} - 2}\Delta F^{\mathrm{p\text{-}s}} \tag{4-4}$$

The F_{bulk} value was roughly estimated from F_{total} at –0.30 V for H_2TMPyP^{4+}, where the interfacial adsorption and distribution into the organic phase are negligibly small. $F(0°)$ and $F(90°)$ in the absence of the distribution of species into the organic phase can be calculated by eqs. 4-3 and 4-4 with F_{total}, $\Delta F^{\mathrm{p-s}}$ and estimated F_{bulk} values.

The average orientation angle of H_2TMPyP^{4+} estimated from eqs. 4-1, 4-3 and 4-4 is shown in **Figure 4-1-4b**. The θ_{OR} values at $-0.18\ \mathrm{V} \le \Delta_{\mathrm{o}}^{\mathrm{w}}\phi \le 0\ \mathrm{V}$ were almost constant at $61 \pm 1°$. The magnitude of $\Delta F^{\mathrm{p-s}}$ is proportional to the interfacial concentration, when the θ_{OR} value is constant. Thus, a gradual increase of $-\Delta F^{\mathrm{p-s}}$ at $\Delta_{\mathrm{o}}^{\mathrm{w}}\phi < \Delta_{\mathrm{o}}^{\mathrm{w}}\phi^{\circ'}_{\mathrm{H_2TMPYP^{4+}}}$ associates with the increase of the interfacial concentration of H_2TMPyP^{4+} depending on the potential. On the other hand, the drastic decrease of $-\Delta F^{\mathrm{p-s}}$ at $\Delta_{\mathrm{o}}^{\mathrm{w}}\phi^{\circ'}_{\mathrm{H_2TMPYP^{4+}}} < \Delta_{\mathrm{o}}^{\mathrm{w}}\phi$ results from the ion transfer of H_2TMPyP^{4+} into the organic phase. The interfacial concentration of ionic species is significantly affected by $\Delta_{\mathrm{o}}^{\mathrm{w}}\phi$ and maximized around $\Delta_{\mathrm{o}}^{\mathrm{w}}\phi^{\circ\prime}$ as expected from simple adsorption models.[11, 58, 59] The potential dependence of PM-TIRF intensity observed in the present work agreed with those theoretical models. Although the small negative $\Delta F^{\mathrm{p-s}}$ values at $0.15\ \mathrm{V} < \Delta_{\mathrm{o}}^{\mathrm{w}}\phi$ may indicate the adsorption of H_2TMPyP^{4+} with a relatively lying orientation at the interface, the θ_{OR} value could not be estimated quantitatively because of large F_{total} values arising from H_2TMPyP^{4+} partitioned into the bulk organic phase. Indeed, the significant increase of F_{total} (cf **Figure 4-1-4a**), which is

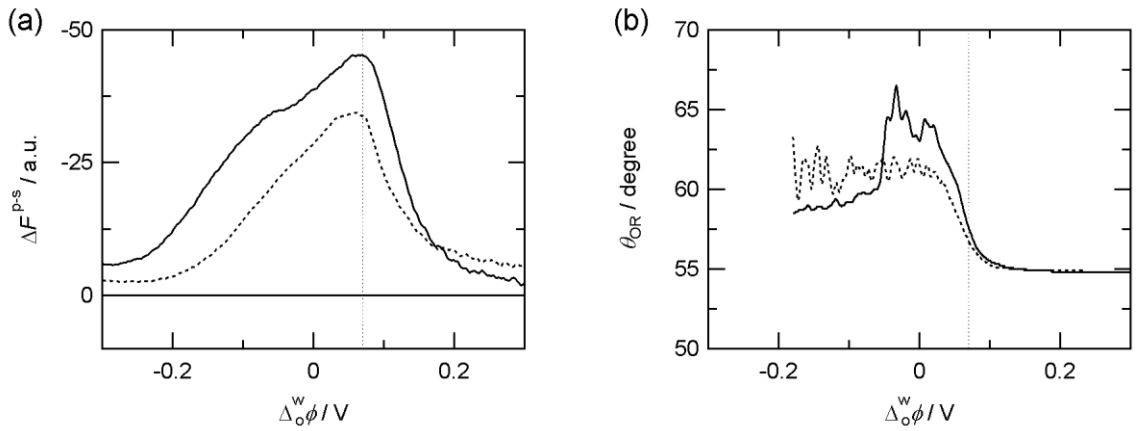

Figure 4-1-5. Potential dependences of (a) PM-TIRF ($\Delta F^{p\text{-}s}$) and (b) orientation angle (θ_{OR}) estimated for H_2TMPyP^{4+} in the presence of Span 20 (**Cell II**). The solid and dashed lines relate to the H_2TMPyP^{4+} systems in the presence and absence of 1.0×10^{-3} mol dm^{-3} Span 20 in the organic phase. The excitation and detected emission wavelengths were 404 nm and 660 nm, respectively. The vertical dotted lines denote the ion transfer potential of H_2TMPyP^{4+} ($\Delta_o^w\phi^{o'}_{H_2TMPyP^{4+}} = 0.07$ V).

mainly correlated to the fluorescence from the bulk organic species on the optical path, was observed at corresponding potentials.

The PM-TIRF responses of H_2TMPyP^{4+} were slightly changed in the presence of nonionic surfactant, Span 20 (**Cell II**, **Figure 3-1**). Span 20 is commonly used as a stabilizer for the electrochemical measurements in the liquid|liquid system in order to minimize the convection of solutions in the vicinity of the interface.[25, 26] **Figure 4-1-5** shows the potential dependence of $\Delta F^{p\text{-}s}$ and θ_{OR} in the presence of Span 20. The $\Delta F^{p\text{-}s}$ value was maximized around $\Delta_o^w\phi^{o'}$ and then approached zero at $0.20\text{ V} < \Delta_o^w\phi$. The smaller θ_{OR} values were estimated at $\Delta_o^w\phi \leq -0.05$ V ($\theta_{OR} = 59 \pm 0.3°$), while those in the presence of Span 20 were $\theta_{OR} = 65 \pm 1.7°$ at $-0.05\text{ V} \leq \Delta_o^w\phi \leq 0.05$ V (**Figure 4-1-5b**), indicating that the addition of nonionic stabilizer certainly affects the adsorption state of ionic analyte molecules at the interface.

The PM-TIRF signals measured in the H_2TPPS^{4-} system (**Figure 4-1-6**) were analyzed in the same manner as described above. The PM-TIRF response was recorded at 649 nm for H_2TPPS^{4-}. The F_{bulk} value was estimated from F_{total} at 0.41 V for H_2TPPS^{4-}. The nonzero $\Delta F^{p\text{-}s}$ was clearly observed even at 0.3 V which was 0.5 V more positive potential than $\Delta_o^w\phi^{o'}_{H_2TPPS^{4-}}$, indicating the high affinity to the water|DCE interface (**Figure 4-1-6a**). The θ_{OR} values for H_2TPPS^{4-} at $-0.10\ \text{V} \le \Delta_o^w\phi \le 0.35\ \text{V}$ were approximately constant at $65 \pm 1°$ (**Figure 4-1-6b**). The negative magnitude of $\Delta F^{p\text{-}s}$ value was remarkably decreased at $\Delta_o^w\phi < \Delta_o^w\phi^{o'}_{H_2TPPS^{4-}}$ and almost zero around −0.30 V. These results indicated that H_2TPPS^{4-} is adsorbed mainly from the aqueous side of the interface prior to the formal ion transfer potential.

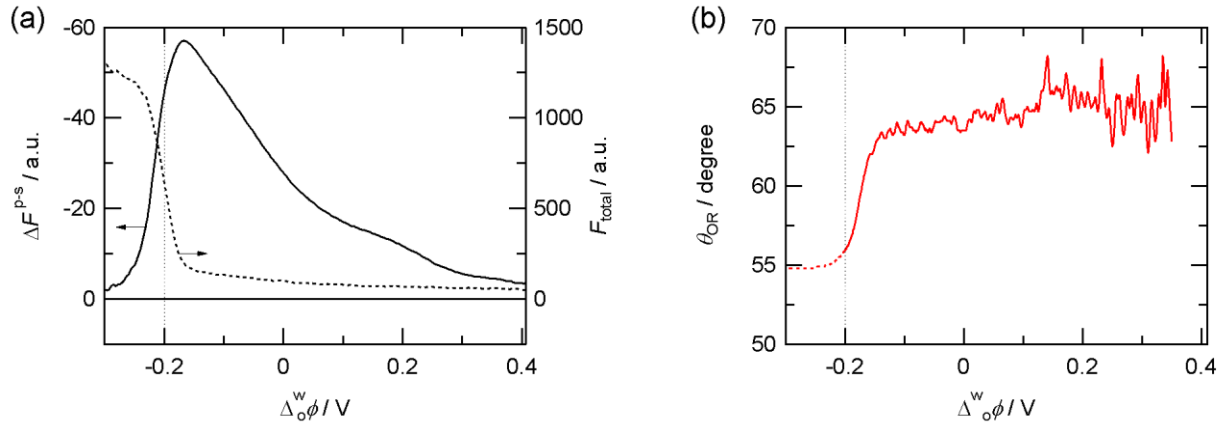

Figure 4-1-6. The potential dependence of (a) PM-TIRF responses ($\Delta F^{p\text{-}s}$) (solid) and F_{total} (dashed) and (b) the orientation angles (θ_{OR}) estimated from eqs. 4-1, 4-3 and 4-4 for H_2TPPS^{4-} system. The potential sweep rate was 5 mV s^{-1}. The fluorescence intensity was detected at 649 nm. The vertical dotted lines depict $\Delta_o^w\phi^{o'}_{H_2TPPS^{4-}} = -0.20\ \text{V}$.

4-1-4. Adsorption States of Porphyrins at the Water|DCE Interface

PM-TIRF spectrum was measured in order to characterize the adsorption state of the porphyrin species at the polarized water|DCE interface. Since PM-TIRF signals result from only the fluorescent dyes with a certain orientation, spectral contributions of randomly oriented species are negligible. The PM-TIRF spectrum is, thus, considered a "pure" emission spectrum of interfacial species oriented at the interface. **Figure 4-1-7** shows the PM-TIRF spectra for H_2TMPyP^{4+} in the absence and presence of Span20 under potentiostatic control. The fluorescence maximum wavelengths (λ_{max}) and peak intensity ratios of the first and second peaks (R_F) of PM-TIRF spectra are summarized in **Table 4-1-1**.

The PM-TIRF spectra in the H_2TMPyP^{4+} system were measured at –0.27 V, –0.15 V and 0.19 V, respectively (**Figure 4-1-7a**). The spectral shape and fluorescence maxima of the PM-TIRF spectra at –0.27 V and 0.19 V were similar to those of the fluorescence spectra measured in the aqueous and organic solutions, respectively. Taking into account $\Delta_o^w\phi^{o'}_{H_2TMPyP^{4+}}$ (= 0.07 V),

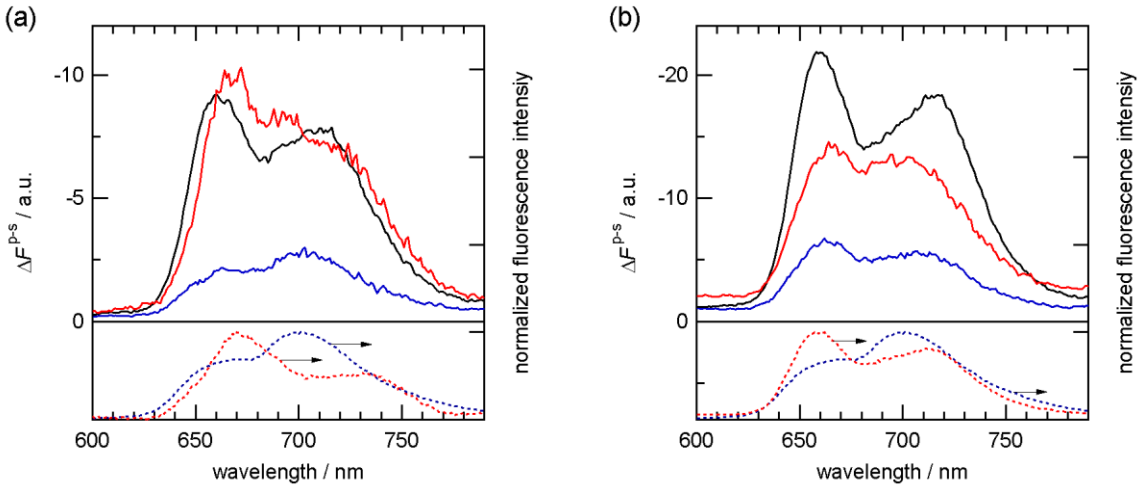

Figure 4-1-7. PM-TIRF spectra for H_2TMPyP^{4+} at the water|DCE interface in the (a) absence and (b) presence of Span 20 (**Cell II**) The blue, black and red solid lines depict PM-TIRF spectra at −0.27 V, −0.15 V and 0.19 V, respectively. The blue and red dashed lines refer to normalized fluorescence spectra measured in the aqueous and organic solutions.

Table 4-1-1. Fluorescence maximum wavelengths (λ_{max}) and peak ratios (R_F) of H_2TMPyP^{4+} and H_2TMPyP^{4+} with Span20 at the water|DCE interface and in solution.

	H_2TMPyP^{4+} system			H_2TMPyP^{4+}–Span20 system		
	$\Delta_o^w\phi$ / V	λ_{max} / nm	R_F[a]	$\Delta_o^w\phi$ / V	λ_{max} / nm	R_F[a]
interface	–0.27	660, 702	0.76	−0.27	662, 708	1.2
	–0.15	660, 710	1.2	−0.15	660, 714	1.3
	0.19	668, 720	1.4	0.19	663, 704	1.1
aqueous phase[b]		660, 702	0.69		660, 702	0.69
organic phase[b]		670, 727	1.6		659, 712	1.2

[a]The peak intensity ratio of the first and second fluorescence peaks. [b]The fluorescence maximum wavelengths measured in the aqueous and organic solutions.

H_2TMPyP^{4+} is stably located in the aqueous phase at –0.27 V, while it is transferred into the organic phase across the interface at 0.19 V. Therefore, the PM-TIRF spectra measured at –0.27 V and 0.19 V associate with H_2TMPyP^{4+} adsorbed at the aqueous and organic sides of the interface. The comparable spectral features of PM-TIRF spectra with relevant bulk spectra exhibit similar solvation states of interfacial species and bulk solution species. On the other hand, the PM-TIRF spectrum measured at –0.15 V was slightly modified from the bulk aqueous spectrum in spite of $\Delta_o^w\phi < \Delta_o^w\phi^{o'}_{H_2TMPyP^{4+}}$. The PM-TIRF maxima were found at around 660 nm and 710 nm at –0.15 V and the peak ratio indicated intermediate value between those of the bulk aqueous and organic spectra. It is reported that the spectral shape and fluorescence maxima of H_2TMPyP^{4+} dissolved in various solvents are affected by polarity of solvents.[60] It has been demonstrated that the solvatochromic dye species located in the interfacial region are influenced from the aqueous and organic solvents, where the spectral features often indicate specific solvation at the interface.[2, 5, 61-65] It has been reported that the spectral shifts of adsorbed species were observed for the free base and zinc(II) porphyrins at polarized water|DCE interfaces

through SSHG and PMF techniques.[25, 49, 55] The potential-dependence of the interfacial species has, however, rarely been studied in detail because of relatively long data acquisition time, e.g., a few hours per spectrum in SHG, and unfavorable contributions from the ion transfer responses in PMF. The spectral features at –0.15 V measured in the present study could be associated with an intermediate solvation structure of H_2TMPyP^{4+} adsorbed at the interface.

As shown in **Figure 4-1-7b**, the PM-TIRF spectrum measured at –0.15 V in the presence of Span20 was identical to the bulk organic spectrum as well as H_2TMPyP^{4+} in the absence of Span20. The change in the spectral features from the bulk aqueous species was also observed even at –0.27 V, suggesting that Span 20 interacts with H_2TMPyP^{4+} at the interface (**Figure 4-1-7** and **Table 4-1-1**). The PM-TIRF spectra similar to the bulk organic spectrum over the measurable potential region ($-0.27\,\mathrm{V} \le \Delta_o^w\phi \le 0.19\,\mathrm{V}$) imply a dehydration of the porphyrin ring induced by sorbitan moiety of Span 20 penetrated into the aqueous side of the interface (**Figure 4-1-8**).

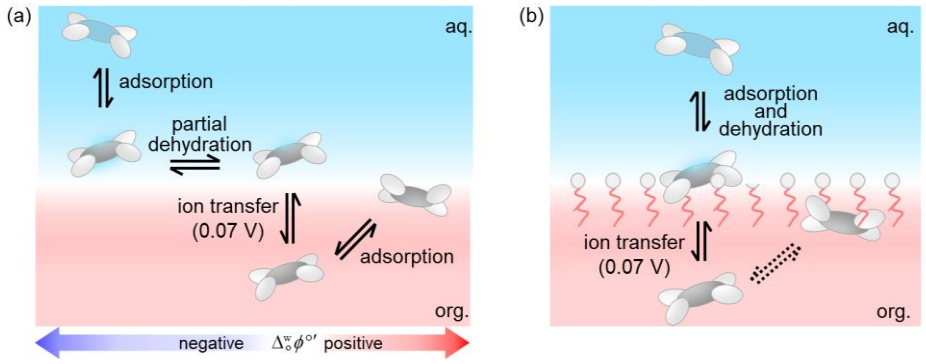

Figure 4-1-8. Schematic representation of (a) the interfacial behavior of H_2TMPyP^{4+} at the water|DCE interface and (b) the interaction of H_2TMPyP^{4+} with Span20 at the water|DCE interface.

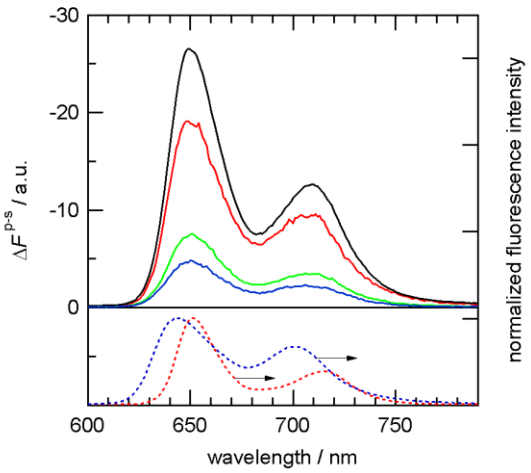

Figure 4-1-9. Potential dependent PM-TIRF spectra for H_2TPPS^{4-} at the water|DCE interface. The blue, green, black and red solid lines depict PM-TIRF spectra at 0.31 V, 0.20 V, −0.10 V and −0.21 V, respectively. The blue and red dashed lines refer to normalized fluorescence spectra measured in the aqueous and organic solutions.

In the H_2TPPS^{4-} system, the PM-TIRF spectra were almost consistent with the bulk organic spectrum at $-0.21\mathrm{V} \le \Delta_o^w\phi \le 0.31\mathrm{V}$ (**Figure 4-1-9** and **Table 4-1-2**), whereas the anionic H_2TPPS^{4-} species should exist stably in the aqueous phase at $\Delta_o^w\phi^{o'}_{H_2TPPS^{4-}} < \Delta_o^w\phi$. It should be noted that the PM-TIRF intensity at given potentials in **Figure 4-1-9** showed essentially the same potential dependence as **Figure 4-1-6a**. The PM-TIRF spectra measured for H_2TPPS^{4-} under potentiostatic control indicate that H_2TPPS^{4-} molecules are preferably dehydrated and solvated at the water|DCE interface and then the porphyrin ring could readily be oriented in plane of the interface (**Figure 4-1-10**).

In the PM-TIRF measurements, both the molecular orientation and spectral feature of the interfacial species are investigated without controversial interference from the bulk solution species. The PMF spectroscopy applied to a variety of dye species provide valuable information about potential-driven transfer and adsorption dynamics in the interfacial region. Although the

orientation parameter and spectral characterization are attained by the PMF technique within limited conditions,[24-26, 66] the PM-TIRF technique shows a significant advantage in terms of the characterization of the species adsorbed at the liquid|liquid interface.

Table 4-1-2. Fluorescence maximum wavelengths (λ_{max}) of H_2TPPS^{4-} at the water|DCE interface.

	H_2TPPS^{4-} system		
	$\Delta_o^w\phi$ / V	λ_{max} / nm	R_F[a]
interface	0.31	650, 707	2.1
	0.20	650, 708	2.2
	−0.10	649, 709	2.1
	−0.21	649, 709	2.1
aqueous phase[b]		644, 701	1.5
organic phase[b]		652, 715	2.5

[a]The peak intensity ratio of the first and second fluorescence peaks. [b]The fluorescence maximum wavelengths measured in the aqueous and organic solutions.

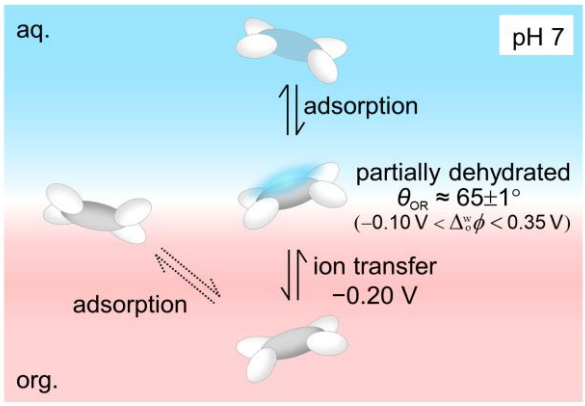

Figure 4-1-10. Schematic representation of the interfacial mechanism of H_2TPPS^{4-} at the water|DCE interface.

4-1-5. Conclusions

PM-TIRF spectroscopy was developed in this work and applied to study the adsorption behavior of *meso*-substituted water-soluble porphyrins at the polarized water|DCE interface. The potential dependences of the molecular orientation and adsorption state of interfacial species were successfully analyzed by PM-TIRF technique. The PM-TIRF response of centrosymmetric $Ru(bpy)_3^{2+}$ was independent of the fluorescence intensity from the bulk solutions and interfacial region, which supports that the PM-TIRF signal is observed only from the species oriented at the interface (cf. **Appendix**). The average orientation angles of H_2TMPyP^{4+} and H_2TPPS^{4-} at the aqueous side of the interface were estimated at $\theta_{OR} = 61 \pm 1°$ and $\theta_{OR} = 65 \pm 1°$, respectively. Furthermore, the PM-TIRF spectra clearly indicated that the free-base porphyrins are adsorbed with a modification of the solvation state at the water|DCE interface. The solvation states of H_2TMPyP^{4+} were also affected by Span 20. These results demonstrated that PM-TIRF spectroscopy is a highly sensitive and selective technique for fluorescent species oriented at a liquid|liquid interface and *in situ* characterization of interfacial species can be achieved without controversial contribution of bulk species. The principle and experimental setup of PM-TIRF spectroscopy is rather simple in comparison with other surface sensitive techniques such as nonlinear spectroscopy and polarized TR-XAFS. In addition, the optical setup for PM-TIRF spectroscopy is analogous to the PMF spectroscopy and the information obtained from both techniques are complementary to each other. Consequently, PM-TIRF spectroscopy allows us to access useful spectroscopic information of interfacial species at a molecular level.

4-2 Potential-Induced Aggregation of Anionic Porphyrins at the Water|1,2-dichloroethane Interface

4-2-1. Introduction

The protonated species of TPPS preferentially form self-aggregates in acidic solutions,[67-69] emulsions,[70, 71] and at liquid interfaces,[16, 72, 73] where the aggregation is significantly affected by the protonation of pyrrole nitrogens in a porphyrin ring as well as counter ions. It has been also reported that the aggregation equilibrium in aqueous solution could be controlled via electric field.[74] The effect of Galvani potential difference on the aggregation is, however, not elucidated at liquid|liquid interface. Protoporphyrin IX (H_2PP) is a direct precursor of heme and is one of the most important natural porphyrins.[75] H_2PP^{2-} also attracts much attention in supramolecular science, nanostructure assembly, energy and electron transfer systems on surfaces and at interfaces.[76] While H_2PP^{2-} has been examined at the water|DCE interface by PMF spectroscopy,[25] The interfacial mechanism of H_2PP^{2-} was hardly elucidated in detail because of its strong interfacial activity, which weakened potential-modulated signals. In this Section, the aggregation mechanisms of H_2TPPS^{4-} and H_2PP^{2-} are successfully analyzed as a function of Galvani potential difference at the water|1,2-dichloroethane interface by PM-TIRF spectroscopy. Furthermore, the adsorption behavior of H_2PP^{2-} at the phospholipid-adsorbed water|DCE interface is examined in order to evaluate its binding characteristics on cell membrane.

4-2-2. Acid-Base Equilibria of Anionic Porphyrins in Aqueous Solution

At lower pHs than pK_a of H_2TPPS^{4-} (pK_{a1} = 4.86, pK_{a2} = 4.96[77, 78]), the free base form (H_2TPPS^{4-}) is protonated and the diacid form (H_4TPPS^{2-}) is a dominant in the aqueous solution. **Figure 4-2-1** shows UV-Vis absorption and fluorescence spectra of TPPS species in the aqueous solution. H_2TPPS^{4-} and H_4TPPS^{2-} have the Soret band around at 413 and 434 nm, respectively. It is known that H_4TPPS^{2-} tends to form J-aggregates under lower pH conditions through a coulomb interaction between its diprotonated porphyrin ring and anionic sulfonatophenyl group.[79-82] The monomeric H_4TPPS^{2-} shows the Soret and Q bands at 434 nm and 645 nm in aqueous solution, respectively, whereas the J-aggregates of H_4TPPS^{2-} exhibit sharp and intense absorption bands at 491 nm and 707 nm (**Figure 4-2-1a**).[79-82] The fluorescence spectra were also red-shifted at pH 1.3 due to the J-aggregation. The fluorescence maximum of the J-aggregates was observed around at 713 nm under the excitation at 488 nm. These spectral shifts allow us to excite the monomer and J-aggregates selectively by using the appropriate excitation wavelength. **Figure 4-2-2** shows the fluorescence spectra of TPPS species transferred into DCE solution. The fluorescence maxima were observed at 651 and 715 nm in DCE, and thus TPPS species in DCE solution exist as the monomer of H_4TPPS^{2-}. No peak corresponding to J-aggregates was found in DCE solution even if the J-aggregate formed at the interface as discussed below. In the H_4TPPS^{2-} system, PM-TIRF measurement were performed by using two excitation wavelengths at 404 and 488 nm to investigate the adsorption behavior of the monomer and J-aggregates selectively.

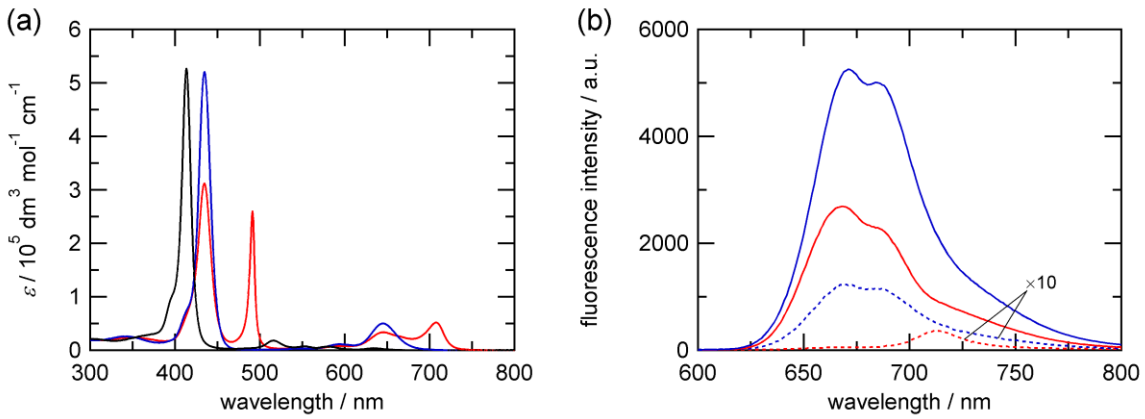

Figure 4-2-1. (a) UV-vis absorption and **(b)** fluorescence spectra measured for TPPS species in aqueous solution. The black, blue and red lines refer to pH 7.2, 2.3 and 1.3, respectively. The excitation wavelengths for the fluorescence measurement were 404 nm (solid line) and 488 nm (dotted line), respectively. The concentration of TPPS species and Li_2SO_4 were 1.0×10^{-5} mol dm^{-3} and 1.0×10^{-2} mol dm^{-3}. The pH condition was adjusted by adding adequate amounts of H_2SO_4 or phosphate buffer.

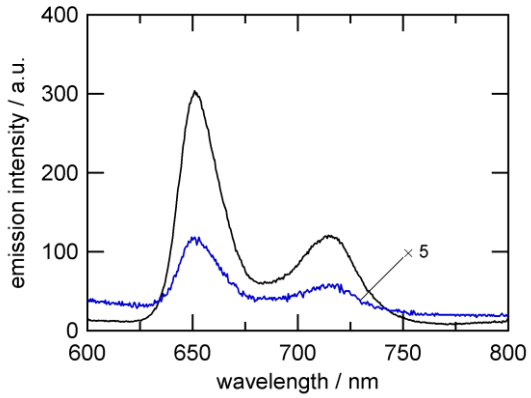

Figure 4-2-2. Fluorescence spectra measured for TPPS species in DCE after the electrochemical measurements for **Cell III**. The excitation light sources for the fluorescence measurement were cw laser diodes of 25 mW at 404 nm (black line) and 488 nm (blue line).

4-2-3. Electrochemical Responses of Anionic Porphyrins at the Water|DCE Interface.

CVs measured for H_4TPPS^{2-} at pH 2.1 (**Cell III**) and H_2PP^{2-} at pH 7.3 (**Cell IV**) are displayed in **Figure 4-2-3**. The positive and negative current peaks were observed around –0.25 V and the peak separation was ca. 16 mV corresponding to a diffusion-controlled transfer process of tetravalent ions (**Figure 4-2-3a**). These voltammetric responses are associated with the ion transfer of H_2TPPS^{4-} across the interface. The ion transfer mechanism of H_4TPPS^{2-} has been reported at the water|nitrobenzene interface,[83] where the deprotonated free base (H_2TPPS^{4-}) was dominant transferred species even under acidic conditions. The protonation of pyrrole nitrogens in a porphyrin ring enhances the hydrophilicity of H_4TPPS^{2-} although the apparent charge number was increased from $z = -4$ to -2. A 50 mV negative shift of the transfer potential of H_2TPPS^{4-} (cf. $\Delta_o^w\phi^{o'}_{H_2TPPS^{4-}} = -0.20$ V[25, 54]) results from the protonation equilibrium in aqueous solutions. In the H_2PP^{2-} system, a pair of positive and negative current peaks was observed at –0.13 V, but the broad positive peaks were relatively small (**Figure 4-2-3b**). These voltammetric features should be attributed to the ion transfer process of H_2PP^{2-} accompanied by the interfacial adsorption since the negative currents at –0.13 V were linearly proportional to sweep rate in

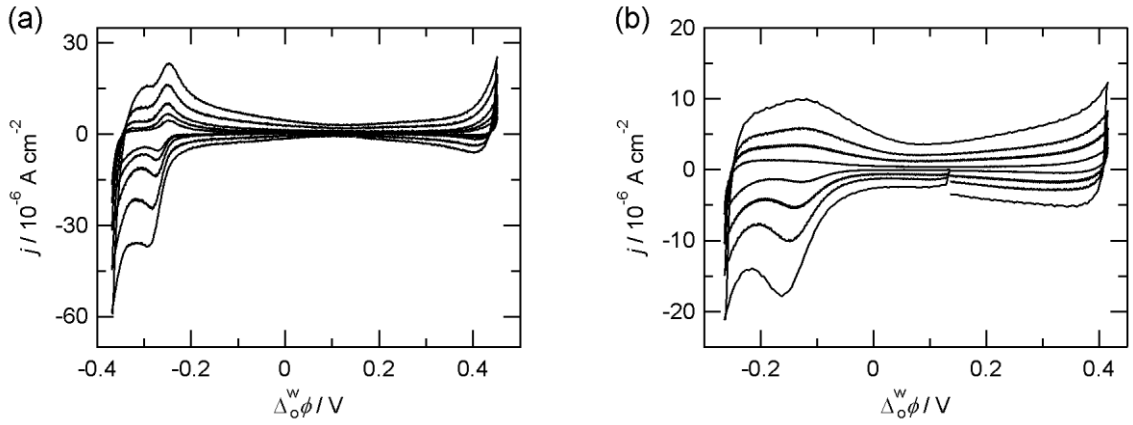

Figure 4-2-3. CVs measured for (a) H_4TPPS^{2-} at pH 2.1 (**Cell III**) and (b) H_2PP^{2-} at pH 7.2 (**Cell IV**). The potential sweep rates were 10, 20, 50, 100 and 200 mV s^{-1}. The concentrations of H_4TPPS^{2-} and H_2PP^{2-} in the aqueous phase were 2.0×10^{-5} mol dm^{-3} and 1.0×10^{-4} mol dm^{-3}, respectively.

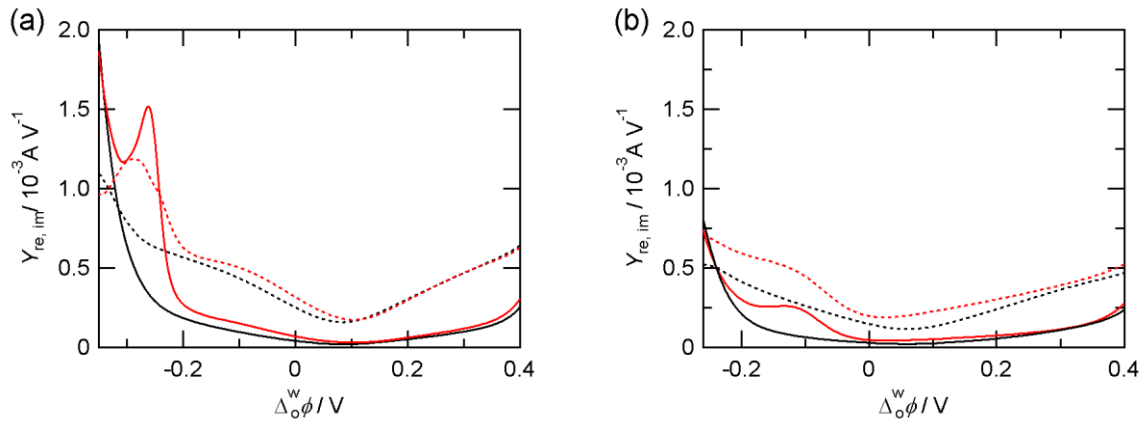

Figure 4-2-4. Ac voltammograms measured for (a) H_4TPPS^{2-} at pH 2.1 and (b) H_2PP^{2-} at pH 7.2. The black lines depict ac voltammograms in the absence of the porphyrins. The solid and dashed lines denote the real and imaginary components of admittance. The potential sweep rate was 5 mV s^{-1}. The potential modulation was 10 mV at 7 Hz. The concentrations of H_4TPPS^{2-} and H_2PP^{2-} in the aqueous phase were 2.0×10^{-5} mol dm^{-3} and 1.0×10^{-4} mol dm^{-3}, respectively.

agreement with the previous report.[25] The formal transfer potential of H_2PP^{2-} was evaluated at $\Delta_o^w\phi^{o'}_{H_2PP^{2-}} = -0.13$ V from ac voltammograms.

The adsorption of the porphyrins at the water|DCE interface can be confirmed by small increments of the admittance. In **Figure 4-2-4**, the real and imaginary components of the admittance increase prior to the transfer potential in both systems, indicating the specific adsorption of the anionic porphyrins at the interface. The adsorption responses of H_4TPPS^{2-} were obtained at $\Delta_o^w\phi < 0.10$ V (**Figure 4-2-4a**), while those of H_2PP^{2-} appeared within the whole potential window (**Figure 4-2-4b**). Indeed, the interfacial tension measurements showed that the interfacial tension (γ_i) values decreased at $\Delta_o^w\phi < 0$ V in the presence of H_4TPPS^{2-} (**Figure 4-2-5**). The interfacial tension lowering by adding H_2PP^{2-} was also measured over the potential window. These results indicate that adsorption process of H_2PP^{2-} is less potential-dependent in comparison with that of H_4TPPS^{2-}.

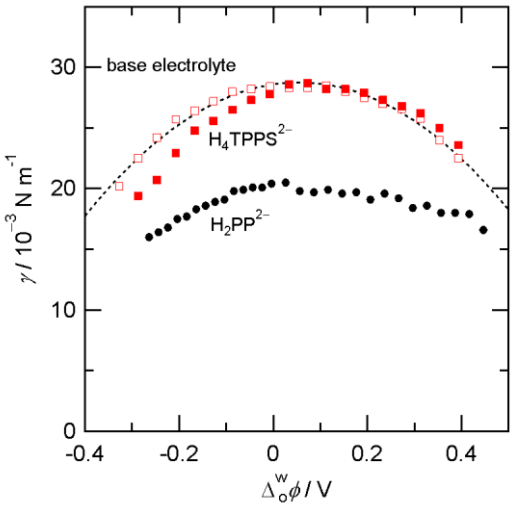

Figure 4-2-5. Electrocapillary curves measured by QELS for H_4TPPS^{2-} system at pH 2.2 (**Cell III**, solid square) and H_2PP^{2-} system at pH 7.2 (**Cell IV**, solid circle). The concentration of H_4TPPS^{2-} and H_2PP^{2-} were 2.0×10^{-5} mol dm^{-3} and 1.0×10^{-4} mol dm^{-3}, respectively. In the base electrolyte system, 1.0×10^{-2} mol dm^{-3} Li_2SO_4 was used as supporting electrolyte for the aqueous phase.

4-2-4. Adsorption and Aggregation of Porphyrins at the Water|DCE Interface

The PM-TIRF spectra measured for H_4TPPS^{2-} at pH 2.2 under potentiostatic control were shown in **Figure 4-2-6**. The incident laser beams of 404 nm and 488 nm were employed for the excitation of the monomer and aggregate species of H_4TPPS^{2-}, respectively. The formation of J-aggregates with red-shifted emission bands at the interface were clearly observed depending on $\Delta_o^w\phi$. The PM-TIRF signals from the interfacial species should be associated with the orientations of the porphyrin ring of monomers[56, 57] or the long axis of J-aggregates.[82, 84, 85] The fluorescence maximum wavelengths of the PM-TIRF spectra are summarized in **Table 4-2-1.** In **Figure 4-2-6a**, the PM-TIRF spectra under the excitation at 404 nm exhibited the spectra similar to the fluorescence spectra of the diacid form in aqueous solution with a negative sign ($\Delta F^{p\text{-}s} <$

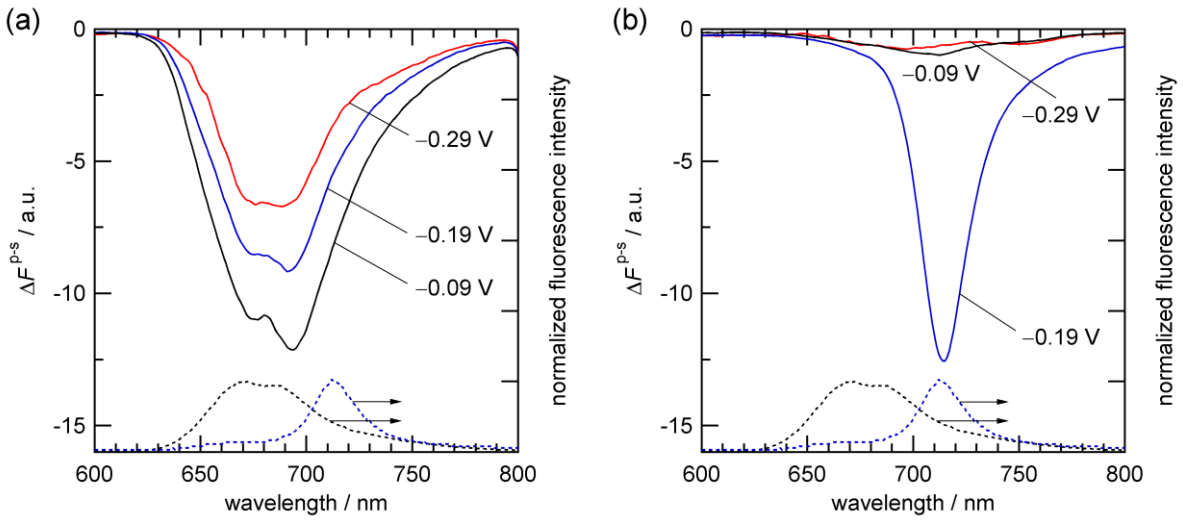

Figure 4-2-6. PM-TIRF spectra for H_4TPPS^{2-} at the water|DCE interface under the excitation at **(a)** 404 nm and **(b)** 488 nm. The pH of the aqueous phase was pH 2.2. The blue and black dotted lines refer to the normalized fluorescence spectra of J-aggregates at pH 1.3 and monomers at pH 2.3 in the aqueous solutions under the excitation at 488 nm.

0), indicating that the H_4TPPS^{2-} monomers were adsorbed with relatively lying orientation ($54.7° < \theta_{OR} \leq 90°$) and its adsorption state was almost consistent with that in the bulk aqueous phase. The non-zero $\Delta F^{p\text{-}s}$ associated with the adsorption of H_4TPPS^{2-} was also observed at –0.29 V, which is 0.04 V more negative potential than that of the ion transfer. These results show that the H_4TPPS^{2-} monomers remain at the aqueous side of the interface even at potentials more negative than that of the ion transfer. In addition, the interfacial adsorption of H_2TPPS^{4-} was not observed under the present experimental conditions.

Under the excitation at 488 nm, the selective detection of J-aggregates of H_4TPPS^{2-} was achieved with negligible interference from the monomer species. As seen in **Figure 4-2-6b**, the intensity of negative PM-TIRF signal was highly dependent on $\Delta_o^w\phi$ and a maximum wavelength of 714 nm clearly shows the formation of the J-aggregates at the interface. The negative $\Delta F^{p\text{-}s}$ also suggests that the long axis of the J-aggregates were lying nearly parallel to the interface. The

Table 4-2-1. Fluorescence maximum wavelengths of the porphyrins at the water|DCE interface and in bulk solutions.

	TPPS system			PP system		
	$\Delta_o^w\phi$ / V	$\lambda_{em,max}^{404}$ / nm[b]	$\lambda_{em,max}^{488}$ / nm[b]	$\Delta_o^w\phi$ / V	$\lambda_{em,max}^{404}$ / nm[b]	R_F[c]
interface (PM-TIRF)[a]	–0.09	676(–), 693(–)	713(–)	0.31	636(+), 702(+)	4.8
	–0.19	676(–), 691(–)	714(–)	−0.11	636(+), 693(–)	
	–0.29	676(–), 688(–)	697(–)	−0.20	640(–), 698(–)	1.2
aqueous phase[d]	(pH 1.3)	671, 684	713		620, 684	2.8
	(pH 2.3)	671, 684	671, 684			
organic phase[d]		651, 715	651, 715		633, 698	2.9

[a]The PM-TIRF spectra were taken at pH 2.2 for TPPS and pH 7.3 for PP systems. [b] $\lambda_{em,max}^{404}$ and $\lambda_{em,max}^{488}$ denote the PM-TIRF maxima under the excitation at 404 nm and 488 nm, respectively. [c]The peak intensity ratio of the first and second fluorescence peaks. [d]The fluorescence maxima measured for the aqueous and organic solutions (cf. **Figures 4-2-1** and **4-2-2**).

PM-TIRF signals of H_4TPPS^{2-} monomer and its aggregates were recorded respectively at 680 nm and 713 nm in the quasi-equilibrium condition with a potential sweep rate of 1 mV s^{-1} (**Figure 4-2-7**). The negative $\Delta F^{p\text{-}s}$ magnitude of the monomer maximized around –0.07 V was decreased simultaneously with increasing negative $\Delta F^{p\text{-}s}$ corresponding to the aggregation at –0.25 V < $\Delta_o^w\phi$ ≤ –0.15 V. At more negative potentials, the magnitude of $\Delta F^{p\text{-}s}$ at 713 nm was reduced eventually to almost zero. A compatible result was observed in the PM-TIRF spectra measured for the J-aggregate (**Figure 4-2-8**). The magnitude of $\Delta F^{p\text{-}s}$ at 713 nm were also maximized around –0.22 V, suggesting that the J-aggregation takes place at less negative potentials than that of the transfer across the interface (**Figure 4-2-8c**). It is noteworthy that the conventional TIR fluorescence spectra indicate that the dominant aqueous and organic species were monomeric H_4TPPS^{2-} and H_2TPPS^{4-}, respectively (**Figure 4-2-9**). Therefore, the J-

aggregates of H_4TPPS^{2-} were formed only at the aqueous side of the interface and were dissociated through the transfer process involving the deprotonation of H_4TPPS^{2-} (**Figure 4-2-10**).

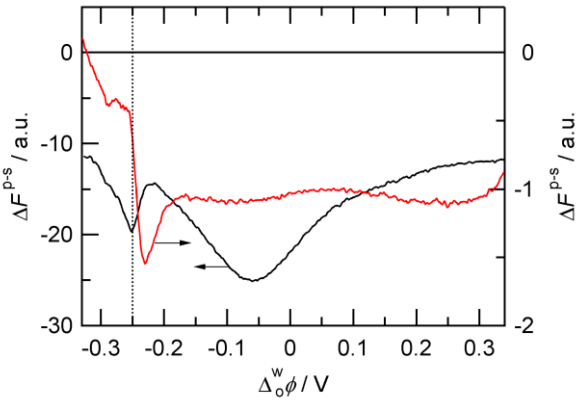

Figure 4-2-7. Typical potential dependence of PM-TIRF responses ($\Delta F^{p\text{-}s}$) for H_2TPPS^{4-} at the water|DCE interface. The excitation and detection wavelengths were 404 nm and 680 nm (black, left axis) and 488 nm and 713 nm (red, right axis), respectively. The potential sweep rate was 1 mV s^{-1}. The vertical dotted lines depict the transfer potential at –0.25 V. The concentration of H_2TPPS^{4-} in the aqueous phase was 2.0×10^{-5} mol dm^{-3}. The pH value of the aqueous phase was adjusted to 2.2.

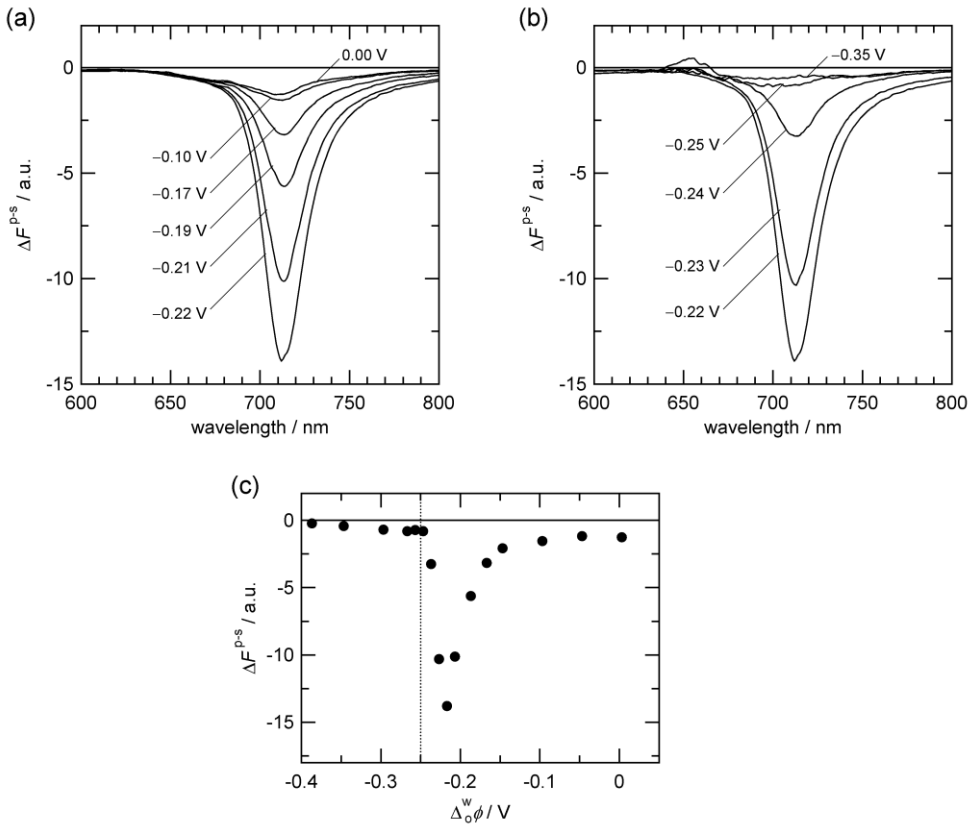

Figure 4-2-8. Typical spectral changes of PM-TIRF spectra for the H_4TPPS^{2-} aggregates measured at the polarized water|DCE interface. The potentiostatic conditions vary from **(a)** 0.00 V to −0.22 V and **(b)** −0.22 V to −0.39 V, respectively. The aqueous phase was adjusted at pH 2.2. The excitation wavelength was 488 nm. **(c)** $\Delta F^{p\text{-}s}$ at 713 nm vs. $\Delta_o^w\phi$ plot. The vertical dotted line depicts the ion transfer potential at pH 2.2.

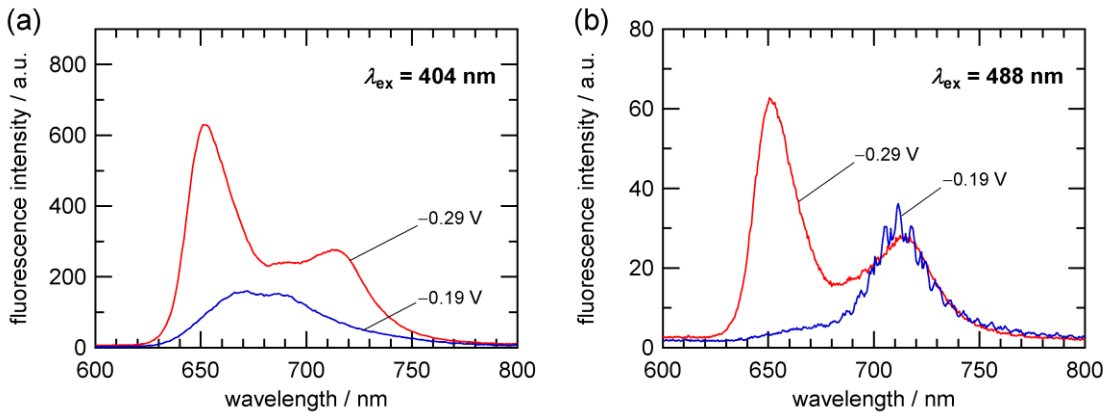

Figure 4-2-9. Conventional TIR fluorescence spectra measured at given potentials (**Cell I**). The excitation wavelengths were **(a)** 404 nm and **(b)** 488 nm, respectively.

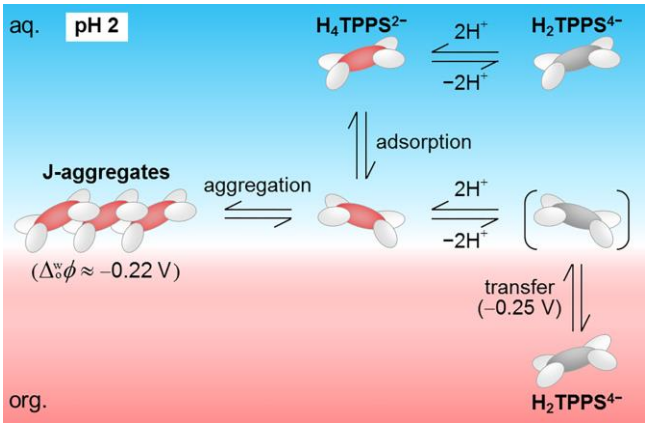

Figure 4-2-10. Schematic representation of the aggregation and transfer of H_4TPPS^{2-} at the polarized water|DCE interface.

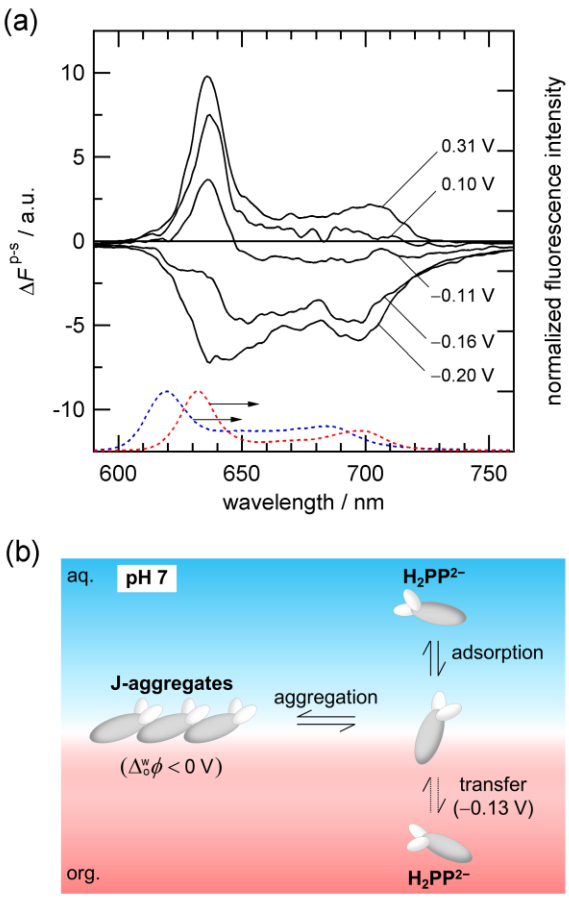

Figure 4-2-11. (a) Typical PM-TIRF spectra for H_2PP^{2-} at the water|DCE interface. The blue and red dotted lines refer to the normalized fluorescence spectra measured in the aqueous and organic solutions. The concentration of H_2PP^{2-} in the aqueous phase at pH 7.3 was 1.0×10^{-4} mol dm^{-3}. The excitation wavelength was 404 nm. **(b)** Schematic representation of the aggregation behavior of H_2PP^{2-} at the polarized water|DCE interface.

The PM-TIRF spectra measured for H_2PP^{2-} exhibited complicated spectral features depending on $\Delta_o^w\phi$ under neutral pH conditions (**Figure 4-2-11**), where the further protonation of the free base is negligible. The PM-TIRF experiments for H_2PP^{2-} were carried out under the excitation at 404 nm. The fluorescence maximum wavelengths and peak intensity ratios of the first and second peaks (R_F) of PM-TIRF spectra are summarized in **Table 4-2-1**. At positive potentials than $\Delta_o^w\phi^{\circ'}_{H_2PP^{2-}} = -0.13$ V, the PM-TIRF spectra exhibited the positive PM-TIRF signals ($\Delta F^{p\text{-}s}$

> 0), suggesting that the H_2PP^{2-} monomers were adsorbed with standing orientation relative to the interface. The PM-TIRF maxima, 636 nm and 702 nm, observed at 0.31 V were consistent with fluorescence maxima of bulk organic species at 633 nm and 698 nm. These spectral features suggest that H_2PP^{2-} adsorbed at the interface has a solvation state similar to the bulk organic species, i.e., dehydration of the porphyrin fluorophore. Taking into account standing orientation of H_2PP^{2-} under positively polarized conditions, the less hydrophilic porphyrin moiety of H_2PP^{2-} could penetrate into the organic side of the interface. In the negative potential region, the positive PM-TIRF responses around 636 nm were gradually weakened and then the negative PM-TIRF spectra were obtained at $\Delta_o^w\phi < \Delta_o^w\phi^{o'}_{H_2PP^{2-}}$. As a result, the PM-TIRF spectrum at –0.20 V exhibited a red-shift of the broad first peak to 640 nm. The similar red-shift has been observed for Fe(III) protoporphyrin IX at the water|DCE interface by surface second harmonic generation (SSHG), where the spectral shift was interpreted by the aggregation and specific polarity in the interfacial region.[86] It has also been reported that the J-aggregation of H_2PP^{2-} derivatives in solutions cause a significant decrease in intensity with a small spectral shift in the fluorescence spectrum.[87-89] A 7 nm red-shift observed in PM-TIRF spectra with $\Delta F^{p\text{-}s} < 0$ should be associated with the formation of J-aggregates at the water|DCE interface. In the present pH condition, the J-aggregates consist of the free base molecules with the π-π interaction. **Figure 4-2-11b** illustrates the interfacial mechanism of H_2PP^{2-}, where the J-aggregation occurs particularly at the negatively polarized interface and H_2PP^{2-} monomers transfer across the interface at –0.13 V. As shown in **Figure 4-2-12**, the positive $\Delta F^{p\text{-}s}$ around 633 nm decreased as a function of time, while the negative $\Delta F^{p\text{-}s}$ around at 650 nm were slightly increased. These temporal changes were equilibrated after 20 minutes, suggesting that the J-aggregation of H_2PP^{2-} was considerably slow process at the polarized water|DCE interface. These results were also supported by the dependence of PM-TIRF signal on the potential sweep rate (**Figure 4-2-13**). The $\Delta F^{p\text{-}s}$ at 1 mV s^{-1} decreased gradually and the sign of $\Delta F^{p\text{-}s}$ was changed in the negative potential region. On the other hand, $\Delta F^{p\text{-}s}$ at 5 mV s^{-1} showed positive value and increased

gradually around at $\Delta_o^w\phi^{o'}_{H_2PP^{2-}}$. The specific interfacial behavior could be attributed to the high surface-activity and well-ordered molecular orientation of H_2PP^{2-} with slow kinetics at the water|DCE interface.

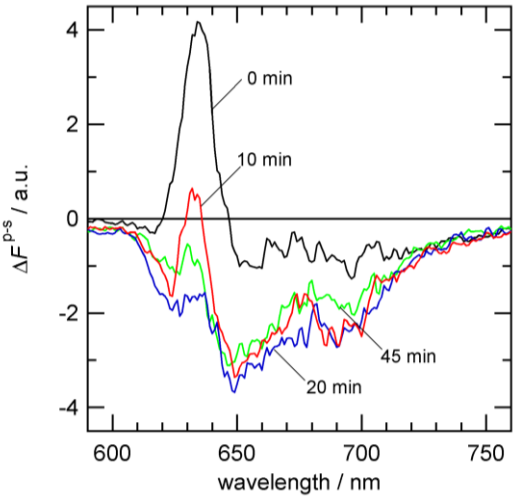

Figure 4-2-12. Time-dependence of PM-TIRF spectra for H_2PP^{2-} at –0.16 V. The concentration of H_2PP^{2-} was 1.0×10^{-4} mol dm^{-3}. The pH value of the aqueous phase was pH 7.2.

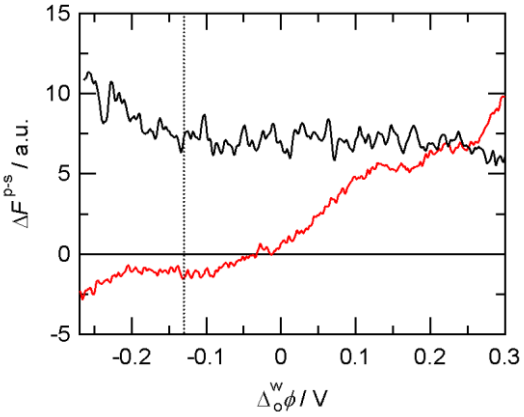

Figure 4-2-13. Typical potential dependence of PM-TIRF responses (ΔF^{p-s}) for H_2PP^{2-} at the water|DCE interface. The potential sweep rates were 1 mV s^{-1} (red line) and 5 mV s^{-1} (black line). The vertical dotted lines depict the transfer potential at –0.13 V. The excitation and detection wavelengths were 404 nm and 633 nm. The concentration of H_2PP^{2-} in the aqueous phase was 1.0×10^{-4} mol dm^{-3}. The pH value of the aqueous phase was adjusted to 7.2.

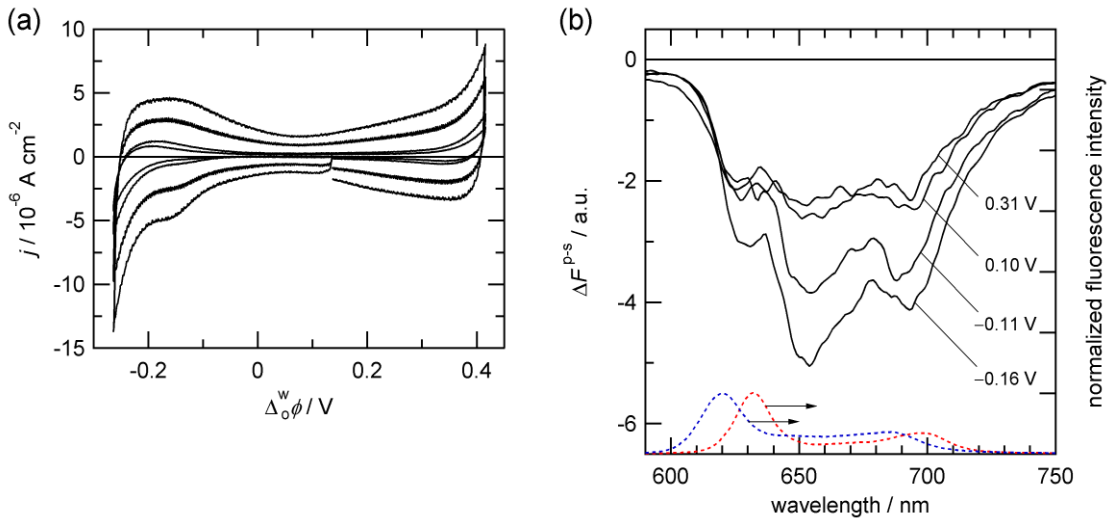

Figure 4-2-14. (a) CVs measured at 10, 20, 50, 100 mV s^{-1} and **(b)** PM-TIRF spectra for H_2PP^{2-} at the water|DCE interface. **(b)** The blue and red dotted lines refer to normalized fluorescence spectra measured in the aqueous and organic solutions. The concentration of H_2PP^{2-} was 2.0×10^{-5} mol dm^{-3}. The pH value of the aqueous phase was pH 7.1.

The red-shifted negative peak at 651 nm were also observed at a H_2PP^{2-} concentration of 2.0×10^{-5} mol dm^{-3}, depending on $\Delta_o^w\phi$ (**Figure 4-2-14**). The PM-TIRF results demonstrated that the potential-dependent aggregation occurs even at dilute concentrations down to 2.0×10^{-5} mol dm^{-3}. **Figure 4-2-15** shows the concentration dependence of PM-TIRF spectra measured at –0.16 V, where the spectral features were changed from the red-shifted spectrum of the J-aggregates with $\Delta F^{p\text{-}s} < 0$ to the monomeric shape with $0 < \Delta F^{p\text{-}s}$ at higher concentrations. It is known that the aggregation of porphyrins was induced by increasing the bulk concentration.[89-91] The PM-TIRF spectrum at 5.0×10^{-4} mol dm^{-3}, however, showed the sharp monomeric response with a positive sign at 636 nm (**Figure 4-2-16**). The possible reason for the H_2PP^{2-} monomer as the dominant interfacial species is the limited interfacial area available for the adsorption since an upstanding molecular orientation of monomeric H_2PP^{2-} can reduce the occupied interfacial area per unit molecule in comparison with the aggregates flattened in the interfacial plane. Furthermore, the weak negative $\Delta F^{p\text{-}s}$ responses observed at –0.16 V (**Figure 4-2-16**) are

analogous to those observed in 1.0×10^{-4} mol dm^{-3} H_2PP^{2-} system at –0.11 V (cf. **Figure 4-2-11**). The J-aggregation, therefore, occurs at more negative potentials than the lower concentration systems, where the interfacial concentration is slightly decreased via ion transfer into the organic phase.

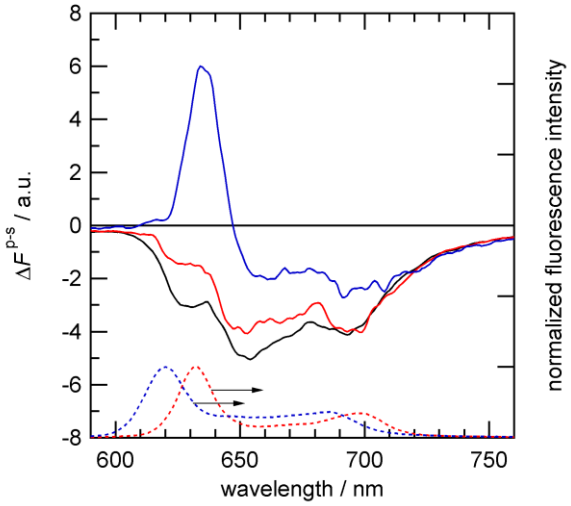

Figure 4-2-15. The dependence of PM-TIRF spectra at $\Delta_o^w\phi = -0.16$ V on the H_2PP^{2-} concentration. The concentrations of H_2PP^{2-} were 2.0×10^{-5} (black), 1.0×10^{-4} (red) and 5.0×10^{-4} mol dm^{-3} (blue). The blue and red dotted lines refer to normalized fluorescence spectra measured in the aqueous and organic solutions.

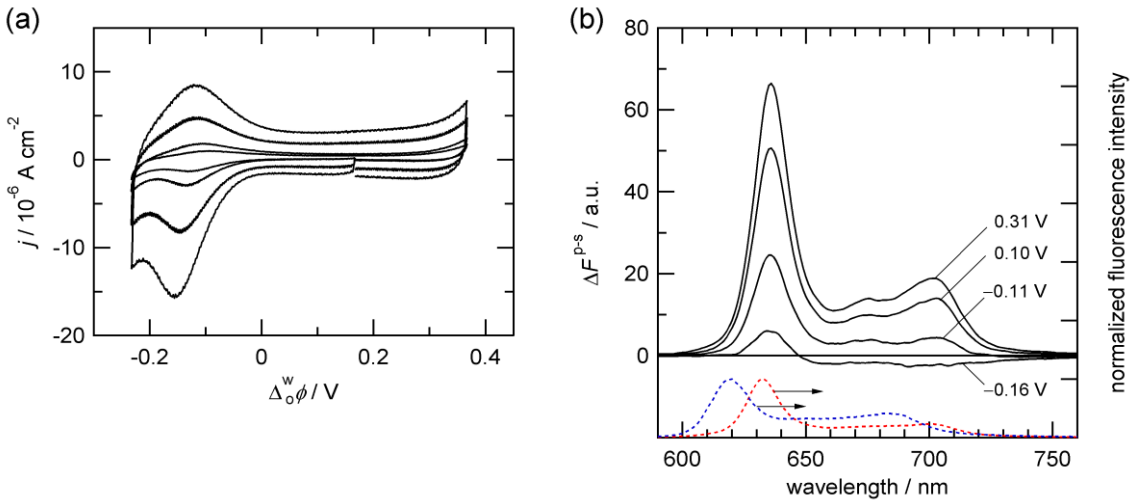

Figure 4-2-16. (a) CVs measured at 10, 20, 50, 100 mV s^{-1} and (b) PM-TIRF spectra for H_2PP^{2-} at the water|DCE interface. (b) The blue and red dotted lines refer to normalized fluorescence spectra measured in the aqueous and organic solutions. The concentration of H_2PP^{2-} was 5.0×10^{-4} mol dm^{-3}. The pH value of the aqueous phase was pH 7.3.

4-2-5. Adsorption Behavior of Protoporphyrin IX at Biomimetic Interfaces.

The phospholipid with a high surface-activity is spontaneously adsorbed at variety of liquid|liquid interfaces and the self-assemble monolayer can be used as a model of biomembrane surfaces.[9, 92-94] In order to evaluate its binding characteristics on cell membrane, the adsorption behavior of H_2PP^{2-} at the phospholipid-adsorbed water|DCE interface was investigated. A neutral glycerophospholipid, DMPC, was added to the organic solution and then the phospholipid monolayer was spontaneously formed at the water|DCE interface.[9, 50, 92] **Figure 4-2-17** shows the CVs and electrocapillary curves for H_2PP^{2-} at the DMPC-adsorbed water|DCE interface. The current increase was observed at 0.20 V < $\Delta_o^w\phi$ in the presence of 1.0×10^{-5} mol dm^{-3} DMPC. The facilitated transfer of Li^+ ions by the monolayer of DMPC formed at the interface through the complexation of a cation (Li^+) with phospholipid and the simultaneous desorption from the interface into organic phase.[50, 95] The voltammetric responses of H_2PP^{2-} around at $\Delta_o^w\phi^{o'}_{H_2PP^{2-}}$ = –0.13 V were decreased with increasing DMPC concentration, suggesting that DMPC inhibited the adsorption and transfer processes of H_2PP^{2-}. The surface-activity of H_2PP^{2-} and DMPC manifested itself in the γ_i lowering in the electrocapillary curves (**Figure 4-2-17b**). DMPC caused a remarkable decrease in γ_i and the additional lowering effect was observed by the coexistence of H_2PP^{2-} at $\Delta_o^w\phi$ < 0.2 V, indicating that H_2PP^{2-} could penetrate into the DMPC layer at the negatively polarized interface.

The spectral shape and signal phase of PM-TIRF were influenced depending on $\Delta_o^w\phi$ by the addition of DMPC (**Figure 4-2-18)**. At 0.31 V, the PM-TIRF signal from H_2PP^{2-} was almost vanished by the competitive adsorption with DMPC and this result agrees with no additional γ_i lowering at 0.2 V < $\Delta_o^w\phi$ in **Figure 4-2-17b**. On the other hand, the PM-TIRF spectra at –0.16 V in the presence of 1.0×10^{-5} mol dm^{-3} DMPC exhibited the negative $\Delta F^{p\text{-}s}$ arising from H_2PP^{2-} relatively parallel to the interface, where the PM-TIRF maximum around 633 nm exhibited the

spectral feature similar to that of the H_2PP^{2-} monomer in the organic solution (cf. **Table 1**). The competitive adsorption of DMPC would reduce the surface amounts of H_2PP^{2-} and then prevent the aggregation process (**Figure 4-2-19**).

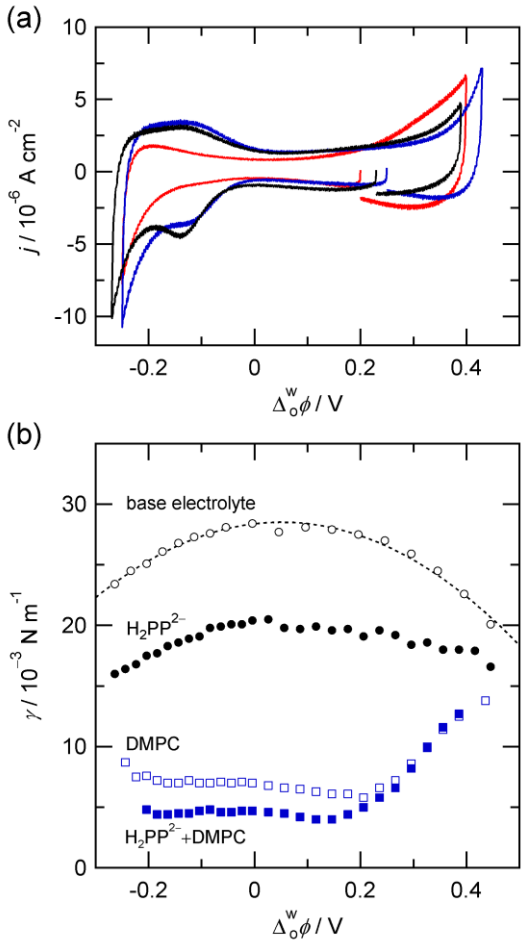

Figure 4-2-17 (a) CVs and **(b)** electrocapillary curves of H_2PP^{2-} at the DMPC-adsorbed water|DCE interface. The concentration of H_2PP^{2-} was 1.0×10^{-4} mol dm^{-3} and the aqueous phase was buffered at pH 7.2–7.3. **(a)** The concentrations of DMPC were 0 (black), 1.0×10^{-6} (blue) and 1.0×10^{-5} mol dm^{-3} (red). The potential sweep rates were 50 mV s^{-1}. **(b)** The electrocapillary curves were measured in the presence of H_2PP^{2-} (solid circle), 1.0×10^{-5} mol dm^{-3} DMPC (open square) and H_2PP^{2-} + DMPC (solid square). The open circles depict the base electrolyte system.

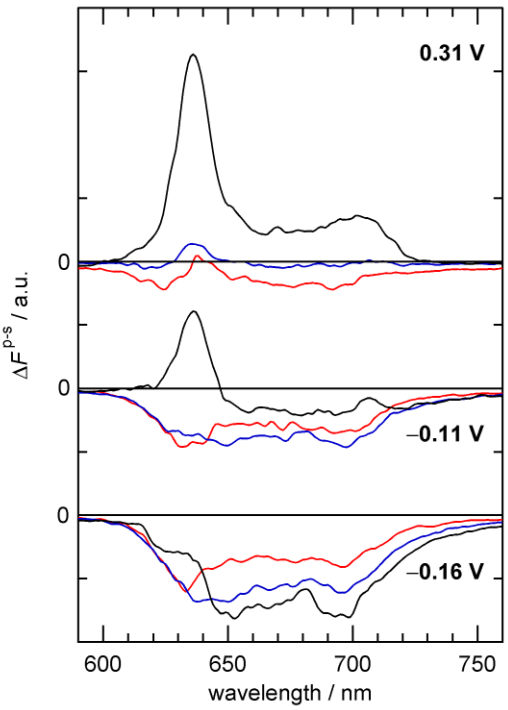

Figure 4-2-18. The dependence of PM-TIRF spectra on DMPC concentration. PM-TIRF spectra were measured in the presence of DMPC at the concentrations of 0 (black), 1.0×10^{-6} (blue) and 1.0×10^{-5} mol dm^{-3} (red). The concentration of H_2PP^{2-} was 1.0×10^{-4} mol dm^{-3}. The bottom blue and red dotted lines refer to normalized fluorescence spectra measured in the aqueous and organic solutions.

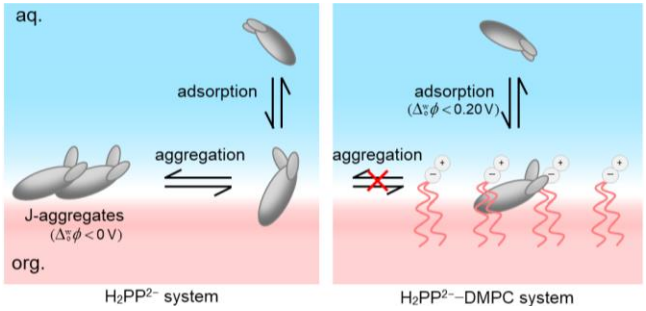

Figure 4-2-19. Schematic representation of the adsorption behavior of H_2PP^{2-} at the polarized water|DCE interface in the absence and presence of DMPC.

4-2-6. Conclusions

The spectroelectrochemical analysis based on the PM-TIRF technique uncovered the potential-dependent adsorption and aggregation mechanism of anionic porphyrins at the polarized water|DCE interface. In the H_4TPPS^{2-} system, the monomeric H_4TPPS^{2-} and its J-aggregates oriented at the interface could be measured separately by selecting the appropriate excitation wavelength. The selective detection of the interfacial species achieved in multi-wavelength excited PM-TIRF experiments is very useful to elucidate the complicated heterogeneous reaction, which is composed of plural surface-active species. The negative PM-TIRF signals exhibited the relatively flat orientation of the *meso*-substituted H_4TPPS^{2-} monomer with four equivalent sulfonatophenyl groups, whereas the potential-induced J-aggregation of H_4TPPS^{2-} proceeded only at the aqueous side of the interface. The slow aggregation process of H_2PP^{2-} was found in the negative potential region. The molecular orientation of H_2PP^{2-} was affected by the J-aggregation at the interface, where the monomers were adsorbed with relatively standing orientation and the long axis of the J-aggregates was nearly in plane of the interface. At the phospholipid-adsorbed water|DCE interface, the competitive adsorption of DMPC effectively inhibited the adsorption and aggregation processes of H_2PP^{2-}. These results indicate that the adsorption and aggregation of charged species can reversibly be controlled as a function of externally applied potential and it will enable a potential-induced self-assembly of 2D supramolecular structure or nanomaterial formation at ITIES.

4-3 Adsorption Behavior of Water-Soluble 8-Quinolinol Complexes at Liquid|Liquid Interfaces

4-3-1. Introduction

8-quinolinol (HQ) derivatives are effective chelating reagents applied for quantitative analysis of various metal ions. It has been reported that the transfer of metal ions at polarized liquid|liquid interfaces is facilitated by HQ, [96-98] where the partition of hydrophobic HQ into the aqueous phase and then the complexation occurs in the aqueous phase. However, the direct characterization of the HQ complexes at liquid|liquid interfaces has been rarely reported.[96-98] Recently, the interfacial behavior of metal (Al(III), Zn(II) and Cu(II)) complexes with QS has been investigated by Marie Takeyama in our group.[99] In the case of a bidentate ligand, 8-quinolinol-5-sulfonate (HQS^-), the stoichiometry and molecular geometry of the metal complex formation in the aqueous solution varies from 1:1 to 1:3 as a function of pH. The capacitance results indicate that the adsorption process of the QS complexes occurs at negatively polarized interface although there is no ion transfer response of the QS complexes in the potential window. The adsorptivity tends to be $Cu(QS)_2^{2-} \geq Al(QS)_3^{3-} > Zn(QS)_2^{2-}$. The lower adsorptivity of $Zn(QS)_2^{2-}$ could be associated with the axial coordination of water molecule to zinc center,[100, 101] which leads to the enhancement of the hydrophilicity. In addition, PMF measurements were carried out for Al(II) and Zn(II) complex systems with their high emission features.[99] The PMF analysis revealed that the ion transfer process of $Al(QS)_3^{3-}$ and $Zn(QS)_2^{2-}$ is accompanied by the adsorption process at the aqueous side of the interface. Furthermore, in the case of the Zn(II) complex system, the effect of molecular geometry on the adsorption behavior was also examined by using a tridentate ligand, 8-quinolinol-2-carboxylate (HQC^-).[99] QC ligand inhibited the axial hydration to the zinc center of 1:2 complex by carboxylate groups, which leads the enhancement of the adsorptivity at the water|DCE interface. Thus, the axial hydration of 8-quinolinol

complexes at the interface plays important roles in the interfacial behavior. In chapter 4-3, the adsorption behavior of Al(III) and Zn(II) complexes is discussed in terms of the stoichiometry for the formation of HQ complexes and molecular geometries as a function of pH in the aqueous solution.

4-3-2. Complexation of 8-Quinolinol Derivatives in Aqueous Solutions

When the acid–base equilibria of QS are described in **Figure 4-3-1**, the dissociation constants pK_{a1} and pK_{a2} given by eq. (4-3-1) and (4-3-2) are 3.8 and 8.4, respectively.[102, 103]

$$K_{a1} = \frac{[HQS^-][H^+]}{[H_2QS]} \tag{4-3-1}$$

$$K_{a2} = \frac{[QS^{2-}][H^+]}{[HQS^-]} \tag{4-3-2}$$

The stoichiometry for metal complex formation with QS varies from 1:1 to 1:3 (matal:ligand) depending on metal ions and pH conditions in the aqueous solution.[100-106] The structures of 1:2 and 1:3 complexes are shown in **Figure 4-3-2**. The stability constants of metal complexes (β_n) in literature are listed in **Table 4-3-1**. The β_n values for complexation with metal ion (M) are defined as

$$M + nQS^{2-} \leftrightharpoons MQS_n$$

$$\beta_n = \frac{[MQS_n]}{[M][QS^{2-}]^n} \tag{4-3-3}$$

Taking account of the formation of metal hydroxide, the total concentration of metal ion (c_M) and ligand (c_L) are given by

$$c_M = [M] + [ML] + \cdots + [ML_n] + [M(OH)] + [M(OH)_2] + \cdots + [M(OH)_m] \tag{4-3-4}$$

$$c_L = [L'] + [ML] + 2[ML_2] + 3[ML_3] \tag{4-3-5}$$

where

$$[L'] = [L] + [HL] + [H_2L] = [L]\left(1 + \frac{[H^+]}{K_{a2}} + \frac{[H^+]^2}{K_{a1}K_{a2}}\right) \tag{4-3-6}$$

Figure 4-3-3 and **4-3-4** show the abundance of Al(III) and Zn(II) complexes with QS as a function of pH calculated from eqs. (4-3-1)–(4-3-6). The dominant species can be controlled by pH in the aqueous solution. In the Al(III)−QS complex system, the population of $Al(QS)_3^{3-}$ at lower pH can be reduced by controlling the concentration ratio of aluminum ion and QS (**Figure 4-3-3a** and **4-3-3b**).

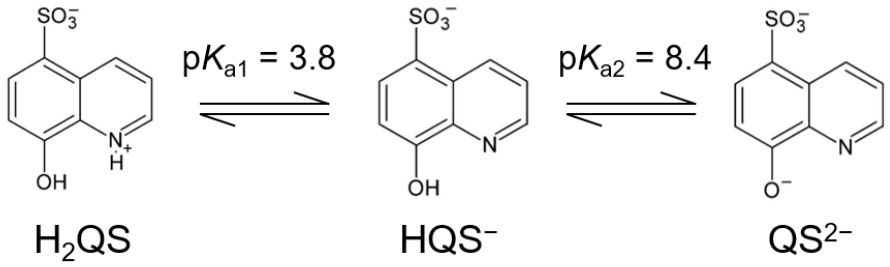

Figure 4-3-1. Dissociation equilibrium of QS.[102, 103]

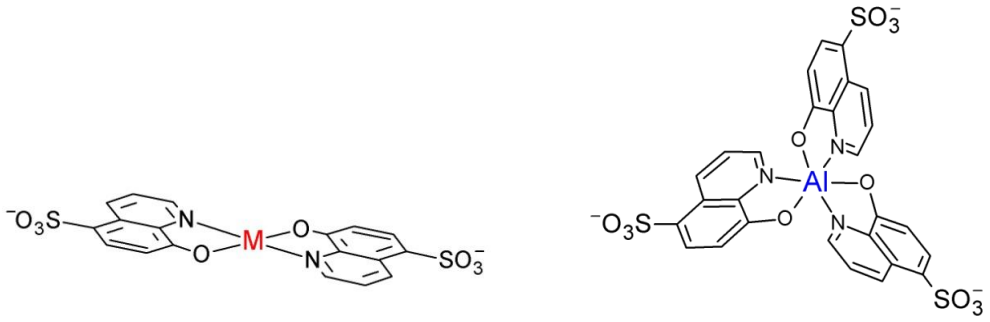

Figure 4-3-2. Molecular structures of QS complexes (M = Al(III) or Zn(II)).[100−106]

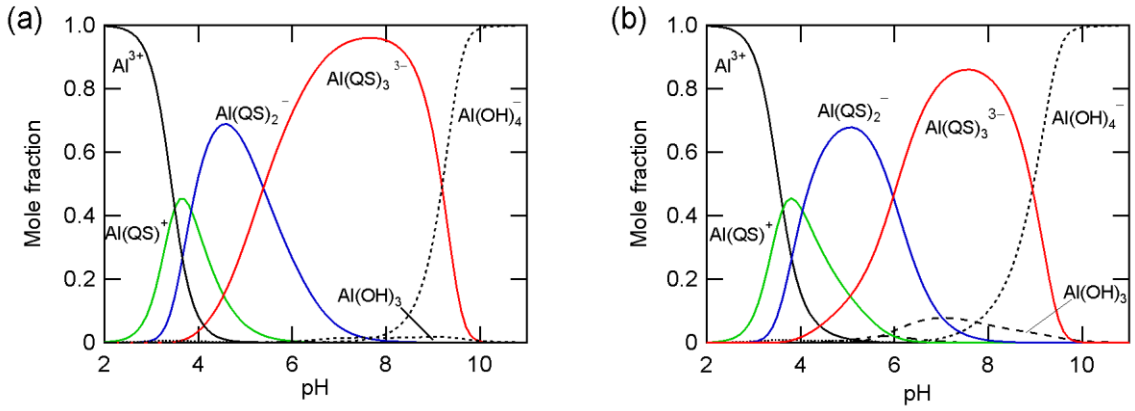

Figure 4-3-3. Abundance of Al(III)−QS complexes as a function of pH. The concentrations of aluminum ion and QS were taken as [Al(III)] = 1.0 ×10^{-4} mol dm^{-3}, [QS] = (a) 3.0 ×10^{-4} mol dm^{-3} and (b) 2.0 ×10^{-4} mol dm^{-3}.

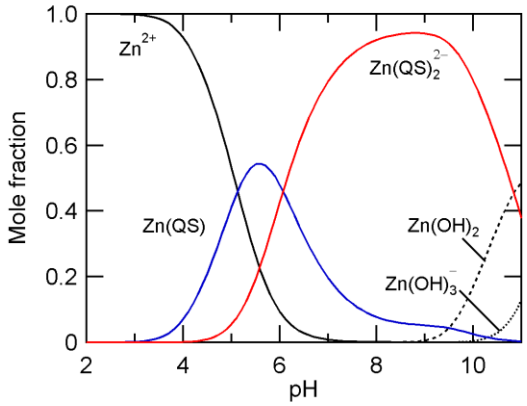

Figure 4-3-4. Abundance of Zn(II)−QS complexes as a function of pH. The concentrations of zinc ion and QS were taken as [Zn(II)] : [QS] = 5.0 ×10^{-5} mol dm^{-3} : 1.0 ×10^{-4} mol dm^{-3}.

Table.4-3-1 Stability constants (β_n) of QS complexes

metal ion	logβ_1	logβ_2	logβ_3	Ref.
Al(III)	8.95	17.43	24.58	[104]
Zn(II)	7.54	14.32	−	[103]

4-3-3. Adsorption Behavior of Al(III)−QS Complexes

Figure 4-3-5 shows CVs for Al(III)−QS complex systems at pH 7.0 and 4.9, where $Al(QS)_3^{3-}$ and $Al(QS)_2^-$ are the dominant species, respectively (cf. **Figure 4-3-3**). At both pHs, a pair of the negative and positive peaks was observed around at −0.24 V. The peak separation was 53 mV, which is close to the theoretical value for the ion transfer of monovalent species across the interface. Considered that the ion transfer of the Al(III)−QS complexes takes place at $\Delta_o^w\phi < -0.30$ V ,[99] this current response is attributable to the ion transfer of the free QS (HQS^-) across the interface.

PM-TIRF measurement were carried out to investigate the adsorption behavior of the QS complexes at the interface. **Figure 4-3-6** shows the potential dependences of $\Delta F^{p\text{-}s}$ measured for the Al(III)−QS complex in the negative potential region. The negative $\Delta F^{p\text{-}s}$ was observed at pH 7.0 and 4.9 over the potential window (**Figure 4-3-6**). The rapid increase of F_{total} at $\Delta_o^w\phi < -0.30$ V suggests that the ion transfer of Al(III)−QS complex occurred. In the present

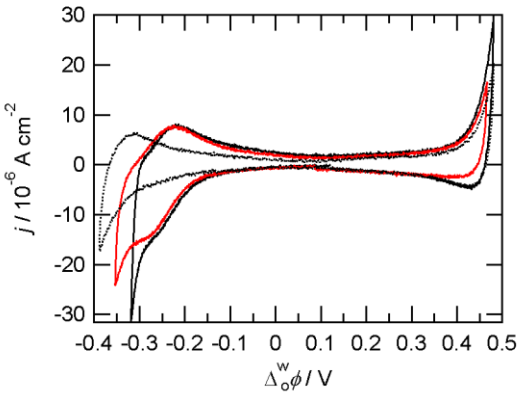

Figure 4-3-5. CVs measured for Al(III)−QS complexes at the water|DCE interface. The pHs in the aqueous phase were pH 7.0 (black) and pH 4.9 (red), respectively. The dotted line refers to the base electrolyte system. The potential sweep rate was 50 mV s^{-1}. [Al(III)] = 1.0×10^{-4} mol dm^{-3}, [QS] = 3.0×10^{-4} mol dm^{-3} at pH 7.0 and [Al(III)] = 1.0×10^{-4} mol dm^{-3}, [QS] = 2.0×10^{-4} mol dm^{-3} at pH 4.9.

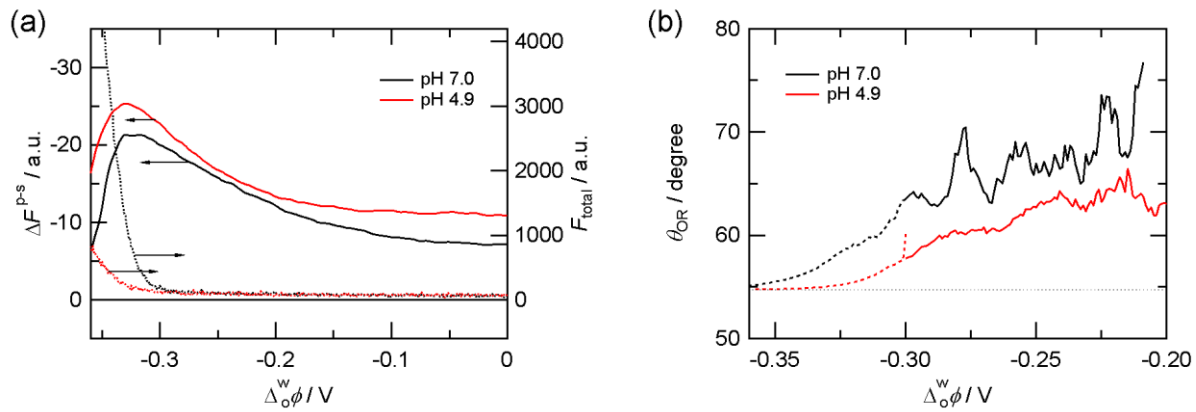

Figure 4-3-6. The potential dependence of (a) PM-TIRF responses ($\Delta F^{p\text{-}s}$) and (b) the orientation angles (θ_{OR}) for the Al(III)–QS complex systems at pH 7.0 (black) and 4.9 (red). The potential sweep rate was 2 mV s^{-1}. $\lambda_{ex} = 376$ nm, $\lambda_{em} = 492$ nm. [Al(III)] = 1.0×10^{-4} mol dm^{-3}, [QS] = 3.0×10^{-4} mol dm^{-3} at pH 7.0 and [Al(III)] = 1.0×10^{-4} mol dm^{-3}, [QS] = 2.0×10^{-4} mol dm^{-3} at pH 4.9.

system, the fluorescence from $Al(QS)_3^{3-}$ could be independent on linear polarizations even if $Al(QS)_3^{3-}$ is adsorbed at the interface because of its D_3 symmetry (cf. $Ru(bpy)_3^{2+}$ system in **Appendix**). Therefore, the non-zero $\Delta F^{p\text{-}s}$ is generated from the planar 1:2 complex, $Al(QS)_2^-$, although the abundance of $Al(QS)_2^-$ is quite small ($Al(QS)_3^{3-}$: $Al(QS)_2^-$ = 93 : 5 at pH 7.0). In addition, the $\Delta F^{p\text{-}s}$ from $Al(QS)_2^-$ associates the plane of 1:2 complex involving the π–π^* transition dipole moment in quinoline ring. The average orientation angles of $Al(QS)_2^-$ is estimated from $\Delta F^{p\text{-}s}$ and shown in **Figure 4-3-6b**. The θ_{OR} values at $-0.25\,V < \Delta^{w}_{o}\phi < -0.20\,V$ were approximately constant at 63±2°. The magnitude of $\Delta F^{p\text{-}s}$ was increased at pH 4.9 in comparison with $\Delta F^{p\text{-}s}$ at pH 7.0, which supports the adsorption of $Al(QS)_2^-$ at pH 7.0 since $Al(QS)_2^-$ is the dominant species in the aqueous phase at pH 4.9 ($Al(QS)_3^{3-} : Al(QS)_2^- : Al(QS)^+$ = 12 : 67 : 18, **Figure 4-3-3b**). The orientation angle was determined as θ_{OR} = 67 ± 3° at $-0.30\,V < \Delta^{w}_{o}\phi < -0.20\,V$. The θ_{OR} values were almost constant. Thus, a gradual increase of the

negative $\Delta F^{\text{p-s}}$ correlates with the increase in the interfacial concentration of $Al(QS)_2^-$. The negative $\Delta F^{\text{p-s}}$ maximized at −0.34 V, and then decreased at $\Delta_o^w\phi < -0.34$ V through the ion transfer of Al(III) complexes into the organic phase.

In order to characterize the interfacial species, PM-TIRF spectra were measured under potentiostatic control. The spectroscopic characteristics were evaluated by comparing the PM-TIRF spectra with the fluorescence spectra measured in the aqueous and organic solutions. An intense Raman scattering from the bulk DCE phase maximized at 424 and 460 nm, respectively, under the excitation at 376 and 404 nm was unfavorably superimposed on the PM-TIRF spectrum. To remove considerable overlap of Raman scattering in the PM-TIRF spectra, the raw PM-TIRF spectra were subtracted by that measured in the bulk organic solution (in transmittance mode).

The baseline subtracted PM-TIRF spectra for Al(III)−QS complexes at pH 7.0 and 4.9 are

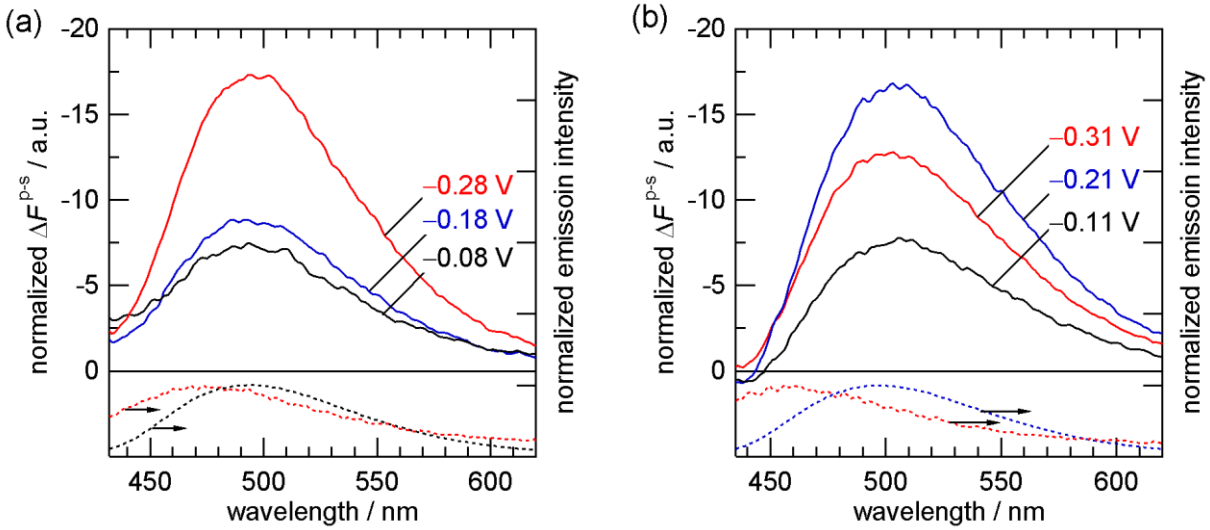

Figure 4-3-7. PM-TIRF spectra for Al(III)−QS complex systems at (a) pH 7.0 and (b) 4.9 at the water|DCE interface. The blue and red dashed lines refer to normalized fluorescence spectra measured in the aqueous and organic solutions. λ_{ex} = 376 nm. [Al(III)] = 1.0 ×10^{-4} mol dm^{-3}, [QS] = 3.0 ×10^{-4} mol dm^{-3} at pH 7.0 and [Al(III)] = 1.0 ×10^{-4} mol dm^{-3}, [QS] = 2.0 ×10^{-4} mol dm^{-3} at pH 4.9.

shown in **Figure 4-3-7**. The maximum wavelengths (λ_{max}) of the PM-TIRF spectra are summarized in **Table 4-3-2**. The PM-TIRF maximum at pH 7.0 was found at around 496 nm. The spectral features were similar to those measured in the aqueous solution at pH 4.9 where the dominant species is $Al(QS)_2^-$. These results suggest that $Al(QS)_2^-$ was adsorbed at the water|DCE interface and the PM-TIRF responses at pH 7.0 are associated with $Al(QS)_2^-$. It should be noted that $Al(QS)_3^{3-}$ would also be adsorbed at the interface but, in principle, the spherical $Al(QS)_3^{3-}$ is not responsible for PM-TIRF signal. The PM-TIRF maxima at pH 4.9 were red-shifted from the fluorescence maximum of the bulk aqueous spectrum at 496 nm. At this pH, the cationic 1:1 complex, $Al(QS)^+$ is one of the major species (18%) but the adsorption of $Al(QS)^+$ hardly occurred in the negative potential region. Thus, the possible reason for the red-shifted PM-TIRF spectra would be the π–π stacking between the QS ligands of $Al(QS)_2^-$ at the interface.[107-109]

Table 4-3-2. Fluorescence maximum wavelengths (λ_{max}) of Al(III)−QS complexes at the water|DCE interface and in solution.

	pH 4.9		pH 7.0	
	$\Delta_o^w\phi$ / V	λ_{max} / nm	$\Delta_o^w\phi$ / V	λ_{max} / nm
interface	–0.11	503	–0.08	494
	–0.21	503	−0.18	496
	–0.31	501	−0.28	496
aqueous phase[a]		496		493
organic phase[a]		456		478

[a]The fluorescence maximum wavelengths measured in the aqueous and organic solutions.

4-3-4. Adsorption Behavior of Zn(II) Complexes

Figure 4-3-8 shows CVs and PMF responses for Zn(II)−QS complex system at pH 7.0 and 6.1. The abundance of Zn(QS) and $Zn(QS)_2^{2-}$ are 45%:48% at pH 6.1 and 20%:80% at pH 7.0, respectively. In **Figure 4-3-8a**, the ion transfer responses of Zn(II)−QS complexes were not observed clearly at pH 7.0 within the potential window. On the other hand, the negative and positive current peaks were observed around at −0.24 V at pH 6.1. These response is attributable to the ion transfer of the free QS (HQS^-) across the interface (cf. **Figure 4-3-5**) since $Zn(QS)_2^{2-}$ could not be transferred in the relevant potential region. As shown in **Figure 4-3-8b**, the PMF responses corresponding to the adsorption of $Zn(QS)_2^{2-}$ at the aqueous side of the interface ($\Delta F_{re} < 0$ and $\Delta F_{im} > 0$) was observed at $-0.3\,\mathrm{V} < \Delta_o^w\phi < 0\,\mathrm{V}$, which is in good agreement with the previous report.[99] Although the ion transfer process of the free QS occurs at pH6.1 in that potential region, the $Zn(QS)_2^{2-}$ can also be adsorbed at the interface.

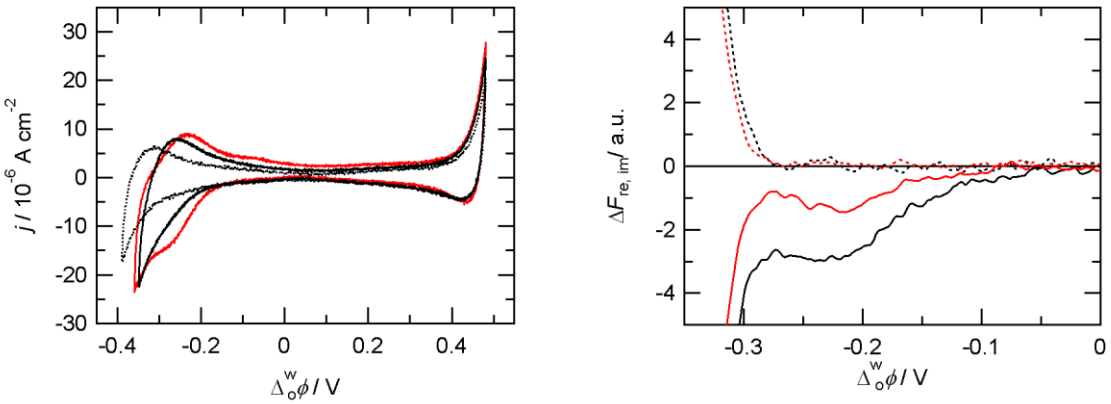

Figure 4-3-8. (a) CVs and (b) potential dependence of PMF responses for $Zn(QS)_2^{2-}$ at pH 7.0 (black) and pH 6.1(red). (a) The dotted line refers to the base electrolyte system. The potential sweep rate was (a) 50 mV s^{-1}. (b) The potential modulation was 20 mV at 1 Hz with the sweep rate of 2 mV s^{-1}. The solid and dotted line was real and imaginary components, respectively. λ_{ex} = 404 nm, λ_{em} = 525 nm. [Zn(II)] = 5.0 ×10^{-5} mol dm^{-3}, [QS] = 1.0 ×10^{-4} mol dm^{-3}.

As shown in **Figure 4-3-9**, the negative $\Delta F^{\text{p-s}}$ values were observed at pH 7.0 and 6.1 in the negative potential region where the PMF response for the adsorption of $Zn(QS)_2^{2-}$ was observed. The magnitude of $\Delta F^{\text{p-s}}$ was depending on $\Delta_o^w\phi$, suggesting that the negative $\Delta F^{\text{p-s}}$ response was generated from the planar $Zn(QS)_2^{2-}$ adsorbed at the interface. The average orientation angles of excitation dipole of $Zn(QS)_2^{2-}$ at $-0.25\ \text{V} < \Delta_o^w\phi < -0.20\ \text{V}$ were determined as 65±2° at pH 7.0 and 70±2° at pH 6.1, respectively (**Figure 4-3-9b**). The magnitude of $\Delta F^{\text{p-s}}$ was maximized around −0.31 V, and then decreased gradually at more negative potentials through the ion transfer of $Zn(QS)_2^{2-}$ into the organic phase. The steep decrease in the negative $\Delta F^{\text{p-s}}$ at pH 6.1 could be due to the simultaneous ion transfer of $Zn(QS)_2^{2-}$ and the free HQS^- across the interface (**Figure 4-3-8**).

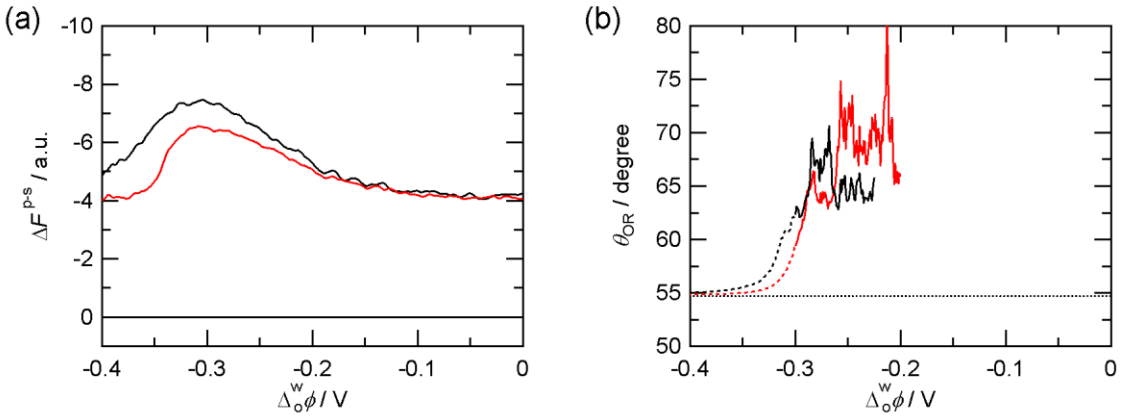

Figure 4-3-9. The potential dependence of (a) PM-TIRF responses ($\Delta F^{\text{p-s}}$) and (b) the orientation angles (θ_{OR}) for Zn(II)−QS complex systems at pH 6.1 (red) and 7.0 (black). The potential sweep rate was 2 mV s^{-1}. λ_{ex} = 404 nm, λ_{em} = 525 nm. [Zn(II)] = 5.0×10^{-5} mol dm^{-3}, [QS] = 1.0×10^{-4} mol dm^{-3}.

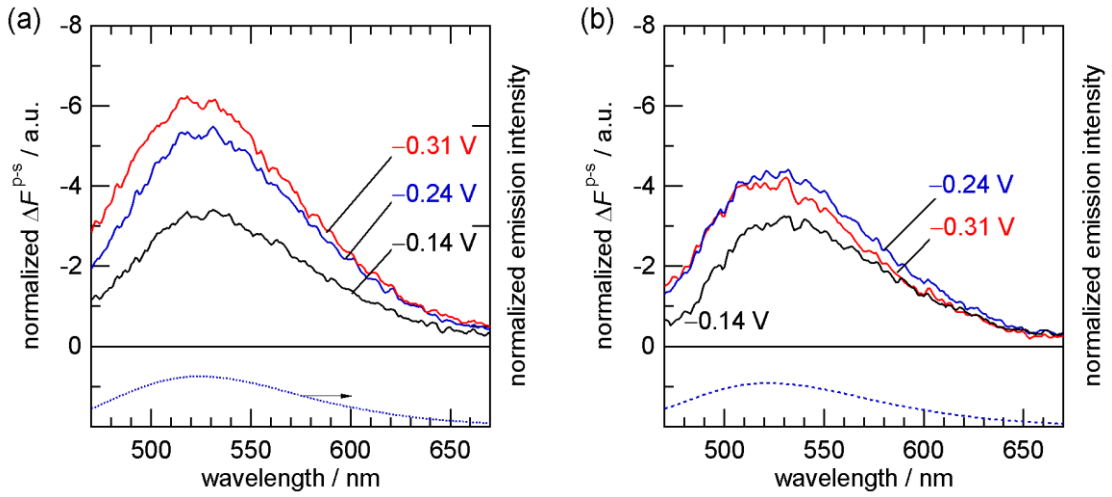

Figure 4-3-10. PM-TIRF spectra for Zn complex systems at (a) pH 7.0 and (b) 6.1 at the water|DCE interface. The blue and red dashed lines refer to normalized fluorescence spectra measured in the aqueous and organic solutions. λ_{ex} = 404 nm. [Zn(II)] = 5.0 ×10^{-5} mol dm^{-3}, [QS] = 1.0 ×10^{-4} mol dm^{-3}.

The PM-TIRF spectra of Zn(II)−QS complexes were shown in **Figure 4-3-10**. The maximum wavelengths of the PM-TIRF spectra are summarized in **Table 4-3-3**. In the Zn(II)−QS complex systems at pH 7.0, the spectral shapes and λ_{max} of PM-TIRF spectra were not significantly affected by $\Delta_o^w\phi$ although the slight spectral shifts should not be discussed because of a low S/N ratio. In addition, the spectral features of PM-TIRF spectra were similar to those of the bulk fluorescence spectra. These results could indicate that $Zn(QS)_2^{2-}$ was adsorbed with the hydration state similar to that in the aqueous solution, that is the effective axial hydration at the interface (**Figure 4-3-11**).[100, 101] In addition, the PM-TIRF spectra at pH 6.1 were analogous to those at pH 7.0, suggesting that the hydrated $Zn(QS)_2^{2-}$ was also adsorbed at the interface. The adsorption of the neutral 1:1 complex, Zn(QS), could not be identified in the present condition.

Table 4-3-3. Fluorescence maximum wavelengths (λ_{max}) of Zn(II) complexes with QS at the water|DCE interface.

	$\Delta_o^w\phi$ / V	λ_{max} / nm	
		pH 6.1	pH 7.0
interface	−0.14	528	526
	−0.24	524	524
	−0.31	519	522
aqueous phase[a]		522	523
organic phase[b]		–	–

[a]The fluorescence maximum wavelengths measured in the aqueous solutions.

[b] $Zn(QS)_2^{2-}$ was hardly partitioned into the organic phase.

In this paragraph, the effect of molecular geometry on the adsorption behavior is discussed. A tridentate QC ligand inhibits the axial hydration to the zinc center of 1:2 complex by carboxylate groups (**Figure 4-3-11**).[101, 110] Interestingly, the apparent $\Delta F^{p\text{-}s}$ was observed in $Zn(QC)_2^{2-}$ system (**Figure 4-3-12a**) and $\Delta F^{p\text{-}s}$ increased with the increase of F_{total} at $\Delta_o^w\phi < -0.30$ V. Although the coordination geometry of $Zn(QC)_2^{2-}$ could be distorted from octahedral geometry, the negative $\Delta F^{p\text{-}s}$ indicates that the net excitation dipole was oriented roughly parallel to the interfacial plane. The non-zero $\Delta F^{p\text{-}s}$ also allows us to investigate the adsorption state of the interfacial species. The PM-TIRF spectra of $Zn(QC)_2^{2-}$ at pH7.5 are shown in **Figure 4-3-12b**. The λ_{max} of the PM-TIRF spectra are summarized in **Table 4-3-4**. The spectral shape was affected by applying $\Delta_o^w\phi$. The PM-TIRF maxima at $\Delta_o^w\phi < -0.30$ V showed intermediate λ_{max} values between the fluorescence maxima in the bulk aqueous (645 nm) and organic solutions (562 nm). The PM-TIRF maximum at –0.33 V was found at around 567 nm, which is close to

the λ_{max} in the organic solution. These results indicate that the hydration states of $Zn(QC)_2^{2-}$ were modified at the interface depending on $\Delta_o^w\phi$, suggesting that the adsorption state of $Zn(QC)_2^{2-}$ is associated with the polarity of the interfacial region. The adsorption plane of $Zn(QC)_2^{2-}$ could be varied according to $\Delta_o^w\phi$.

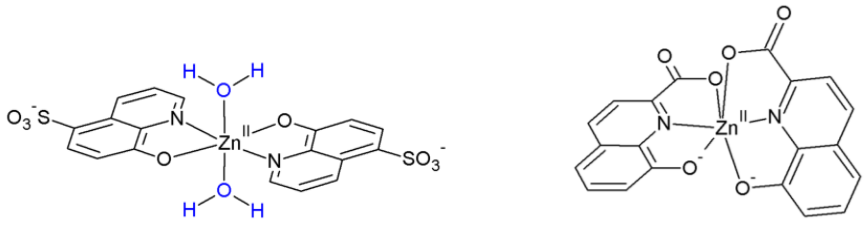

Figure 4-3-11. Molecular structures of $Zn(QS)_2^{2-}$ [101] and $Zn(QC)_2^{2-}$ [110].

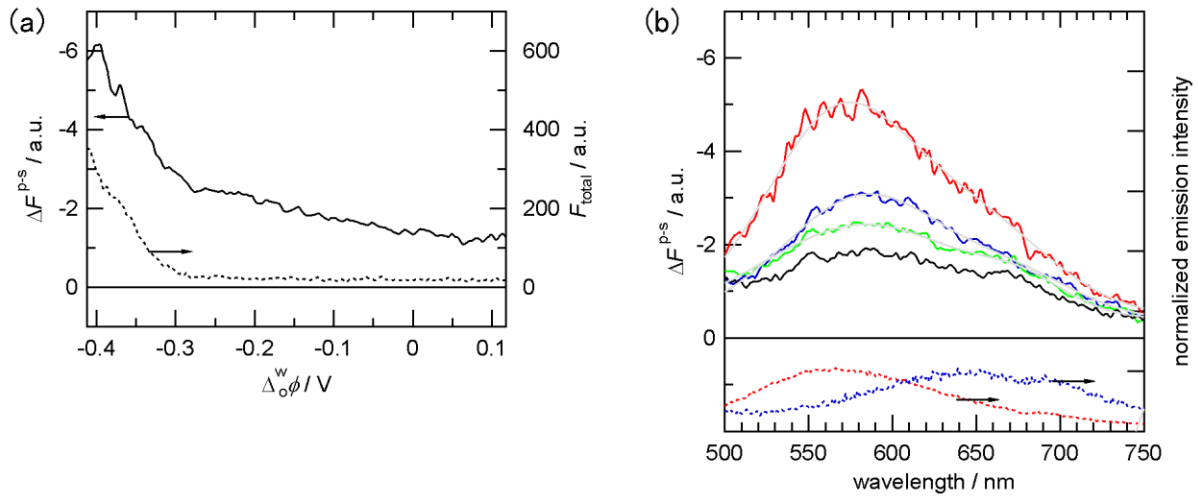

Figure 4-3-12. PM-TIRF spectra measured for $Zn(QC)_2^{2-}$ systems at pH 7.5. The black, green, blue and red solid lines depict PM-TIRF spectra measured at −0.08 V, −0.18 V −0.28 V and −0.33 V, respectively. The blue and red dashed lines refer to normalized fluorescence spectra measured in the aqueous and organic solutions. λ_{ex} = 404 nm. [Zn(II)] = [QC] = 1.0 ×10^{-4} mol dm^{-3}.

Table 4-3-4. Fluorescence maximum wavelengths (λ_{max}) of Zn complexes with QC at the water|DCE interface.

	$\Delta_o^w\phi$ / V	λ_{max} / nm
interface	−0.08	584
	−0.18	584
	−0.28	584
	−0.33	567
aqueous phase[a]		645
organic phase[a]		562

[a]The fluorescence maximum wavelengths measured in the aqueous and organic solutions.

4-3-5. Conclusions

The interfacial behavior of water-soluble 8-quinolinol complexes was strongly affected by the central metal ion as well as molecular geometry. The adsorption state of the 8-quinolinol complexes at the water|DCE interface was successfully characterized by PM-TIRF spectroscopy. Although the spherical 1:3 complex, $Al(QS)_3^{3-}$, cannot respond in PM-TIRF measurements, the planar 1:2 complexes, $Al(QS)_2^-$ and $Zn(QS)_2^{2-}$ showed roughly parallel orientation to the interface. In the case of Al(III)−QS complexes, the hydration state of $Al(QS)_2^-$ at pH 7.0 was analogous to that in the bulk aqueous solution. At pH 4.9, the π−π stacking of $Al(QS)_2^-$ occurred especially at the interface. In the Zn(II) complex system, the effect of molecular geometry on the adsorption behavior were highlighted by using bidentate QS and tridentate QC ligands. $Zn(QS)_2^{2-}$ was adsorbed with axial hydration to the zinc center, while QC ligand inhibited the axial coordination of the water molecule and enhanced adsorptivity at the water|DCE interface. Thus, the axial hydration of Zn(II) complexes at the interface plays important roles in the interfacial behavior.

5. CONCLUDING REMARKS

PM-TIRF spectroscopy is a high sensitive and selective to fluorescent species oriented at a liquid|liquid interface. By using this technique, the direct characterization of interfacial species has been achieved without controversial contribution of bulk species. The potential-dependence of the adsorption states of the interfacial species has been analyzed successfully by PM-TIRF spectroscopy even when several reactions occur simultaneously such as ion transfer, adsorption and aggregation. In this dissertation, PM-TIRF was applied to the fluorescent species in order to evaluate the interfacial mechanism at liquid|liquid interfaces. The solvation states of water-soluble porphyrins at the water|DCE interface were modified from those in the bulk solutions depending on the Galvani potential difference. The anionic porphyrins showed high surface activities at the polarized water|DCE interface. In addition, the J-aggregation of the anionic porphyrins was observed at the interface and it can be controlled reversibly as a function of externally applied potential. In H_2PP^{2-} system, the adsorption behavior of H_2PP^{2-} at the phospholipid-adsorbed water|DCE interface was investigated to evaluate its binding characteristics on the cell membranes. The results demonstrated that the adsorption state of H_2PP^{2-} is drastically affected at the phospholipid-adsorbed interface in comparison with the bare water|DCE interface. These findings can contribute to the study of the mass transfer process in biological system. Furthermore, in the case of 8-quinolinol complexes, the results indicated that the axial coordination of water molecules to metal center plays important roles in the interfacial mechanism. PM-TIRF spectroscopy allows us to access useful spectroscopic information of interfacial species at a molecular level such as molecular orientation, intermediate solvation properties and specific aggregation. It will help us understanding of 2D structure of self-assembly at liquid|liquid interfaces and the extraction mechanism of metal ions in the liquid|liquid extraction system.

6. REFERENCES

(1) Benjamin, I., Chemical Reactions and Solvation at Liquid Interfaces: A Microscopic Perspective. *Chem. Rev.* **1996,** *96*, 1449-1475.

(2) Benjamin, I., Reaction Dynamics at Liquid Interfaces. *Annu. Rev. Phys. Chem.* **2015,** *66*, 165-188.

(3) Watarai, H.; Tsukahara, S.; Nagatani, H.; Ohashi, A., Interfacial Nanochemistry in Liquid-Liquid Extraction Systems. *Bull. Chem. Soc. Jpn.* **2003,** *76*, 1471-1492.

(4) Tsukahara, S., Recent Analytical Methodologies on Equilibrium, Kinetics, and Dynamics at Liquid/liquid Interface. *Anal. Chim. Acta* **2006,** *556*, 16-25.

(5) Benjamin, I., Static and Dynamic Electronic Spectroscopy at Liquid Interfaces. *Chem. Rev.* **2006,** *106*, 1212-1233.

(6) Watarai, H.; Adachi, K., Measuring the Optical Chirality of Molecular Aggregates at Liquid-Liquid Interfaces. *Anal. Bioanal. Chem.* **2009,** *395*, 1033-1046.

(7) Nagatani, H., *In Situ* Spectroscopic Characterization of Porphyrins at Liquid Interfaces. In *Handbook of Porphyrin Science*, Kadish, K. M.; Smith, K. M.; Guilard, R., Eds. World Scientific Publishing Co.: Singapore, 2014; Vol. Volume 34: Harnessing Solar Energy pp 51-96.

(8) Samec, Z., Electrochemistry at the Interface between Two Immiscible Electolyte Solutions. *Pure Appl. Chem.* **2004,** *76*, 2147-2180.

(9) Girault, H. H., Electrochemistry at Liquid-Liquid Interfaces. In *Electroanalytical Chemistry*, Bard, A. J.; Zoski, C. G., Eds. CRC Press: 2010; Vol. 23, pp 1-104.

(10) Piron, A.; Brevet, P. F.; Girault, H. H., Surface Second Harmonic Generation Monitoring of the Anion Methyl Orange during Ion Transfer Reactions across a Polarised Water | 1,2-Dichloroethane Interface. *J. Electroanal. Chem.* **2000,** *483*, 29-36.

(11) Nagatani, H.; Fermín, D. J.; Girault, H. H., A Kinetic Model for Adsorption and Transfer of Ionic Species at Polarized Liquid|liquid Interfaces as Studied by Potential Modulated Fluorescence Spectroscopy. *J. Phys. Chem. B* **2001,** *105*, 9463-9473.

(12) Volkov, A. G., *Liquid Interfaces in Chemical, Biological, and Pharmaceutical Application*. Marcel Dekker: New York, 2001.

(13) Watarai, H.; Teramae, N.; Sawada, S., *Interfacial Nanochemistry*. Kluwer Academic/Plenum Publishers: New York, 2005.

(14) Perera, J. M.; Stevens, G. W., Spectroscopic Studies of Molecular Interaction at the Liquid-Liquid Interface. *Anal. Bioanal. Chem.* **2009,** *395*, 1019-1032.

(15) Axelrod, D.; Burghardt, T. P.; Thompson, N. L., Total Internal Reflection Fluorescence. *Annual review of biophysics and bioengineering* **1984,** *13*, 247-268.

(16) Okumura, R.; Hinoue, T.; Watarai, H., Ion-Association Adsorption of Water-Soluble Porphyrin at a Liquid-Liquid Interface and an External Electric Field Effect on the Adsorption. *Anal. Sci.* **1996,** *12*, 393-397.

(17) Ishizaka, S.; Kitamura, N., Time-Resolved Total Internal Reflection Fluorometry Study on Chemical and Structural Characteristics at Water/Oil Interfaces. *Bull. Chem. Soc. Jpn.* **2001,** *74*, 1983-1998.

(18) Pant, D.; Girault, H. H., Time-Resolved Total Internal Reflection Fluorescence Spectroscopy: Part I. Photophysics of Coumarin 343 at Liquid/liquid Interface. *Phys. Chem. Chem. Phys.* **2005,** *7*, 3457-3463.

(19) Sutherland, R. L., *Handbook of Nonlinear Optics*. 2nd ed.; Marcel Dekker: New York, 2003.

(20) Roy, S.; Covert, P. A.; Fitzgerald, W. R.; Hore, D. K., Biomolecular structure at solid-liquid interfaces as revealed by nonlinear optical spectroscopy. *Chemical Reviews* **2014,** *114*, 8388-8415.

(21) Zaera, F., Surface chemistry at the liquid/solid interface. *Surf. Sci.* **2011,** *605*, 1141-1145.

(22) Corn, R. M.; Higgins, D. A., Optical Second Harmonic Generation as a Probe of Surface Chemistry. *Chem. Rev.* **1994,** *94*, 107-125.

(23) Eisenthal, K. B., Liquid Interfaces Probed by Second-Harmonic and Sum-Frequency Spectroscopy. *Chem. Rev.* **1996,** *96*, 1343-1360.

(24) Nagatani, H.; Iglesias, R. A.; Fermín, D. J.; Brevet, P. F.; Girault, H. H., Adsorption Behavior of Charged Zinc Porphyrins at the Water/1,2-Dichloroethane Interface Studied by Potential Modulated Fluorescence Spectroscopy. *J. Phys. Chem. B* **2000,** *104*, 6869-6876.

(25) Nagatani, H.; Ozeki, T.; Osakai, T., Direct Spectroelectrochemical Observation of Interfacial Species at the Polarized Water/1,2-Dichloroethane Interface by Ac Potential Modulation Technique. *J. Electroanal. Chem.* **2006,** *588*, 99-105.

(26) Osakai, T.; Yamada, H.; Nagatani, H.; Sagara, T., Potential-Dependent Adsorption of Amphoteric Rhodamine Dyes at the Oil/Water Interface as Studied by Potential-Modulated Fluorescence Spectroscopy. *Journal of Physical Chemistry C* **2007,** *111*, 9480-9487.

(27) Nagatani, H.; Sakamoto, T.; Torikai, T.; Sagara, T., Encapsulation of anilinonaphthalenesulfonates in carboxylate-terminated PAMAM dendrimer at the polarized water|1,2-dichloroethane interface. *Langmuir* **2010,** *26*, 17686-17694.

(28) Yoshimura, T.; Nagatani, H.; Osakai, T., Combined use of two membrane-potential-sensitive dyes for determination of the Galvani potential difference across a biomimetic oil/water interface. *Anal. Bioanal. Chem.* **2014,** *406*, 3407-3414.

(29) Sakae, H.; Nagatani, H.; Imura, H., Ion transfer and adsorption behavior of ionizable drugs affected by PAMAM dendrimers at the water|1,2- dichloroethane interface. *Electrochim. Acta.* **2016,** *191*, 631-639.

(30) Blaudez, D.; Castano, S.; Desbat, B., PM-IRRAS at Liquid Interfaces. In *Biointerface Characterization by Advanced IR Spectroscopy*, Elsevier: 2011; pp 27-55.

(31) Blaudez, D.; Buffeteau, T.; Cornut, J. C.; Desbat, B.; Escafre, N.; Pezolet, M.; Turlet, J. M., Polarization Modulation FTIR Spectroscopy at the Air-Water Interface. *Thin Solid Films* **1994,** *242*, 146-150.

(32) Cornut, I.; Desbat, B.; Turlet, J. M.; Dufourcq, J., In situ study by polarization modulated Fourier transform infrared spectroscopy of the structure and orientation of lipids and amphipathic peptides at the air-water interface. *Biophysical journal* **1996,** *70*, 305-312.

(33) Buffeteau, T.; Blaudez, D.; Pere, E.; Desbat, B., Optical Onstant Determination in the Infrared of Uniaxially Oriented Monolayers from Transmittance and Reflectance Measurements. *J. Phys. Chem. B* **1999,** *103*, 5020-5027.

(34) Mendelsohn, R.; Flach, C. R., Infrared Reflection-Absorption Spectroscopy of Lipids, Peptides, and Proteins in Aqueous Monolayers. In *Curr. Top. Membr.*, Academic Press: 2002; Vol. 52, pp 57-88.

(35) Tanida, H., Total-reflection X-ray absorption fine structure on liquid surface. *Spectrochim. Acta B* **2004,** *59*, 1071-1076.

(36) Watanabe, I.; Tanida, H.; Kawauchi, S., Coordination structure of zinc(II) ions on a Langmuir monolayer, observed by total-reflection X-ray absorption fine structure. *J. Am. Chem. Soc.* **1997,** *119*, 12018-12019.

(37) Watanabe, I.; Tanida, H.; Kawauchi, S.; Harada, M.; Nomura, M., X-ray absorption spectroscopy of liquid surface. *Rev. Sci. Instrum.* **1997,** *68*, 3307-3311.

(38) Nagatani, H.; Tanida, H.; Ozeki, T.; Watanabe, I., Zinc(II) Porphyrins at the Air-Water Interface as Studied by Polarized Total-Reflection X-ray Absorption Fine Structure. *Langmuir* **2006,** *22*, 209-212.

(39) Nagatani, H.; Tanida, H.; Watanabe, I.; Sagara, T., Extended X-ray Absorption Fine Structure of Copper(II) Complexes at the Air-Water Interface by a Polarized Total-Reflection X-ray Absorption Technique. *Anal. Sci.* **2009,** *25*, 475-480.

(40) Nagatani, H.; Tanida, H.; Harada, M.; Asada, M.; Sagara, T., Polarized total-reflection X-ray absorption fine structure of zinc(II) porphyrin at the heptane-water interface. *Journal of Physical Chemistry C* **2010,** *114*, 18583-18587.

(41) Ohta, N.; Matsunami, S.; Okazaki, S.; Yamazaki, I., Polarized absorption spectra and molecular orientation of some cyanine dyes in Langmuir-Blodgett monolayer films. *Langmuir* **1994,** *10*, 3909-3912.

(42) Akutsu, H.; Kyogoku, Y.; Nakahara, H.; Fukuda, K., Conformational Analysis of Phosphatidylethanolamine in Multilayers by Infrared Dichroism. *Chem. Phys. Lipids* **1975,** *15*, 222-242.

(43) Fermín, D. J.; Duong, H. D.; Ding, Z.; Brevet, P. F.; Girault, H. H., Photoinduced Electron Transfer at Liquid/Liquid Interfaces. Part II. A Study of the Electron Transfer and Recombination Dynamics by Intensity Modulated Photocurrent Spectroscopy (IMPS). *Phys. Chem. Chem. Phys.* **1999,** *1*, 1461-1467.

(44) Toshiyuki, O.; Tadaaki, K.; Mitsugi, S., A.c. Polarographic Study of Ion Transfer at the Water/Nitrobenzene Interface. *Bull. Chem. Soc. Jpn.* **1984,** *57*, 370-376.

(45) Toshiyuki, O.; Tadaaki, K.; Mitsugi, S., Kinetics of the Transfer of Picrate Ion at the Water/Nitrobenzene Interface. *Bull. Chem. Soc. Jpn.* **1985,** *58*, 2626-2633.

(46) Nagatani, H.; Sagara, T., Potential-modulation spectroscopy at solid/liquid and liquid/liquid interfaces. *Anal. Sci.* **2007,** *23*, 1041-1048.

(47) Langevin, D., *Light Scattering by Liquid Surfaces and Complementary Techniques*. Marcel Dekker: New York, 1992; p 89-104.

(48) Trojanek, A.; Krtil, P.; Samec, Z., Quasi-Elastic Laser Light Scattering from Thermally Excited Capillary Waves on the Polarised Water/1,2-Dichloroethane Interface. *Electrochem. Commun.* **2001,** *3*, 613-618.

(49) Nagatani, H.; Samec, Z.; Brevet, P. F.; Fermín, D. J.; Girault, H. H., Adsorption and Aggregation of *meso*-Tetrakis(4-Carboxyphenyl)Porphyrinato Zinc(II) at the Polarized Water|1,2-Dichloroethane Interface. *J. Phys. Chem. B* **2003,** *107*, 786-790.

(50) Samec, Z.; Trojanek, A.; Girault, H. H., Thermodynamic Analysis of the Cation Binding to a Phosphatidylcholine Monolayer at a Polarised Interface between Two Immiscible Electrolyte Solutions. *Electrochem. Commun.* **2003,** *5*, 98-103.

(51) Takahashi, S.; Harata, A.; Kitamori, T.; Sawada, T., Quasi-Elastic Laser Scattering Method for Monitoring Capillary Wave Frequency at a Water/Nitrobenzene Interface. *Anal. Sci.* **1994,** *10*, 305-308.

(52) Zhang; Tsuyumoto, I.; Takahashi, S.; Kitamori, T.; Sawada, T., Monitoring of Molecular Collective Behavior at a Liquid/Liquid Interface by a Time-Resolved Quasi-Elastic Laser Scattering Method. *The Journal of Physical Chemistry A* **1997,** *101*, 4163-4166.

(53) Sakae, H.; Nagatani, H.; Morita, K.; Imura, H., Spectroelectrochemical Characterization of Dendrimer-Porphyrin Associates at Polarized Liquid|liquid Interfaces. *Langmuir* **2014,** *30*, 937-945.

(54) Yamamoto, S.; Nagatani, H.; Morita, K.; Imura, H., Potential-Dependent Adsorption and Orientation of *meso*-Substituted Porphyrins at Liquid|Liquid Interfaces Studied by Polarization-Modulation Total Internal Reflection Fluorescence Spectroscopy. *J. Phys. Chem. C* **2016,** *120*, 7248-7255.

(55) Nagatani, H.; Piron, A.; Brevet, P. F.; Fermín, D. J.; Girault, H. H., Surface second harmonic generation of cationic water-soluble porphyrins at the polarized water. *Langmuir* **2002,** *18*, 6647-6652.

(56) Gouterman, M., Spectra of Porphyrins. *J. Mol. Spectrosc.* **1961,** *6*, 138-163.

(57) Improta, R.; Ferrante, C.; Bozio, R.; Barone, V., The Polarizability in Solution of Tetra-Phenyl-Porphyrin Derivatives in their Excited Electronic States: A PCM/TD-DFT Study. *Phys. Chem. Chem. Phys.* **2009,** *11*, 4664-4673.

(58) Kakiuchi, T., Potential-dependent adsorption and partitioning of ionic components at a liquid|liquid interface. *J. Electroanal. Chem.* **2001,** *496*, 137-142.

(59) Piron, A.; Brevet, P. F.; Girault, H. H., Surface second harmonic generation monitoring of the anion methyl orange during ion transfer reactions across a polarized water. *Journal of Electroanalytical Chemistry* **2000,** *483*, 29-36.

(60) Kano, K.; Nakajima, T.; Takei, M.; Hashimoto, S., Self aggregation of cationic porphyrin in water. *Bulletin of the Chemical Society of Japan* **1987,** *60*, 1281-1287.

(61) Wang, H.; Borguet, E.; Eisenthal, K. B., Polarity of Liquid Interfaces by Second Harmonic Generation Spectroscopy. *J. Phys. Chem. A* **1997,** *101*, 713-718.

(62) Wang, H.; Borguet, E.; Eisenthal, K. B., Generalized Interface Polarity Scale Based on Second Harmonic Spectroscopy. *J. Phys. Chem. B* **1998,** *102*, 4927-4932.

(63) Steel, W. H.; Walker, R. A., Measuring Dipolar Width across Liquid-Liquid Interfaces with 'Molecular Rulers'. *Nature* **2003,** *424*, 296-299.

(64) Steel, W. H.; Beildeck, C. L.; Walker, R. A., Solvent polarity across strongly associating interfaces. *Journal of Physical Chemistry B* **2004,** *108*, 16107-16116.

(65) Siler, A. R.; Brindza, M. R.; Walker, R. A., Hydrogen-bonding molecular ruler surfactants as probes of specific solvation at liquid/liquid interfaces. *Analytical and Bioanalytical Chemistry* **2009,** *395*, 1063-1073.

(66) Osakai, T.; Sawada, J.; Nagatani, H., Potential-modulated fluorescence spectroscopy of the membrane potential-sensitive dye di-4-ANEPPS at the 1,2-dichloroethane/water interface. *Analytical and Bioanalytical Chemistry* **2009,** *395*, 1055-1061.

(67) Gandini, S. C. M.; Gelamo, E. L.; Itri, R.; Tabak, M., Small Angle X-ray Scattering Study of *Meso*-Tetrakis (4-Sulfonatophenyl) Porphyrin in Aqueous Solution: A Self-Aggregation Model. *Biophys. J.* **2003,** *85*, 1259-1268.

(68) Choi, M. Y.; Pollard, J. A.; Webb, M. A.; McHale, J. L., Counterion-Dependent Excitonic Spectra of Tetra(*p*-Carboxyphenyl)Porphyrin Aggregates in Acidic Aqueous Solution. *J. Am. Chem. Soc.* **2003,** *125*, 810-820.

(69) De Luca, G.; Romeo, A.; Scolaro, L. M., Counteranion Dependent Protonation and Aggregation of Tetrakis(4-Sulfonatophenyl)Porphyrin in Organic Solvents. *J. Phys. Chem. B* **2006,** *110*, 7309-7315.

(70) Castriciano, M. A.; Romeo, A.; Villari, V.; Angelini, N.; Micali, N.; Scolaro, L. M., Aggregation Behavior of Tetrakis(4-Sulfonatophenyl)Porphyrin in AOT/Water/Decane Microemulsions. *J. Phys. Chem. B* **2005,** *109*, 12086-12092.

(71) Castriciano, M. A.; Romeo, A.; Villari, V.; Micali, N.; Scolaro, L. M., Nanosized Porphyrin J-aggregates in Water/AOT/Decane Microemulsions. *J. Phys. Chem. B* **2004,** *108*, 9054-9059.

(72) Fujiwara, K.; Wada, S.; Monjushiro, H.; Watarai, H., Ion-Association Aggregation of an Anionic Porphyrin at the Liquid/Liquid Interface Studied by Second Harmonic Generation Spectroscopy. *Langmuir* **2006,** *22*, 2482-2486.

(73) Fujiwara, K.; Monjushiro, H.; Watarai, H., Non-Linear Optical Activity of Porphyrin Aggregate at the Liquid/Liquid Interface. *Chem. Phys. Lett.* **2004,** *394*, 349-353.

(74) Nakata, K.; Kobayashi, T.; Tokunaga, E., Electric Field-Controlled Dissociation and Association of Porphyrin J-aggregates in Aqueous Solution. *Phys. Chem. Chem. Phys.* **2011,** *13*, 17756-17767.

(75) Smith, K. M., *Porphyrins and Metalloporphyrins*. Elsevier Amsterdam: 1975.

(76) Bhosale, S. V.; Shitre, G. V.; Bobe, S. R.; Gupta, A., Supramolecular Chemistry of Protoporphyrin IX and its Derivatives. *Eur. J. Org. Chem.* **2013**, 3939-3954.

(77) Delmarre, D.; Meallet-Renault, R.; Bied-Charreton, C.; Pasternack, R. F., Incorporation of Water-Soluble Porphyrins in Sol-Gel Matrices and Application to pH Sensing. *Anal. Chim. Acta* **1999,** *401*, 125-128.

(78) Chen, J.; Collier, C. P., Noncovalent Functionalization of Single-Walled Carbon Nanotubes with Water-Soluble Porphyrins. *J. Phys. Chem. B* **2005,** *109*, 7605-7609.

(79) Ribo, J. M.; Crusats, J.; Farrera, J.-A.; Valero, M. L., Aggregation in Water Solutions of Tetrasodium Diprotonated *meso*-Tetrakis(4-Sulfonatophenyl)Porphyrin. *J. Chem. Soc., Chem. Commun.* **1994**, 681-682.

(80) Maiti, N. C.; Ravikanth, M.; Mazumdar, S.; Periasamy, N., Fluorescence Dynamics of Noncovalently Linked Porphyrin Dimers, and Aggregates. *J. Phys. Chem.* **1995,** *99*, 17192-17197.

(81) Maiti, N. C.; Mazumdar, S.; Periasamy, N., J- and H-Aggregates of Porphyrin-Surfactant Complexes: Time-Resolved Fluorescence and Other Spectroscopic Studies. *J. Phys. Chem. B* **1998,** *102*, 1528-1538.

(82) Würthner, F.; Kaiser, T. E.; Saha-Möller, C. R., J-Aggregates: From Serendipitous Discovery to Supramolecular Engineering of Functional Dye Materials. *Angew. Chem. Int. Ed.* **2011,** *50*, 3376-3410.

(83) Osakai, T.; Muto, K., Ion Transfer and Photoinduced Electron Transfer of Water-Soluble Porphyrin at the Nitrobenzene|Water Interface. *J. Electroanal. Chem.* **2001,** *496*, 95-102.

(84) Watarai, H.; Wada, S.; Fujiwara, K., Spectroscopic Detection of Chiral Aggregation at Liquid-Liquid Interfaces. *Tsinghua Sci. Technol.* **2006,** *11*, 228-232.

(85) Kobayashi, T., *J-aggregates*. World Scientific: 2012; Vol. 2.

(86) Perrenoud-Rinuy, J.; Brevet, P.-F.; Girault, H. H., Second Harmonic Generation Study of Myoglobin and Hemoglobin and their Protoporphyrin IX Chromophore at the Water/1,2-Dichloroethane Interface. *Phys. Chem. Chem. Phys.* **2002,** *4*, 4774-4781.

(87) Margalit, R.; Shaklai, N.; Cohen, S., Fluorimetric Studies on the Dimerization Equilibrium of Protoporphyrin IX and its Haemato Derivative. *Biochem. J* **1983,** *209*, 547-552.

(88) Bobe, M. S. R.; Al Kobaisi, M.; Bhosale, S. V., Solvent-Tuned Self-Assembled Nanostructures of Chiral $_{L}/_{D}$-Phenylalanine Derivatives of Protoporphyrin IX. *ChemistryOpen* **2015,** *4*, 516-522.

(89) Monsu Scolaro, L.; Castriciano, M.; Romeo, A.; Patane, S.; Cefali, E.; Allegrini, M., Aggregation Behavior of Protoporphyrin IX in Aqueous Solutions: Clear Evidence of Vesicle Formation. *J. Phys. Chem. B* **2002,** *106*, 2453-2459.

(90) Brault, D., Physical Chemistry of Porphyrins and their Interactions with Membranes: The Importance of pH. *J. Photochem. Photobiol., B* **1990,** *6*, 79-86.

(91) Inamura, I.; Uchida, K., Association Behavior of Protoporphyrin IX in Water and Aqueous Poly (N-Vinylpyrrolidone) Solutions. Interaction between Protoporphyrin IX and Poly (N-Vinylpyrrolidone). *Bull. Chem. Soc. Jpn.* **1991,** *64*, 2005-2007.

(92) Walker, R. A.; Conboy, J. C.; Richmond, G. L., Molecular Structure and Ordering of Phospholipids at a Liquid-Liquid Interface. *Langmuir* **1997,** *13*, 3070-3073.

(93) Santos, H. A.; García-Morales, V.; Pereira, C. M., Electrochemical Properties of Phospholipid Monolayers at Liquid-Liquid Interfaces. *ChemPhysChem* **2010,** *11*, 28-41.

(94) Pichot, R.; Watson, R. L.; Norton, I. T., Phospholipids at the Interface: Current trends and Challenges. *Int. J. Mol. Sci.* **2013,** *14*, 11767-11794.

(95) Yoshida, Y.; Maeda, K.; Shirai, O., The Complex Formation of Ions with a Phospholipid Monolayer Adsorbed at An Aqueous|1,2-Dichloroethane Interface. *J. Electroanal. Chem.* **2005,** *578*, 17-24.

(96) Sawada, S.; Osakai, T.; Sawada, S., Mechanism of Electrochemical Solvent Extraction of Divalent Metal Ions With Quinolin-8-ol. *Analyst* **1997,** *122*, 1597-1600.

(97) Itagaki, M.; Fukushima, H.; Watanabe, K., Studies on Electrochemical Solvent Extraction of Metal Ions at Water/1,2-dichloroethane Interface. *Anal. Sci.* **2001,** *17*, 819-824.

(98) Yoshida, Z., Electrochemical Study of Solvent Extraction Based on Ion Transfer at the Aqueous/Organic Solution Interface. *Solvent Extraction Research and Development, Japan* **2011,** *18*, 15-35.

(99) Takeyama, M. Adsorption Behavior of Water-Soluble 8-Quinolinol Complexes at Liquid|Liquid Interface. Bachelor's thesis, Kanazawa University, Unpublished, 2013.

(100) Das, A. K., Studies on mixed Ligand Complexes of Cobalt(II), Nickel(II), Copper(II) and Zinc(II) Involving 8-Hydroxyquinoline-5-Sulphonic Acid as a Primary Ligand and Substituted Catechols as Secondary Ligands. *Transition Met. Chem.* **1989,** *14*, 200-202.

(101) Luisa Ramos, M.; Justino, L. L. G.; Branco, A.; Duarte, C. M. G.; Abreu, P. E.; Fonseca, S. M.; Burrows, H. D., NMR, DFT and Luminescence Studies of the Complexation of Zn(II) with 8-Hydroxyquinoline-5-Sulfonate. *Dalton Transactions* **2011,** *40*, 11732-11741.

(102) Richard, C. F.; Gustafson, R. L.; Martell, A. E., Stability of Metal Chelates of 8-Quinolinol-5-Sulfonate. *J. Am. Chem. Soc.* **1959,** *81*, 1033-1040.

(103) Beltrán, J. L.; Codony, R.; Prat, M. D., Evaluation of stability constants from multi-wavelength absorbance data: program STAR. *Anal. Chim. Acta* **1993,** *276*, 441-454.

(104) Badocco, D.; Dean, A.; Di Marco, V.; Pastore, P., Electrochemical Characterization of 8-Hydroxyquinoline-5-Sulphonate/Aluminium(III) Aqueous Solutions. *Electrochim. Acta* **2007,** *52*, 7920-7926.

(105) Ramos, M. L.; Justino, L. L. G.; Salvador, A. I. N.; de Sousa, A. R. E.; Abreu, P. E.; Fonseca, S. M.; Burrows, H. D., NMR, DFT and Luminescence Studies of the Complexation of Al(iii) with 8-Hydroxyquinoline-5-Sulfonate. *Dalton Transactions* **2012,** *41*, 12478-12489.

(106) Conradi, S.; Vogt, C.; Wittrisch, H.; Knobloch, G.; Werner, G., Capillary electrophoretic separation of metal ions using complex forming equilibria of different stabilities. *J. Chromatogr. A* **1996,** *745*, 103-109.

(107) Brinkmann, M.; Gadret, G.; Muccini, M.; Taliani, C.; Masciocchi, N.; Sironi, A., Correlation between Molecular Packing and Optical Properties in Different Crystalline Polymorphs and Amorphous Thin Films of mer-Tris(8-hydroxyquinoline)aluminum(III). *J. Am. Chem. Soc.* **2000,** *122*, 5147-5157.

(108) Gao, H.-L.; Jiang, S.-X.; Hu, Y.-M.; Li, F.-F.; Zhang, Q.-Q.; Shi, X.-Y.; Cui, J.-Z., Syntheses, Structures and Luminescent Properties of the Metal Complexes Based on Zn(II) or Cd(II) with 5-Nitro-8-Hydroxyquinoline. *Inorg. Chem. Commun.* **2014,** *44*, 58-62.

(109) Li, S.; Lu, J.; Ma, H.; Xu, J.; Yan, D.; Wei, M.; Evans, D. G.; Duan, X., Ordered Blue Luminescent Ultrathin Films by the Effective Coassembly of Tris(8-hydroxyquinolate-5-sulfonate)aluminum and Polyanions with Layered Double Hydroxides. *Langmuir* **2011,** *27*, 11501-11507.

(110) McDonald, F. C.; Applefield, R. C.; Halkides, C. J.; Reibenspies, J. H.; Hancock, R. D., A Thermodynamic and Crystallographic Study of Complexes of the Highly Preorganized Ligand 8-Hydroxyquinoline-2-Carboxylic Acid. *Inorg. Chim. Acta* **2008,** *361*, 1937-1946.

(111) Ding, Z.; Wellington, R. G.; Brevet, P. F.; Girault, H. H., Differential Cyclic Voltabsorptometry and Chronoabsorptometry Studies of Ion Transfer Reactions at the Water|1,2-Dichloroethane Interface. *J. Electroanal. Chem.* **1997,** *420*, 35-41.

ACKNOWLEDGMENTS

I would like to express my gratitude to Associate professor, Hirohisa Nagatani of Kanazawa University for the continuous support of my study. His guidance helped me in all the time of research and writing of this dissertation.

Besides my chief advisor, I would like to thank *Prof.* Tsuyoshi Asakawa, *Prof.* Motohiro Mizuno, *Prof.* Shigehisa Akine, and *Prof.* Hisanori Imura of Kanazawa University for their insightful comments and encouragement.

Finally, I am grateful to all members of Analytical Chemistry Laboratory for their support in everyday life.

PUBLICATION LIST

[1] Sho Yamamoto, Hirohisa Nagatani, Kotaro Morita, Hisanori Imura,
"Potential-Dependent Adsorption and Orientation of *meso*-Substituted Porphyrins at Liquid|Liquid Interfaces Studied by Polarization-Modulation Total Internal Reflection Fluorescence Spectroscopy", *The Journal of Physical Chemistry C*, **120**, 7248–7255 (2016).

[2] Sho Yamamoto, Hirohisa Nagatani, Hisanori Imura,
"Potential-Induced Aggregation of Anionic Porphyrins at Liquid|Liquid Interfaces", *Langmuir*, **33**, 10134–10142 (2017).

Appendix

PM-TIRF Analysis of tris(2,2′-bipyridine)ruthenium(II) system

In order to clarify the surface sensitivity of the PM-TIRF technique, the PM-TIRF spectroscopy was applied to the tris(2,2′-bipyridine)ruthenium(II) ($Ru(bpy)_3^{2+}$) system. $Ru(bpy)_3^{2+}$ is an efficient fluorescent dye and it has been studied at the polarized water|DCE interface,[24, 111] in which $Ru(bpy)_3^{2+}$ exhibited a quasi-reversible ion transfer feature without the interfacial adsorption. The formal transfer potential was observed as $\Delta_o^w\phi^{o'}_{Ru(bpy)_3^{2+}} = -0.10$ V in the voltammetric measurements (**Figure A1**). A *D*3 symmetry of $Ru(bpy)_3^{2+}$ ensures independence of the fluorescence intensity on linear polarizations of the excitation beam, even if $Ru(bpy)_3^{2+}$ is adsorbed at the interface. The $Ru(bpy)_3^{2+}$ system is therefore suitable to examine the selectivity of the PM-TIRF technique for the species "oriented" at the interface. As shown in **Figure A1b**, the PM-TIRF signals ($\Delta F^{p\text{-}s}$) were almost constant in the whole potential region and negligibly small in comparison with the total fluorescence intensity (F_{total}). In the absence of the interfacial adsorption, eq. (4-2) is simplified to $F_{total} = F_{bulk}$. Thus, $\Delta_o^w\phi < \Delta_o^w\phi^{o'}_{Ru(bpy)_3^{2+}}$ is identical to the fluorescence from the bulk aqueous phase and the significant increment of F_{total} at $\Delta_o^w\phi^{o'}_{Ru(bpy)_3^{2+}} < \Delta_o^w\phi$ associates with the fluorescence from $Ru(bpy)_3^{2+}$ transferred into the organic phase. The potential dependence of F_{total} clearly showed that the fluorescence from the bulk organic phase effectively increases only at potentials beyond $\Delta_o^w\phi^{o'}$. It is noteworthy that $\Delta F^{p\text{-}s}$ was also independent on the F_{total} value consisting of the fluorescence intensities from both bulk solutions and interfacial region. **Figure A2** shows the relative intensity of $\Delta F^{p\text{-}s}$ with respect to F_{total}, $\left|\Delta F^{p\text{-}s} / F_{total}\right|$. The $\left|\Delta F^{p\text{-}s} / F_{total}\right|$ values observed for $Ru(bpy)_3^{2+}$ were much smaller than those for H_2TMPyP^{4+} or H_2TPPS^{4-}. These experimental results clearly demonstrate that only the

species which have the excitation dipole moment oriented at the interface can generate strong PM-TIRF signals.

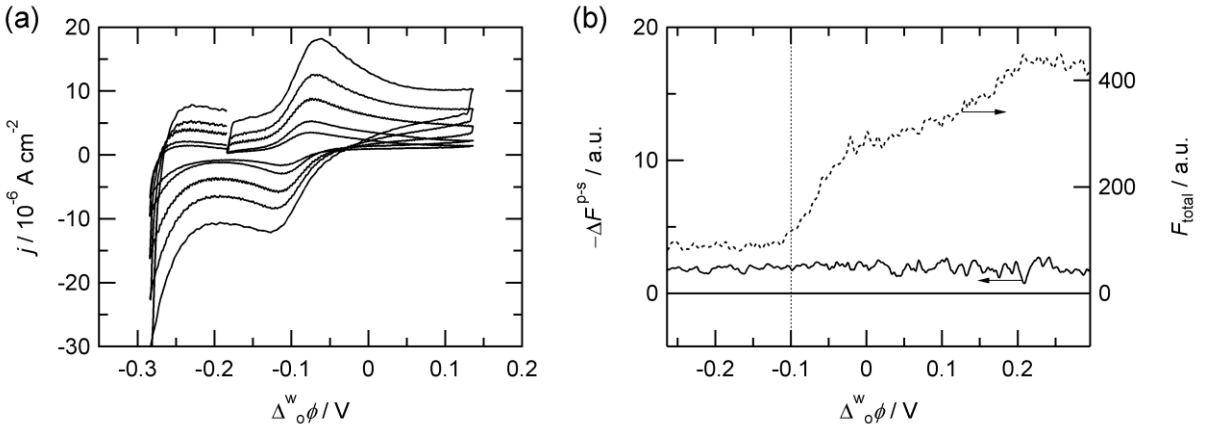

Figure A1. (a) Typical cyclic voltammograms and potential dependence of (b) PM-TIRF responses ($\Delta F^{\text{p-s}}$) measured for $Ru(bpy)_3^{2+}$ at the water|DCE interface. The potential sweep rates were (a) 10, 20, 50, 100 and 200 mV s^{-1}, (b) 5 mV s^{-1}. The concentration of $Ru(bpy)_3^{2+}$ derivatives in the aqueous phase was 2.0×10^{-5} mol dm^{-3}. The pH values of the aqueous phase were pH 7.0. The excitation and detected emission wavelengths were 404 nm and 609 nm, respectively. The vertical line indicates $\Delta^{w}_{o}\phi^{\circ'}_{Ru(bpy)_3^{2+}} = -0.10$ V.

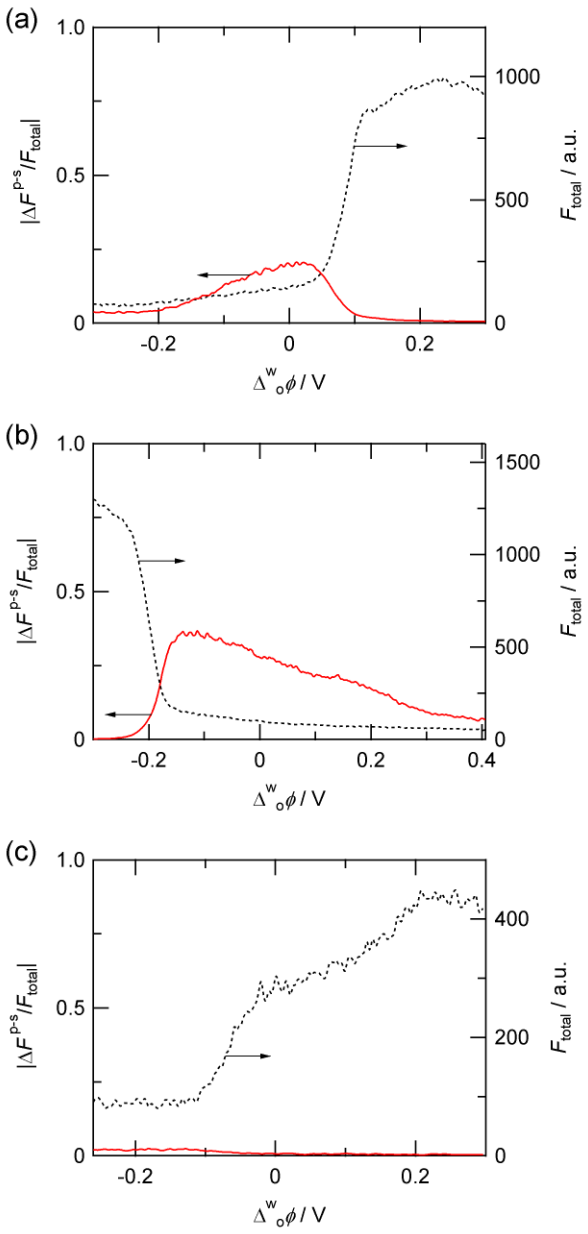

Figure A2. Potential dependences of $\left|\Delta F^{\text{p-s}} / F_{\text{total}}\right|$ and F_{total} for (a) H_2TMPyP^{4+}, (b) H_2TPPS^{4-} and (c) $Ru(bpy)_3^{2+}$ systems. The dotted lines depict F_{total}.

SYMBOL LIST

Greek

α : overall transfer coefficient for adsorption

β_n : stability constants of metal complexes

γ_i : interfacial tension

Γ_s : saturated interfacial concentration

ε, : molar absorption coefficient

ϕ^w : inner potential of an aqueous phase.

ϕ^o : inner potential of an organic phase.

$\Delta_o^w\phi$: Galvani potential difference

$\Delta_o^w\phi^\circ$: standard ion transfer potential

$\Delta_o^w\phi_{ac}$: amplitude of the ac potential modulation

$\Delta_{aw}^w\phi$: the potential difference between the bulk and adsorption plane

$\Delta_o^w\phi^{\circ\prime}$: formal ion transfer potential of species

Φ_f : fluorescence quantum yield

λ_L : wavelength of incident beam

λ_{max} : fluorescence maximum wavelength

θ : surface coverage

θ^w : potential dependent surface coverage at the aqueous side of the interface

θ_{ac} : ac modulated surface coverage

θ_{OR} : orientation angle

θ_{scat} : scattered angle

ρ : density of a solvent

ω : angular frequency

ω_f : frequency of fundamental wave

ω_{SH} : frequency of SH wave

ψ_i : angle of incidence

ψ_c : critical angle

Ψ : angle of polarization of excitation beam with respect to the normal to the interface

Alphabet

a_x^w : activity of x^{z+} in an aqueous phase

a_x^o : activities of x^{z+} in an organic phase

b : the portion of the applied potential

c^w : concentration in an aqueous phase

c_0 : concentration in bulk solution

c_M : the total concentration of metal ion.

c_L : the total concentration of and ligand

C : proportional factor

C_{dl} : capacitance

$\tilde{E}$: ac potential

f_L : fundamental frequency of incident beam

f_0 : frequency of capillary wave.

f_{ac} : potential modulation frequency

F : Faraday constant

F_{bulk} : fluorescence intensity from bulk solution species in evanescent region and on the optical path of the excitation beam

$\Delta F^{p\text{-}s}$: PM-TIRF signal

F_m^p : total intensities of the modulated fluorescence in the p-polarization modes

$F_{\mathrm{m}}^{\mathrm{s}}$: total intensities of the modulated fluorescence in the s-polarization modes

F_{total} : total fluorescence intensity

ΔF_{re} : real part of PMF response

ΔF_{im} : imaginary part of PMF response

ΔF_{t} : PMF response associated with the quasi-reversible ion transfer (ΔF_{t}) in a TIR mode

ΔF_{a} : PMF response associates with adsorption

$\Delta G_{\mathrm{t}}^{\circ,\mathrm{w}\to\mathrm{o}}$: standard Gibbs free energy of the ion transfer from the aqueous and organic phases.

$\Delta G_{\mathrm{a}}^{\circ}$: Gibbs free energy of adsorption

$i_{\mathrm{f,ac}}$: ac faradic current

I_0 : excitation photon flux

$\tilde{I}$: ac current

I^{p} : intensity of p-polarized incident beam

I^{s} : intensity of s-polarized incident beam

j : the imaginary number

$k_{\mathrm{a}}^{\mathrm{w}}$: rate constant for the adsorption at the aqueous plane

$k_{\mathrm{a}}^{\mathrm{w}\circ}$: rate constant for the adsorption at the potential of zero charge

$k_{\mathrm{d}}^{\mathrm{w}}$: rate constant for the desorption at the aqueous plane

$k_{\mathrm{d}}^{\mathrm{w}\circ}$: rate constant for the desorption at the potential of zero charge

$k_{\mathrm{a,dc}}$: dc component of the adsorption rate constant at given potentials

$k_{\mathrm{d,dc}}$: dc component of the desorption rate constant at given potentials

k : wavenumbers of capillary wave

K : wavenumbers of incident beam

K_{a} : acid dissociation constant

n_{i} : refractive index of a medium i

n : order of the diffraction spot

P_m : polarization modulation efficiency

R : gas constant

R_F : peak intensity ratio of the first and second peaks of PM-TIRF spectra

R_s : solution resistance

S : illuminated interfacial area.

T : temperature

x^{z+} : ion in a solution:

Y : admittance

z : charge number